Hypoxic Intrusions to Puget Sound from the Pacific Ocean

Robert W. Deppe

A thesis submitted in partial fulfillment of the requirements for the degree of

Master of Science in Mechanical Engineering

University of Washington

2014

Reading Committee:

Jim Thomson, Chair

Brian Polagye

Christopher Krembs

Program Authorized to Offer Degree:
Mechanical Engineering

University of Washington

Abstract

Hypoxic Intrusions to Puget Sound from the Pacific Ocean

Robert W. Deppe

Chair of the Supervisory Committee:
Dr. Jim Thomson
Applied Physics Lab, Adjunct in Mechanical Engineering

Oceanic intrusions of dense, hypoxic water regularly occur at the entrance to Puget Sound, WA (USA), and may be significant to regional dissolved oxygen levels. Seabed observations at Admiralty Inlet from 2009 to 2013 show a strong correlation of low dissolved oxygen concentrations with high salinity, coincident with landward bottom residual currents. Intrusions of dense water to Puget Sound are likely related to estuarine exchange flows expected to occur during conditions for minimal tidal mixing. Observations agree with minimal mixing occurring during neap tides and maximum diurnal inequalities. Tidal conditions alone cannot predict intrusions of hypoxic ocean water to Puget Sound. Coastal upwelling and Fraser River discharge influence the availability of dense, hypoxic water outside of Puget Sound, likely due to the larger-scale exchange flow in the Strait of Juan de Fuca. This large-scale process adds a strong seasonal and interannual modulation to the intrusions of hypoxic water. This thesis develops a method to diagnose hypoxic intrusion events at Admiralty Inlet. The method is based, empirically, on seabed observations, but its application relies on operational data products. Using only tidal elevation signals and indices for coastal upwelling and river discharge, 98% of events with dissolved oxygen less than 4.0 mg/L are identified in the 3 year record. Two-layer exchange flow conditions during intrusions are confirmed with surface observations and CTDO casts. Effects of landward propagation of hypoxic intrusions are shown to be very diffuse and more prominent in the probable cumulative response. Hypoxic water in Hood Canal cannot be directly tied to these oceanic intrusions.

TABLE OF CONTENTS

LIST OF FIGURES

LIST OF TABLES

GLOSSARY

DO: Dissolved Oxygen

CT: Conductivity, Temperature

CTD: Conductivity, Temperature, Depth

CTDO: Conductivity, Temperature, Depth, Oxygen

ADCP: Acoustic Doppler Current Profiler

TEI: Tidal Elevation Index

MLLW: Mean Low-Low Water

$\mathcal{F}_{40}$: Low-pass filter notation (40 hour half-amplitude period)

$\mathcal{F}_{610}$: Low-pass filter notation (610 hour half-amplitude period)

$\mathcal{F}_{12.5}$: Low-pass filter notation (12.5 hour half-amplitude period)

UI: Upwelling Index

IEI: intrusion Event Index

NTI: Neap Tide Index

DII: Diurnal Inequality Index

UPI: Upwelling Persistence Index

FRDI: Fraser River Discharge Index

DOD: Dissolved Oxygen Deficit

DO_{AP}: Dissolved Oxygen Availability Prediction

$_{ST}DO_{P}$: Sub-tidal Dissolved Oxygen Prediction

TGI: Tidal Gradient Index

PFEL: Pacific Fisheries Environmental Laboratory

NOAA: National Oceanic and Atmospheric Administration

USNO: United States Naval Observatory

ACKNOWLEDGMENTS

I would like to thank the Washington State Department of Ecology, the Environmental Protection Agency, the Northwest National Marine Renewable Energy Center, and all involved in maintaining the sensors and moorings at Admiralty Inlet, especially: Joe Talbert, Alex deKlerk, and Capt. Andy Reay-Ellers. Thank you especially to the members of my reading committee for their time, contributions, and commitment to this project: Jim Thomson, Brian Polagye, and Christopher Krembs.

DEDICATION

To Jim and Ellen Deppe for supporting me in all of my endeavors and for being inspiring role models.

Chapter 1

INTRODUCTION

The waters of Puget Sound, WA (USA), are periodically subject to very low dissolved oxygen levels. These hypoxic events can be extremely harmful to biological life and consequentially to ecosystem-based industries like fishing and aquaculture. Within Puget Sound, Hood Canal is particularly susceptible to hypoxic events that lead to fish kills and to the decimation of populations of other marine life [1]. The origin of this low dissolved oxygen water can be attributed to two major scales of forcing: local and external. One possible local force is anthropogenic modulation. Runoff from farmland and other untreated wastewater that is high in nutrients can cause widespread algae blooms under certain conditions, which quickly consume dissolved oxygen in the water upon decay, reducing the concentration to hypoxic levels [1]. However, algae blooms can also occur naturally in the spring and summer [1]. These local forces, whether natural or anthropogenic, may play a role in the modulation of dissolved oxygen levels in Puget Sound, but there is also an external forcing factor. The external forcing is the natural modulation of dissolved oxygen concentration by oceanographic processes, particularly the intrusion of hypoxic water from the Pacific Ocean [1].

The overwhelming majority of the water leaving and entering Puget Sound does so through Admiralty Inlet, and this study focuses on this location (Figure 1.1). Admiralty Inlet has a unique bathymetry in that it has a long, shallow sill compared to most glacially carved estuaries. The sill region is about 30 kilometers in length and has a minimum depth of about 60 meters with two major peaks along the region [2]. This distinctive geometry plays an important role in determining the physical behavior of the flow of water between the Strait of Juan de Fuca and Puget Sound. Another important characteristic in this region is the presence of strong tidal currents (> 3 m/s) [3]. This is not an isolated system as the Strait of Juan de Fuca and Puget Sound are both part of the Salish Sea. Puget Sound is

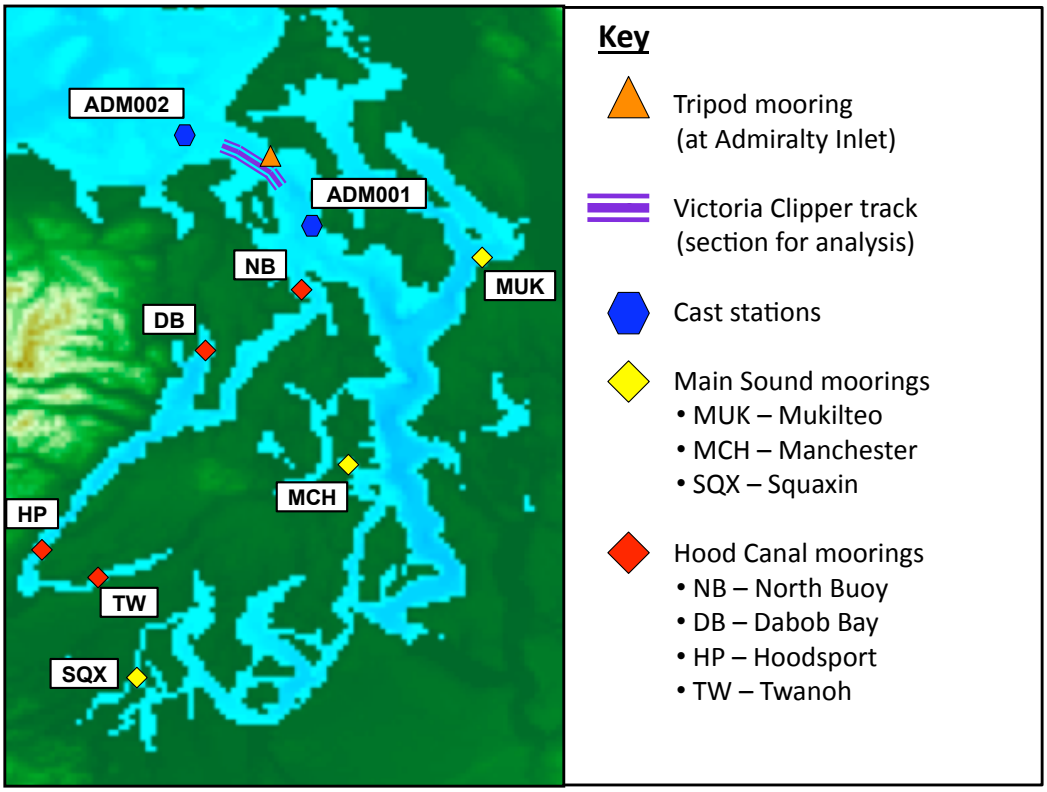

Figure 1.1: Map of Puget Sound with measurement locations marked. Tripod data were collected by the University of Washington and Washington Ecology. Victoria Clipper data, cast data, and main Sound mooring data, were collected by Washington Ecology. Hood Canal mooring data were collected by the ORCA group at the University of Washington.

connected to the North Pacific Ocean by the Strait of Juan de Fuca, making it an estuary within a larger estuary. The Fraser River, as the primary source of fresh water into the Salish Sea, is also important in these regional dynamics [4].

The external modulation of dissolved oxygen has not been studied enough to sufficiently understand the processes involved and its relative contribution to the overall modulation of dissolved oxygen levels in Puget Sound. It is understood that dense, low dissolved oxygen water can be upwelled from the deep ocean and carried through Admiralty Inlet into the Sound under certain tidal conditions as part of a bottom intrusion [2]. A bottom intrusion

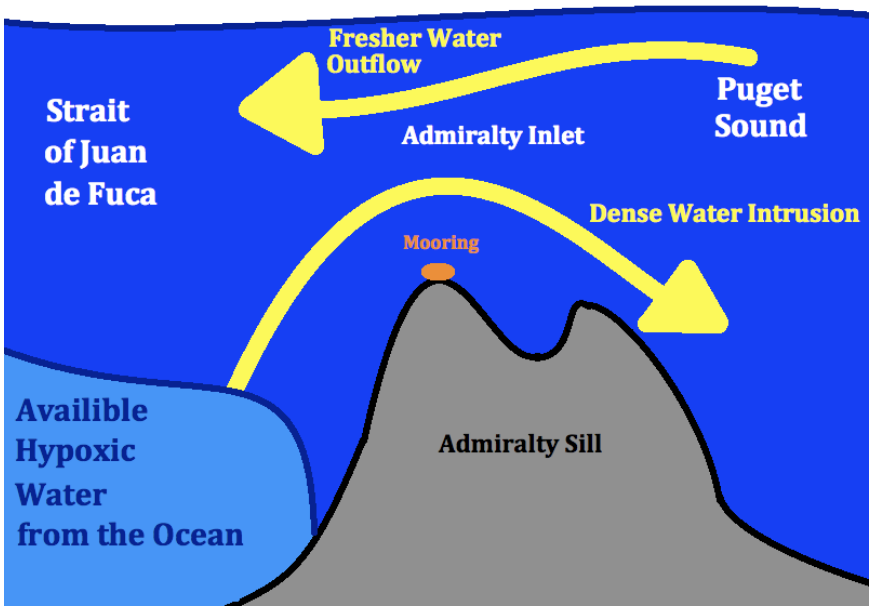

Figure 1.2: Schematic of exchange flow dynamics at Admiralty Inlet and the importance of the availability of hypoxic water in the Strait of Juan de Fuca. The orange marker indicates the location of the tripod mooring from which observational data were collected.

over the sill is considered to be the transport of water in the bottom-layer portion of a two-layer exchange flow in Admiralty Inlet, in which dense water flows into Puget Sound along the bottom (Figure 1.2). This water then makes its way through the main basin and eventually may become involved in hypoxia events in certain areas of the Sound [5]. The relative importance of natural modulation compared to that of anthropogenic modulation is not well known. The driving forces involved in the availability and physical transport of these low dissolved oxygen water intrusions are expected to include coastal upwelling, tidal currents, and river discharge.

Geyer and Cannon determined that high salinity (relatively dense water) intrusions into Puget Sound occur during periods of minimal mixing at Admiralty Inlet, when tidal turbulence generation is the weakest [2]. Consequently, they found that the two most important conditions favoring dense water intrusions over the sill are the maximum diurnal inequality and the neap tides, which coincide at the equinoxes [2]. Geyer and Cannon also mention that

during the strongest spring-tide currents in a year (solstice), tidal advection can generate strong dense-water inflows to Puget Sound but that these instances are rare due to the long length of Admiralty Sill [2]. While two-layer estuarine exchange flow is the dominant process governing water exchange at Admiralty Inlet, Yang and Wang also investigate residual tidal eddies (related complex bathymetry and headlands) as another dynamic phenomena that further complicates the cross-channel variations and current dynamics in the region [6]. Although the current dynamics and exchange flow processes are complex, tidally-forced mixing is considered the dominant factor controlling dense water intrusion development over Admiralty Sill [2][6]. The methods developed in this thesis will focus on the simplified, dominant control of exchange flow development by the strength of mixing at Admiralty Inlet.

Geyer and Cannon also note that the presence of these favorable minimal mixing conditions for dense water intrusions do not guarantee that a high salinity intrusion will occur and that there are other forcing factors like increased river runoff that may account for the availability of dense water [2]. Cannon, Holbrook, and Pashinski, discuss that coastal upwelling and downwelling may be important factors for availability as well [7]. In particular, Cannon, Holbrook, and Pashinski, observed that coastal storms in the winter, which cause downwelling, may suppress high-salinity water intrusions [7]. They also calculated a strong negative correlation between bottom salinity near Admiralty Sill and wind measurements at N 48, W 125, with a lag in the bottom salinity of about 7.25 days following wind events [7]. In order to asses the seasonal availability of hypoxic water in the Strait of Juan de Fuca reaching Puget Sound, the persistence of coastal upwelling conditions and the discharge signal of the Fraser River must be quantified. Both upwelling and Fraser River discharge influence the density difference between deep oceanic waters and fresher surface waters. An increase in this density difference could increase the strength a two-layer exchange flow in the Strait [8]. Given that Juan de Fuca conditions are favorable for hypoxic availability at a given time, an intrusion at Admiralty Sill would be expected to occur during neap tides with maximum diurnal inequality. Figure 1.2 illustrates the general dynamics involved in an estuarine exchange flow over Admiralty Sill and the importance of the seasonal availability of hypoxic water for entrainment in a dense water intrusion.

During a dense water bottom intrusion, there would not only be evidence of the event at the bottom. Due to the conservation of mass involved in a two-layer exchange flow, there would also be an outflow of fresher, less dense water that would be observed at the surface as part of the estuarine salinity balance, strengthening the pycnocline [8]. Therefore, any time that a high-salinity bottom water intrusion develops over the sill and there is a temporary salinity surplus observed (and potentially a dissolved oxygen deficit if hypoxic water is seasonally available), the juxtaposition of this signal may be observed at the surface. There would likely be a coincidental decrease in surface salinity and there would be a noticeable pycnocline in the vertical salinity profile over Admiralty Sill, as is demonstrated by Geyer and Cannon [2].

While there is indication in the literature of the conditions necessary to expect an intrusion of hypoxic water at the bottom of Admiralty Inlet, there is far less understanding of the dynamics of the propagation of these intrusions through Puget Sound and its tributaries after they traverse the sill. There is agreement that the dense, hypoxic water is no longer subject to strong tidal currents after traversing the sill and takes the form of a gravity current that carries this water through the main basin until it is mixed into the existing water masses by other processes [1][2][5]. Lavelle, et al., uses a model to support observations that intrusions propagate along the bottom of Puget Sound at current speeds between 7 and 14 cm/s, much lower than the current speeds observed over Admiralty Sill [9][10]. Due to the complex bathymetry and significant mixing induced by internal sills, the dynamics of propagations of intrusions through Puget Sound and its tributaries are somewhat unclear and likely very complicated.

The following analysis enhances the understanding of the conditions necessary for the development of hypoxic bottom water intrusions from the ocean over Admiralty Sill, as well as the response in Puget Sound to these events. In Chapter 2, a two-stage prediction method is developed for determining periods favorable for hypoxic intrusion events at Admiralty Inlet. The first part of the prediction method uses tidal conditions to identify intrusion events. The second part of the method predicts the seasonal availability of hypoxic water in the Strait of Juan de Fuca that can be entrained into Puget Sound in an intrusion event. The prediction is based on an upwelling index at the mouth of the Strait and discharge from the

Fraser River. Chapter 2 includes two sections that describe vertical gradients associated with two-layer estuarine exchange flows at Admiralty Inlet using existing monitoring data. Temperature and salinity data collected from the Victoria Clipper during its transit through Admiralty Inlet are used to observe the surface signals coincident with active bottom water intrusions. Cast data taken during Ecology's float plane surveys near Admiralty Inlet provide vertical profiles for dissolved oxygen, temperature, and salinity (monitoring data from Washington Department of Ecology). These cast profiles are examined for relationships to tidal conditions and intrusion events.

In Chapter 3, observations from other moorings throughout the Sound are compared to those at Admiralty Sill (monitoring data from Washington Department of Ecology and the ORCA group at the University of Washington). The Main Basin of the Sound is considered separately from Hood Canal in this chapter as they are both distinct portions of the Sound with unique dynamics. The traceability of cumulative and direct responses to modulations in dissolved oxygen are assessed. Chapter 4 operationally tests the prediction method explained in Chapter 2. Rather than using in situ measurements to determine tidal elevation data as was done in the development of the method, the operational run uses publicly available tidal elevation data from online from NOAA (National Oceanic and Atmospheric Administration). The operational prediction method for hypoxic oceanic intrusions into Puget Sound outlined in this chapter does not require any in situ measurements at Admiralty Sill and all of its inputs are publicly available online. Chapter 5 integrates and discusses the different parts of the analysis conducted in the previous chapters. Three appendices provide additional information that may be useful for follow-on work.

Chapter 2

INTRUSION ANALYSIS AND PREDICTION FOR ADMIRALTY INLET

This chapter presents a method to quantify the combined tidal and regional conditions necessary for hypoxic intrusion events and examines different ways to observe two-layer exchange flow development over the sill at Admiralty Inlet. Section 2.1 describes seabed observations of hypoxic intrusions and develops indices for the relevant conditions. Section 2.2 applies these indices to predict (or rather, hindcast) the seabed observations and correctly identify hypoxic intrusion events. Figure 2.1 outlines the prediction method covered in Sections 2.1 and 2.2. Section 2.3 discusses implications and potential applications of the predictions for future intrusion events. Section 2.4 explores temperature and salinity signals in the surface waters Admiralty Inlet indicative of intrusions using data from the Victoria Clipper. Section 2.5 explores data records from float plane surveys of stations in the proximity of Admiralty Inlet considering the conditions necessary to observe two-layer exchange flows. Section 2.6 summarizes the conclusions of this analysis local to Admiralty Inlet.

2.1 Methods for Predicting

2.1.1 Field Observations

From August 2009 to October 2013, a Seabird 16plusv2 CTDO (Conductivity, Temperature, Depth, Oxygen) sensor was deployed on a Sea Spider tripod on the bottom of Admiralty Inlet off of Admiralty Head at approximately N 48 09.172, W 122 41.170 (Figure 1.1). The water depth at the site is approximately 55 m (ref. MLLW). The CTDO was mounted on the tripod 0.5 m above the seabed to sample every 30 minutes. The tripod was recovered and redeployed every 3 months, and each time the CTDO was replaced and calibrated.

A Nortek Continental ADCP (Acoustic Doppler Current Profiler) and a number of other

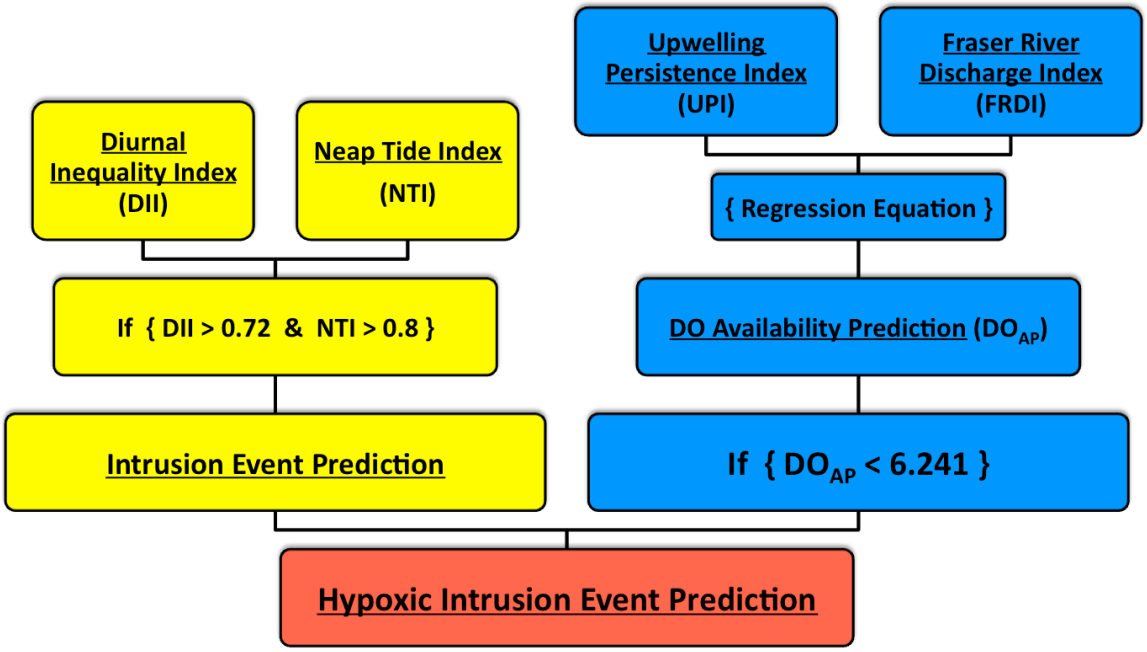

Figure 2.1: Flow chart outlining the prediction method for identifying hypoxic intrusion events.

sensors were mounted to the tripod. (The tripod deployments were motivated originally by a tidal energy site characterization, see [3] [11]). The ADCP sampled currents in 1 m bins from 1.7 to 50.7 m above the seabed[1] and recorded ensemble averages every 1 minute. Prior to analysis, all CTDO and ADCP data were interpolated to a uniform hourly time base. This obscures the small scale variations, but provides high statistical confidence in resolving processes on tidal and seasonal time scales.

The CTDO sensor is a single point measurement and thus cannot be used to estimate the flux of dissolved oxygen through the Inlet. Rather, we focus on diagnosing events of low dissolved oxygen and related conditions. Collocated salinity and temperature readings were used to identify the water mass associated with low dissolved oxygen. As shown in Figure 2.2, low dissolved oxygen levels measured at the site correspond with high salinity water

[1]For the final deployment, July to October 2013, the ADCP range only reaches up to 20 m above the seabed.

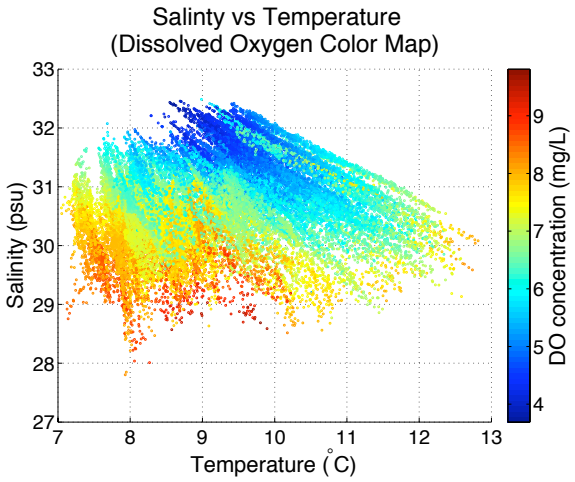

Figure 2.2: Salinity (psu) versus temperature (C) at Admiralty Inlet from August 2009 to October 2013. Data (30534 data points) colored according to corresponding dissolved oxygen concentration (mg/L).

and a narrow temperature range, suggesting an oceanic source (water from Puget Sound is expected to be fresher as result of the large river outflows). This confirms that occurrences of low dissolved oxygen water in Admiralty Inlet can be paired with the dynamics of dense water intrusions, which have been studied previously at this location [2].

The full time series of dissolved oxygen concentration from the CTDO sensor, shown in Figure 2.3a, covers a span of over four years. Missing sections of data are due to instrument failure or corrupted data. There is noticeable seasonality in the time series with the lowest dissolved oxygen levels occurring in the late summer and early autumn and higher levels occurring in the spring. There is also significant variance on shorter time scales. Figure 2.3b(I) shows a four-week period in which dissolved oxygen levels are low and in which the tidal dynamics are theoretically favorable for exchange flow. In Figure 2.3b(II), a Tidal Elevation Index derived via de-meaning (by deployment) and normalizing the pressure signal from the CTDO is shown in conjuction with the neap tides, which are shaded blue.

$$TEI = \frac{\text{demean}\,(Pressure)}{-MLLW} \tag{2.1}$$

As expected, the neap tides and the maximum diurnal inequality occur simultaneously during the equinox, and thus there are protracted periods of weak tidal currents. The weak

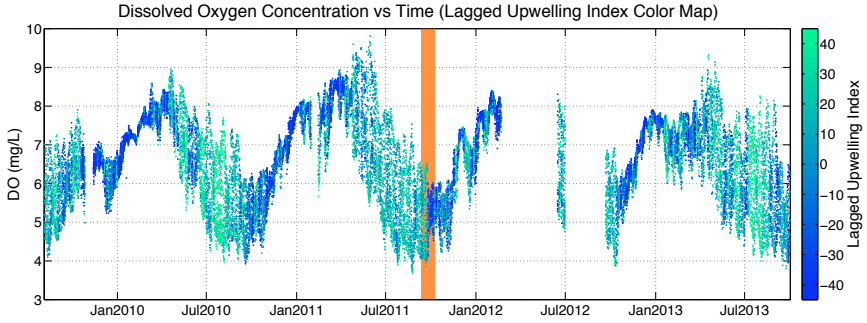

(a) Full time series

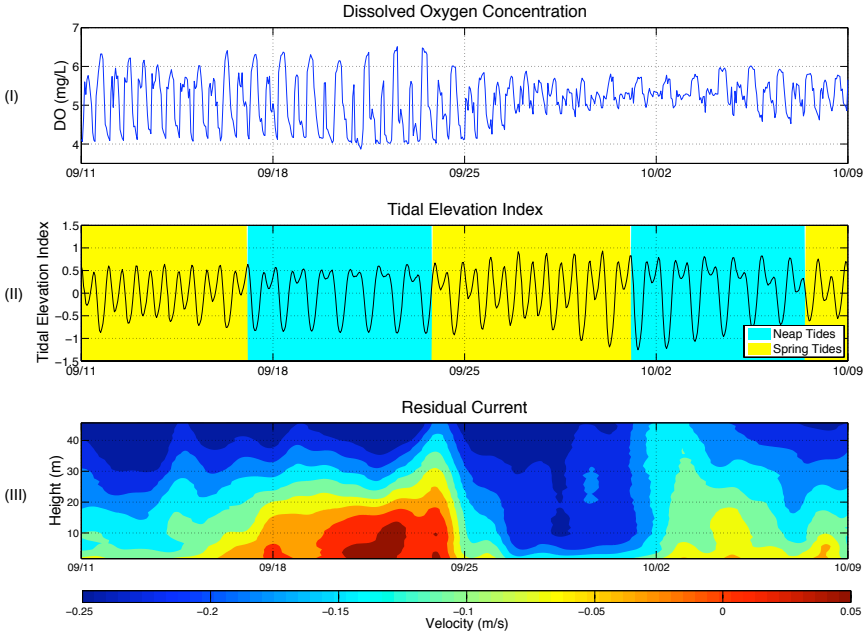

(b) Zoom-in of period shaded orange in full time series plot

Figure 2.3: (a) Time series of dissolved oxygen concentration (mg/L) at Admiralty Inlet from August 2009 to October 2013. Data points colored according to an Upwelling Index obtained from the Pacific Fisheries Environmental Laboratory [12], linearly interpolated to an hourly time scale, and lagged 7.25 days (following [7]). (b) A four-week subset of data surrounding the 2011 autumnal equinox, showing: (I) dissolved oxygen concentration (mg/L), (II) Tidal Elevation Index (from demeaned pressure measurements), and (III) low-pass filtered residual currents (m/s), height measured from sea floor. Spring and neap tide periods are shaded for the Tidal Elevation Index time series.

currents are associated with weak mixing, and thus exchange flow is strong [2]. The residual currents, calculated using a low-pass filter $\mathcal{F}_{40}$ (low-pass filter notation) on the ADCP current velocity data with a half-amplitude period of 40 hours [11], show significant exchange flow occurring coincident with the minima in dissolved oxygen (Figure 2.3b(II)). It is apparent that strong exchange flows and lower dissolved oxygen concentrations develop during periods of weak tidal amplitude. These flows and concentrations appear to be subsequently mixed out during periods of large tidal amplitude, consistent with Geyer and Cannon [2].

Related to this tidal modulation of exchange flow development via mixing, there is a significant negative correlation between dissolved oxygen and tidal elevation during the period from August to November of 2011, an example of a period with a fairly constant background dissolved oxygen (DO) signal. While this correlation cannot be observed for the full data set due to seasonal trends, it suggests that tidal elevation may be a useful predictor of exchange flow conditions. However, whether low dissolved oxygen water is available to enter the Sound during these conditions likely depends on other forcing factors such as coastal upwelling and river discharge. Revisiting Figure 2.3a during the same time period, it appears that coastal downwelling is also initiated at the end of September 2011, eliminating the transport of the most dense, hypoxic ocean water toward Puget Sound by way of the Strait.

To examine the influence of upwelling, records of an Upwelling Index UI from the same longitude and latitude as the wind data used by Cannon, Holbrook, and Pashinski [7], were obtained from the Pacific Fisheries Environmental Laboratory [12], lagged by 7.25 days, and then compared with the dissolved oxygen time series from the mooring at Admiralty Inlet, as shown in Figure 2.3a. The factor of upwelling favorable winds appears to play an important role in determining the availability of low dissolved oxygen water at Admiralty Inlet. Positive values indicate winds from the North that favor upwelling and negative values indicate winds from the South that favor downwelling. It appears that, on a seasonal time scale, downwelling conditions reduce the availability of low dissolved oxygen water that can be transported over the sill while upwelling conditions increase the availability of this dense upwelled water.

This mechanism also seems to have an effect on dissolved oxygen availability on shorter,

sub-tidal time scales and influences temporary changes in average dissolved oxygen concentrations. Sustained periods of upwelling-favorable winds at the coast are related to a sub-tidal-scale decrease in DO concentrations over time while downwelling-favorable winds have the opposite relationship Figure 2.3a. Upwelling and downwelling also appear to be related to the degree of variance in DO concentration on a tidal time-scale. During sustained upwelling time periods, tidal variance in DO concentrations is larger than during sustained downwelling time periods. This observation agrees with the concept of availability of dense water. During upwelling periods, dense, lower-DO water is available near the sill so that when bottom water intrusions develop during the small-amplitude portion of the mixed semi-diurnal tidal cycle, DO concentration near the bottom decreases drastically as this dense, lower-DO water traverses the sill [2]. Subsequently, when strong currents during the large-amplitude portion of the tidal cycle induce mixing over the sill, the DO concentration quickly increases as less dense, higher-DO water is mixed into the water mass near the bottom [2]. During downwelling periods, the difference between the DO concentration of bottom water entrained in intrusions and the other water in the region is less drastic, reducing the tidally-induced variance.

2.1.2 Intrusion Event Index

An Intrusion Event Index is developed based on the ADCP data and is used to quantify the duration and magnitude of a bottom water intrusion event at the tripod location in Admiralty Inlet. This index is independent of dissolved oxygen levels and identifies active exchange flow intrusions into Puget Sound. Thus, the index is expected to modulate with spring-neap tidal cycles and diurnal inequality signals. Due to a new tripod location starting May 2010, only the time series from May 2010 to October 2013 was considered in the intrusion analysis in order to preserve consistency in the index related to site-specific residual current patterns. Residual current data was first interpolated to create consistent bin sizes and heights between different ADCP deployments. Then residual current velocities were vertically averaged for all bins with positive (into the Sound) current velocities from the seabed up to the zero crossing (i.e., where residual current velocity switches to negative [out

of the Sound]). This depth-averaged intrusion velocity provided average positive residual current velocities of bottom water intrusions to the Sound and has a value of zero for all negative bottom current velocities, at each time step.

Next, the positive (inward) average bottom residual current velocities are integrated in time. Once this time-integral reaches a point where the depth-averaged intrusion velocity is zero or undefined, it resets to zero and remains so until the depth-averaged intrusion velocity is positive again and time-integration resumes. The result of this integral is a length scale representing the distance that a water parcel would travel under an assumption of homogenous flow. Comparing this length scale to the approximate $L = 30$ km length of Admiralty Sill [2], it can be assumed that if the time-integrated intrusion distance of a water mass carried by residual currents is greater than 30 km, then a dense-water intrusion could potentially traverse all the way over the sill and into the main basin of Puget Sound. Thus, a non-dimensional intrusion index is given by

$$IEI = \frac{\int \mathcal{F}_{40}\left(u\right) dt}{L}, \tag{2.2}$$

in which any intrusion that exceeds one before reseting to zero is considered a major bottom water intrusion event into Puget Sound. The maximum magnitude of the IEI during each event is a product of the vertically averaged residual bottom-current speed and duration, independent from dissolved oxygen levels.

2.1.3 Neap Tide Index

The spring tide to neap tide cycle has a fortnightly period and is based on lunar orientation[2]. Since spring tides reach their peak during the new moon and full moon and neap tides are prominent during periods of the quarter-moons [13], lunar phase data can be used as a basis for quantifying the neap-spring cycle. Daily lunar phase data downloaded from the Astronomical Applications Department of the US Naval Observatory provide a strong historical and predictive record for this application [14]. This daily raw data is formatted on a scale where a full moon has a value of 1, a quarter moon has a value of 0.5, and a new moon has a value of 0. The equation in (2.3) is used to formulate a Neap Tide Index, a form where a

value of 1 represents peak neap period and a value of 0 represents peak spring period.

$$NTI = (-2 \times |LunarPhase - 0.5|) + 1 \tag{2.3}$$

Since the NTI has a period of about 14 days, it does not need to be filtered to remove a tidal signal to be compared with residual current data or the Intrusion Event Index.

2.1.4 Diurnal Inequality Index

The maximum diurnal inequality occurs when the difference between the semidiurnal tidal amplitudes is largest. This means that there is about a half-day period of very gradual change in tidal elevation followed by about a half-day period of very rapid change in tidal elevation, as can be seen in Figure 2.3b(II). During the small-amplitude portion of the signal, tidal currents are weak with minimal mixing. Therefore, during the maximum diurnal inequality, average daily tidal elevation changes are moderated by these slow elevation-change periods. Conversely, during periods of diurnal equality, large-amplitudes dominate the entire signal and tidal currents are strong with maximal mixing. In order to capture this phenomena and its sub-tidal signal, the absolute value of the time gradient of the Tidal Elevation Index is low-pass filtered. The sign of the result is reversed for maximum values to indicate periods of maximum diurnal inequality and then normalized on a scale from 0 to 1 for the given time series, producing the Diurnal Inequality Index.

$$DII = -\mathcal{F}_{40}\left(\left|\frac{d}{dt}TEI\right|\right) \tag{2.4}$$

Values closer to 1 suggest the tidal elevation signal is in a period of maximum diurnal inequality, characterized by minimal average mixing, while values closer to 0 suggest the tidal elevation signal is in a period of near-diurnal-equality, characterized by strong mixing. Strong exchanges can happen during spring tides, but only during the lesser flood tide of a diurnal cycle. A subsequent greater ebb will cause mixing, and the exchanges are not sustained unless the diurnal inequality and the neap tide are coincident.

2.1.5 Upwelling Persistence Index

Persistent periods of upwelling or downwelling at the mouth of the Strait of Juan de Fuca influence a seasonal trend in dissolved oxygen concentration at Admiralty Inlet (Figure 2.3a). A new index is defined in order to capture the influence of sustained upwelling or downwelling conditions over time. Since the upwelling index has a much greater average magnitude during downwelling conditions than during upwelling conditions (due to more intense storms in the winter than summer), a conditional time integral is used to capture this persistence signal. First, the 7.25 day lagged Upwelling Index UI from PFEL is low-pass filtered. Second, the filtered result is set to +1 if positive (upwelling condition) and -1 if negative. Third, this binary result is time-integrated over the series. Finally, the integrated result is de-trended by subtracting a fit-line according to a 2nd-order polynomial fit for the time period between Jan 1, 2010 to Jan 1, 2013 (to capture seasonality). This de-trended result (removing interannual variability) is termed the Upwelling Persistence Index:

$$UPI = \text{detrend}\left(\int \text{sign}\left[\mathcal{F}_{40}\left(UI - 7.25\text{days}\right)\right] dt\right) \tag{2.5}$$

2.1.6 Fraser River Discharge Index

Discharge data D for the Fraser River measured at Hope, British Columbia, Canada, were obtained from the Water Survey of Canada website [15]. This station was the nearest main-channel station to the Strait of Juan de Fuca for the Fraser River that had complete discharge data for the appropriate time period. The data obtained was linearly interpolated to an hourly time scale, then low-pass filtered with $\mathcal{F}_{40}$, and finally normalized to a scale of 0 to 1.

$$FRDI = \frac{\mathcal{F}_{40}\left(D\right)}{\max[\mathcal{F}_{40}\left(D\right)]} \tag{2.6}$$

The resulting time series is the Fraser River Discharge Index.

2.1.7 Dissolved Oxygen Deficit

A Dissolved Oxygen Deficit index is defined to quantify temporary decreases in dissolved oxygen concentration from the background seasonal modulation of the dissolved oxygen.

First, the measured dissolved oxygen is low-pass filtered by $\mathcal{F}_{40}$ with the same 40-hour half-amplitude period as the other signals. Then, the result is filtered again with a 610-hour half-amplitude period filter $\mathcal{F}_{610}$ that is chosen as 1.6 times the period associated with the maximum observed intrusion event duration (the distinct time period in which the IEI is positive, from initiation to termination of an event)[2]. The Dissolved Oxygen Deficit (DOD) is determined by the difference in these signals:

$$DOD = \mathcal{F}_{610}\left(DO\right) - \mathcal{F}_{40}\left(DO\right) \tag{2.7}$$

The Dissolved Oxygen Deficit value will be positive during an intrusion event and will indicate a hypoxic intrusion if the observed seasonal dissolved oxygen signal $\mathcal{F}_{610}$ is low enough for a drop in dissolved oxygen concentration from seasonal levels at that time associated with an intrusion event to reach critically low concentrations .

2.2 Results At Admiralty Inlet Using Mooring Data

This section presents the two-part prediction developed to determine whether a hypoxic bottom water intrusion into Puget Sound is expected to occur in Admiralty Inlet at a given time. The prediction methods are based solely on indices that can be accurately determined without any in situ data collection in Admiralty Inlet. The first part of the method uses the Neap Tide Index NTI and Diurnal Inequality Index DII, the tidal conditions, to conditionally predict that a major bottom water intrusion event is likely. The second part of the method uses the Upwelling Persistence Index UPI and Fraser River Discharge Index $FRDI$, the availability conditions, to empirically predict availability of hypoxic water. When both the tidal and availability conditions are met, hypoxic intrusions are successfully identified. The Intrusion Event Index IEI is used as a metric for assessing the success of these predictions.

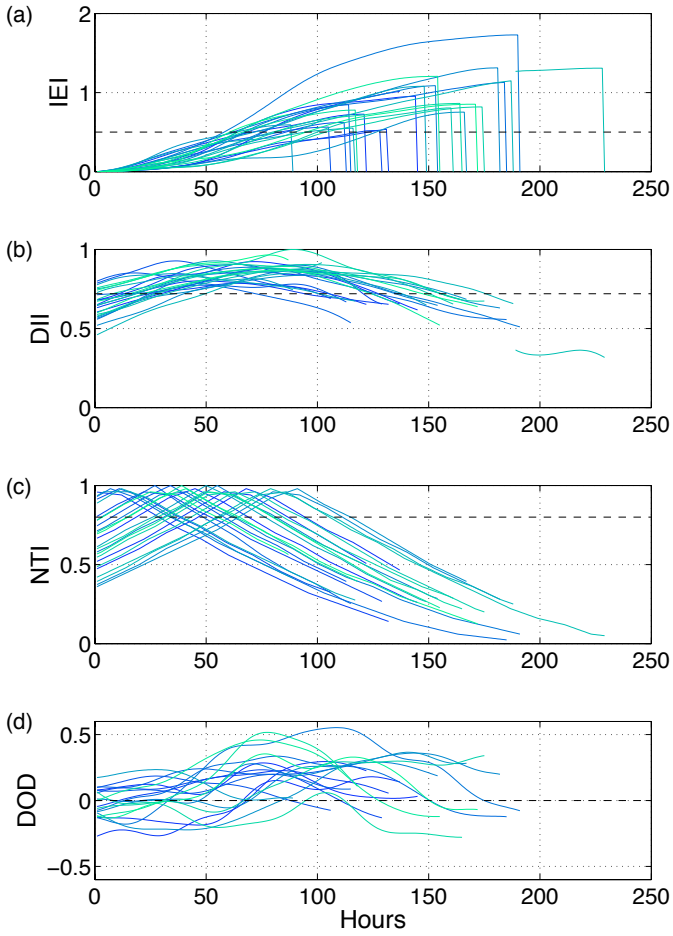

Figure 2.4: Composite in time of intrusion events that obtain an IEI value of at least 0.5, showing the signals of (a) Intrusion Event Index, (b) Diurnal Inequality Index, (c) Neap Tide Index, and (d) Dissolved Oxygen Deficit.

2.2.1 Intrusion Event Predictions

All observed intrusion events that reach an IEI of at least 0.5 are shown in Figure 2.4a as a function of time during the event (i.e., from intrusion initiation to intrusion termination). Figure 2.4 shows theDII (b) and the NTI (c) signals during these large intrusion events.

[2]The maximum observed intrusion event is about 191 hours (likely related to to the fortnightly neap-spring cycle). Accounting for the periodicity of intrusions, the maximum period of the intrusion cycle is about 382 hours. Since the ratio of the 40-hr half-amplitude period for residual currents to the 25-hr tidal period was 1.6, this ratio was used to determine a 610-hr half-amplitude period to remove fluctuations associated with the intrusion cycle.

Both the NTI and the DII must be elevated at the same time in order for an large intrusion event to develop and be sustained. Events evolve according to these indices, such that intrusions terminate as soon as tidal conditions are no longer favorable (i.e., when tides become stronger and mixing becomes dominant). Other variables, such as local winds, and discharge from the major rivers into Puget Sound, and lagged Upwelling Index do not have noticeable patterns during Intrusion Events. Thus, Intrusion Events are predicted solely based on choosing thresholds in NTI and DII:

$$\text{If} \quad NTI > 0.8 \quad \& \quad DII > 0.72, \quad \text{Intrusion} = 1 \tag{2.8}$$

Dashed black lines in Figure 2.4 mark these threshold values. As is shown in Table 2.1, using these two conditional thresholds achieves a high success rate for correctly identifying an observed intrusion event at least one time-step in its duration. In fact, these threshold conditions can correctly identify all events that reach an Intrusion Event Index of at least 0.5. Futhermore, using these threshold conditions only produce a false positive prediction 1.52 % of the times that the true Intrusion Event Index is observed to be zero.

2.2.2 Empirical Prediction of Seasonal Dissolved Oxygen Availability

The second portion of the method requires an empirical prediction of the background (seasonal) dissolved oxygen signal to asses the DO availability. Figure 2.4d supports the hypothesis that intrusion events cause temporary a deficit in dissolved oxygen levels compared with the background, seasonal signal of dissolved oxygen in Puget Sound. The deficit only produces hypoxia if the seasonal background levels are already low, and thus a prediction of background levels is necessary to predict hypoxic intrusions.

The Upwelling Persistence Index and the Fraser River Discharge Index are regressed against observed dissolved oxygen levels to determine an empirical equation for predicting seasonal dissolved oxygen trends in Admiralty Inlet. Figure 2.5 shows that the Upwelling Persistence Index follows the reverse seasonal signal of the seasonally filtered ($\mathcal{F}_{610}$) dissolved oxygen data, consistent with the mechanism of upwelling bringing low dissolved oxygen up from the deep ocean and into the Strait of Juan de Fuca. However, there is a lag in the correlation, indicating the Fraser River Discharge Index (also shown in Figure 2.5) must

Table 2.1: Intrusion Event prediction results

Intrusion Events with IEI	Number of Events	Percent Identified
≥ 1.0	9	100
≥ 0.9	10	100
≥ 0.8	15	100
≥ 0.5	25	100
≥ 0.4	28	92.9
≥ 0.3	33	84.8
≥ 0.2	37	78.4
≥ 0.1	49	69.4
> 0.0	88	43.2

be considered as it modulates the signal further. The mid-year peak in river discharge would decrease the surface salinity, increasing the density difference between the two-layers of the exchange flow in the Strait of Juan de Fuca, and therefore making the exchange flow stronger. This would increase the availability of hypoxic waters in Admiralty Inlet and Puget Sound in conjunction with upwelling persistence.

Performing a multi-linear regression, the Upwelling Persistence Index and the Fraser River Discharge Index fit the observed seasonal dissolved oxygen data as

$$DO_{AP} = 7.0343 - [0.0013 \times UPI] - [2.0535 \times FDI], \tag{2.9}$$

where the R-squared correlation value is 0.7745. The resultant empirical Dissolved Oxygen Availability Prediction DO_{AP} is shown in Figure 2.5c, where it is compared with the observed seasonal dissolved oxygen pattern at the bottom-mounted mooring site. While this DO Availability Prediction does not precisely predict the observed seasonally filtered DO data, it does perform adequately in reproducing a similar pattern, which is important in assessing the availability of hypoxic water for a given intrusion prediction. The availability

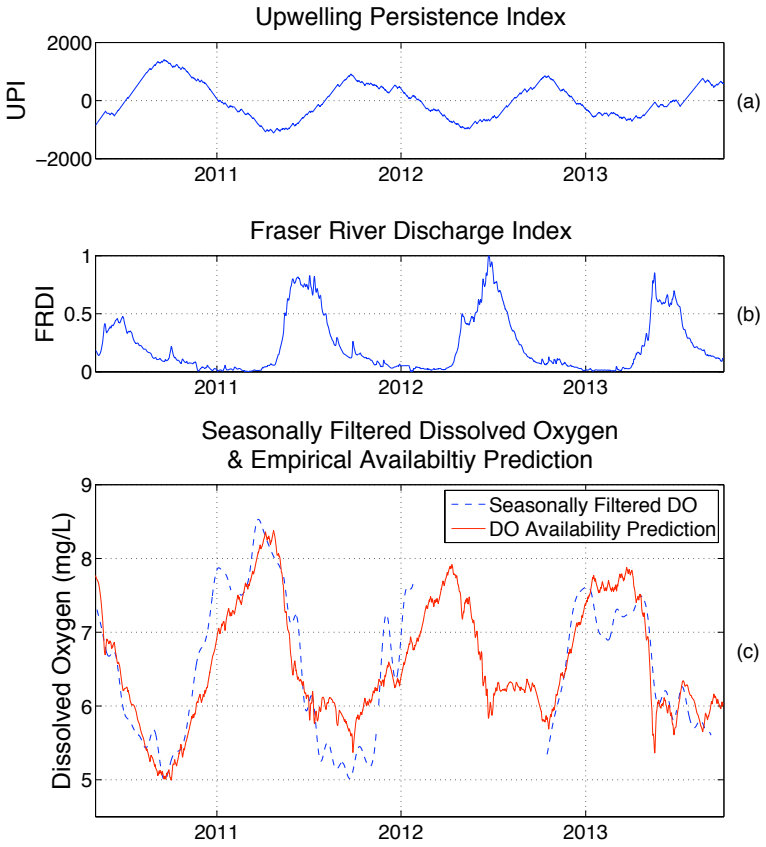

Figure 2.5: (a) Upwelling Persistence Index time series from May 2010 to October 2013. (b) Fraser River Discharge Index time series from May 2010 to October 2013; (c) Time Series of observed seasonally filtered $\mathcal{F}_{610}$ DO from May 2010 to October 2013 and the Dissolved Oxygen Availability Prediction constructed though regression.

prediction for DO was not designed to strictly follow the observed hourly DO time series because of the degree of local variance and because the prediction addresses the availability of hypoxic water in the Strait As a result, seasonal dissolved oxygen trends are modeled and the relationship between the DOD and IEI becomes important for predicting reductions in dissolved oxygen concentration from seasonal background levels.

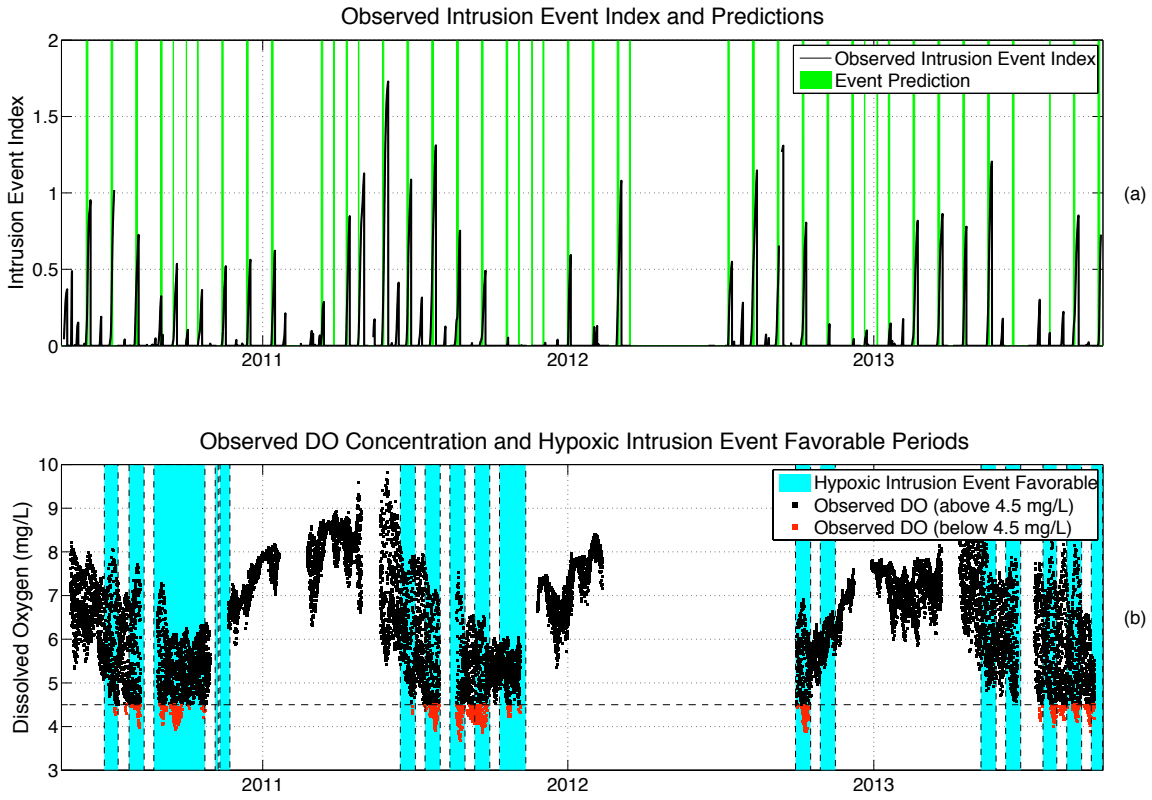

Figure 2.6: (a) The observed Intrusion Event Index time series from May 2010 to October 2013 with marks indicating when the tidal condition indices are both above the proposed threshold for prediction ($NTI > 0.8$, $DII > 0.72$). (b) Hourly dissolved oxygen observations (points less than or equal to 4.5 mg/L marked red) from May 2010 to October 2013, with background shaded blue for Hypoxic Intrusion Event Favorable Periods.

2.2.3 Hypoxic Intrusion Event Predictions

Finally, a combined set of thresholds is established, empirically, to predict hypoxic intrusion events. If an Intrusion Event Prediction from the first part of the method coincides with an empirical Dissolved Oxygen Availability Prediction less than or equal to 6.241 mg/L, a predicted intrusion event characterized by hypoxic water (less than 4.0 mg/L) is expected.

$$\begin{aligned} \text{If} \quad & NTI > 0.8 \quad \& \quad DII > 0.72 \\ \& \quad & DO_{AP} < 6.241, \quad \text{Hypoxic Intrusion Event} = 1 \end{aligned} \tag{2.10}$$

Table 2.2: Hypoxic Intrusion Event prediction results.

Observed DO (mg/L) Below	Percent of Points Identified
4.0	97.8
4.25	90.4
4.50	83.7
4.75	80.7
5.0	77.9
5.25	74.9
5.5	73.7
5.75	71.0
6.0	68.9
6.25	66.2
6.5	62.8

Conditions are regarded as favorable for dissolved oxygen to drop to hypoxic levels in any time period of 8 days[3] before or after an Intrusion Event Prediction that has a Dissolved Oxygen Availability Prediction below this threshold of 6.241. The combined result is shown in Figure 2.6 and Table 2.2, in which identified events are shaded in blue and percent identification is listed, respectively.[4] The top panel, Figure 2.6a, shows the observed Intrusion Event Index over the time series and marks when the tidal condition indices are both above the chosen threshold. The lower panel shows the observed dissolved oxygen and predicted hypoxic events. Figure 2.6 demonstrates the success of this two-part method for

[3]8 days is chosen because it is the maximum observed intrusion event duration and if an intrusion event prediction is made only at the beginning or end of an event, this window ensures that all intrusion event-related modulations of DO are accounted for over the entire event duration.

[4]Dissolved oxygen data that is within 8 days before or after periods of no raw DO data collection or undefined NTI and DII points are removed in order to remove bias due to gaps in data.

predicting intrusions of hypoxic water. Observed dissolved oxygen data less than or equal to 4.5 mg/L is marked red to highlight near-hypoxic dissolved oxygen measurements at the mooring site. As Table 2.2 demonstrates, the predicted hypoxic intrusion event favorable periods encompass 97.8 % of observed DO concentrations below 4.0 mg/L and 83.7 % of observed DO concentrations below 4.5 mg/L. These hypoxic intrusion favorable periods do include many DO observations above 4.5 mg/L, since predictions are based on a sub-tidal time-scale, making these false positives an inevitable part of the prediction. A hypoxic intrusion favorable period is only meant to indicate when Puget Sound is at "high risk" for a near-hypoxic intrusion event.

2.3 Discussion Of Prediction Outcomes

The two-part method for prediction of hypoxic intrusions to Puget Sound can be used to assess the likelihood that low dissolved oxygen water will be transported over the sill at Admiralty Inlet and into the main basin of Puget Sound in a given time period. The first part of the method independently predicts major bottom water intrusion events (which may carry nutrients or other water properties of interest). A key aspect of the two pronged approach is the use of readily available information from routine monitoring of tidal elevation, rather than detailed in situ measurements. Lunar phase data (for NTI) and tidal elevation data (for DII) have enough skill to identify intrusion events, so ADCP data may not significantly increase the predictability. However, ADCP point measurements at one location allows for observation and quantification of the duration and magnitude of events and provides a better indication of whether a given bottom water intrusion is entering significantly into the main basin of Puget Sound. The limitation of the present method is that it identifies events; it does not prescribe the severity.

The second part of the method specifically addresses hypoxia in Puget Sound and may help to better understand the natural forcing of dissolved oxygen levels in the Sound at depth. This part of the method uses publicly available data (Upwelling Index and Fraser River Discharge) and does not require in situ observations. However, a similar limitation to event identification remains; the present method does not prescribe the severity of the hypoxic intrusion or the overall impact to Puget Sound water quality. These details will

require comprehensive in situ monitoring and hydrodynamic modeling. Such efforts can be guided and optimized by the dominant variables identified herein. It is also important to note that the thresholds are empirically-derived and customized based on the observations from May 2010 to October 2013. Accuracies of the thresholds were based on maximizing the success of the prediction method during this time period in agreeing with observations at this particular mooring site. The sensitivity of indices to normalization and de-trending is discussed in Chapter 4.

2.4 Victoria Clipper: Surface Temperature and Salinity Observations

The Victoria Clipper makes frequent trips between Seattle, WA, USA, and Victoria, BC, Canada. During these trips, spatial and temporal data is collected for temperature and salinity of the surface waters. This section studies temperature and salinity signals in the surface waters of the Sound in Admiralty Inlet, particularly the modulation of these signals by exchange flow conditions at depth. Bottom water intrusions of dense water discussed in the previous sections should be accompanied by outflows of fresher, less dense water at the surface. This is part of the salt balance that drives these exchange flows [8]. Consequentially, observations of a temporary decrease in salinity and increase in temperature are expected in the surface water of the Puget Sound in the vicinity of Admiralty Inlet during residual exchange flow conditions. The following analysis provides evidence that some of the modulation of salinity and temperature in the surface waters is driven by intrusion events at depth and counteracts the modulation of the salinity and temperature in the bottom waters in Admiralty Inlet. In order to isolate the Victoria Clipper data associated with processes at Admiralty Inlet, data between 48.1 N to 48.2 N and 122.6 W to 122.8 W were considered (Figure 1.1). Data records that include both temperature and salinity from the Victoria Clipper are from June, 2012, to January, 2013. Fortunately this is a period marked by significant intrusion events and some hypoxic intrusions. Data is linearly interpolated to a 1-minute time scale in order to sufficiently sample the vessel's observations within the spatial domain during its quick transit through Admiralty Inlet.

Figure 2.7 shows the spatial temporal trends for both surface salinity and temperature within the spatial bounds in relation to residual currents at the bottom at Admiralty Inlet.

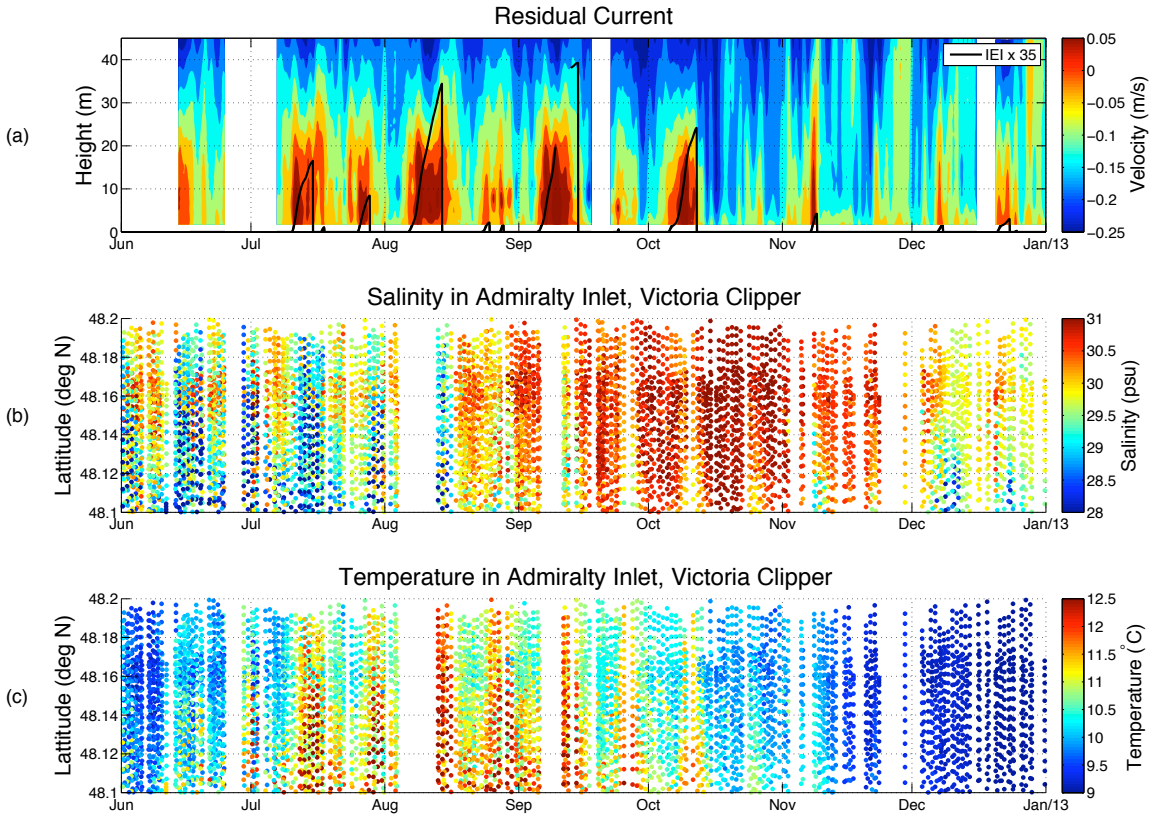

Figure 2.7: Time series presentation of salinity and temperature observations by latitude at Admiralty Inlet from the Victoria Clipper in relation to residual currents. (a) low-pass filtered, residual currents (m/s), height measured from the sea floor, overlaid with magnified Intrusion Event Index values to demonstrate intrusion activity, (b) time series of latitude positions from the Victoria Clipper, colored by salinity (psu) observed at each location and time, (c) time series of latitude positions from the Victoria Clipper, colored by temperature (°C) observed at each location and time.

There is a noticeable seasonal trend in the data from June to July (salinity increases from June to November and then begins to decrease; temperature increases through September and then begins to decrease). But there are also temporary spikes in temperature as well as drops in salinity on smaller time scales. These short-term modulations occur simultaneously in both variables and appear to coincide with bottom intrusion events (Figure 2.7c).

Focusing on a period from late-September to mid-November 2012 (Figure 2.8), it is possible to examine the sub-tidal trends in salinity and temperature at both the surface and

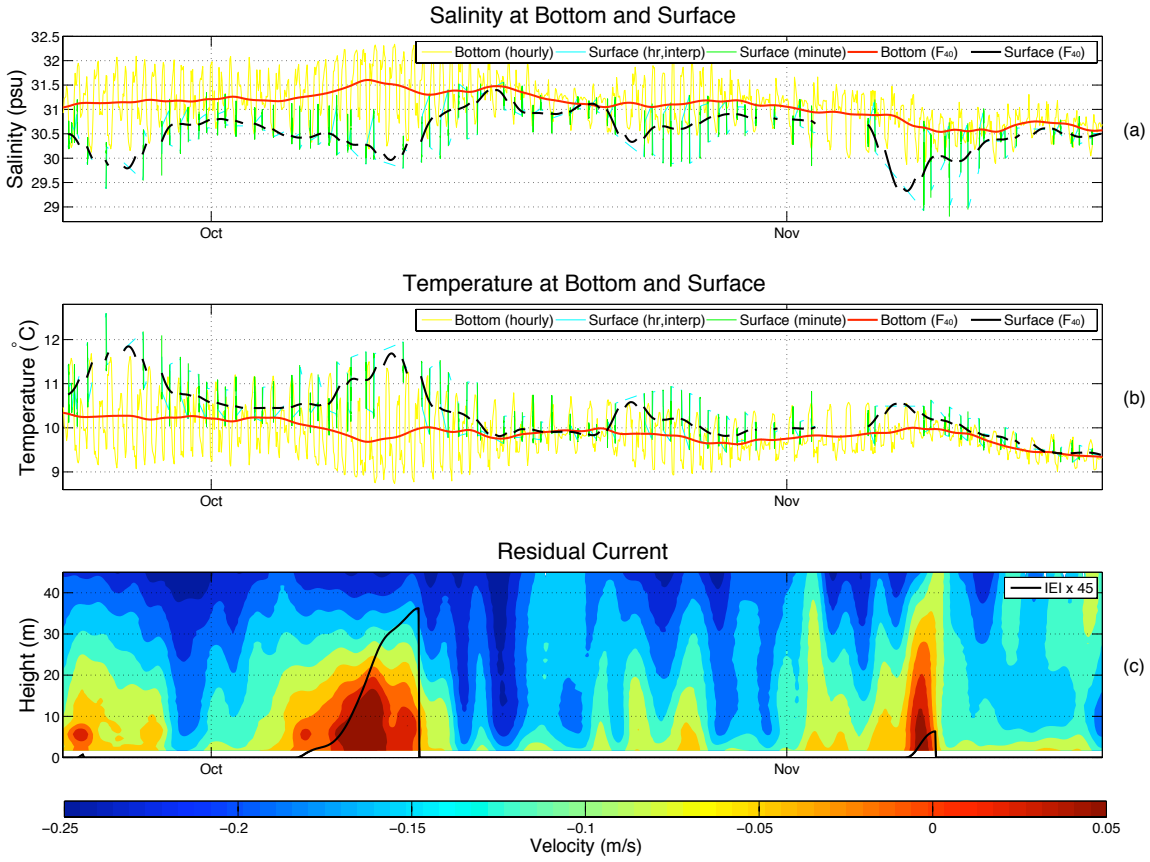

Figure 2.8: Time series presentation of salinity and temperature signals at the bottom and surface of Admiralty Inlet in relation to residual currents. (a) salinity signals at the bottom from the tripod (hourly and sub-tidal) and at the surface from the Victoria Clipper (minute-observations, hourly interpolation, and sub-tidal), (b) temperature signals at the bottom from the tripod (hourly and sub-tidal) and at the surface from the Victoria Clipper (minute-observations, hourly interpolation, and sub-tidal), (c) low-pass filtered, residual currents (m/s), height measured from the sea floor, overlaid with magnified Intrusion Event Index values to demonstrate intrusion activity.

the bottom of Admiralty Inlet to assess whether exchange flow conditions are observed. To determine the sub-tidal signals in the bottom waters, the measured salinity and temperature were low-pass filtered by $\mathcal{F}_{40}$ with the same 40-hour half-amplitude period as the residual currents. The surface temperature and salinity data within the spatial boundaries was interpolated from the minute-scale record to an hourly time scale for the time periods in which the Victoria Clipper was actively collecting data. Interpolated hourly data were low-

pass filtered by $\mathcal{F}_{40}$ to get the sub-tidal signal of salinity and temperature at the surface of Admiralty Inlet. Figure 2.8a demonstrates that periods with bottom water intrusions demonstrate increased exchange flow characteristics in the sub-tidal $\mathcal{F}_{40}$ salinity signals at the surface and bottom. Intrusion events coincide with a drop in surface salinity and a slight spike in bottom salinity from the longer-scale trends. A similar relationship is shown for the temperature signals in Figure 2.8b. Small drops in bottom temperature and large spikes in surface temperature from the longer-scale trends are observed during intrusion events. Sub-tidal $\mathcal{F}_{40}$ salinity and temperature signals have nearly equal magnitude during periods when the residual current velocity is nearly uniform from top-to-bottom. This demonstrates that during periods of high mixing (i.e. uniform vertical water properties), two-layer exchange flows are not able to develop [2].

Salinity vs. temperature diagrams for the surface are shown in Figure 2.9a and for the bottom in Figure 2.9b. For the surface, the open circle scatter points represent the minute-scale Victoria Clipper data within the Admiralty boundaries. Overlaid are the data points that occur during an active intrusion event colored by the maximum IEI reached during each discrete intrusion event. At the bottom, hourly data from the tripod mooring is interpolated to the minute-scale, selected for time-points in which the Victoria Clipper is within the Admiralty spatial boundaries, and plotted as open circles. The bottom data during active intrusion events are also overlaid with the same intrusion event color scale. In the surface and bottom diagrams, there is a negative correlation between temperature and salinity during specific intrusion events. During discrete intrusion events, water masses at the surface tend to have a lower average salinity than water masses at the bottom of Admiralty inlet, consistent with a two-layer exchange flow.

To compare the vertical difference in signals for individual parameters in Admiralty Inlet, surface data and bottom data are plotted against each other in Figure 2.10 for both minute-scale and sub-tidal ($\mathcal{F}_{40}$, low-pass filtered) data sets. For the minute-scale data (Figure 2.10a,b), there is nearly no statistically significant overall correlation between surface and bottom salinity or surface and bottom temperature. However, during many discrete, intrusion events (colored) a negative correlation appears between surface and bottom data. The first half of Table 2.3 catalogues the statistically significant correlation coefficients be-

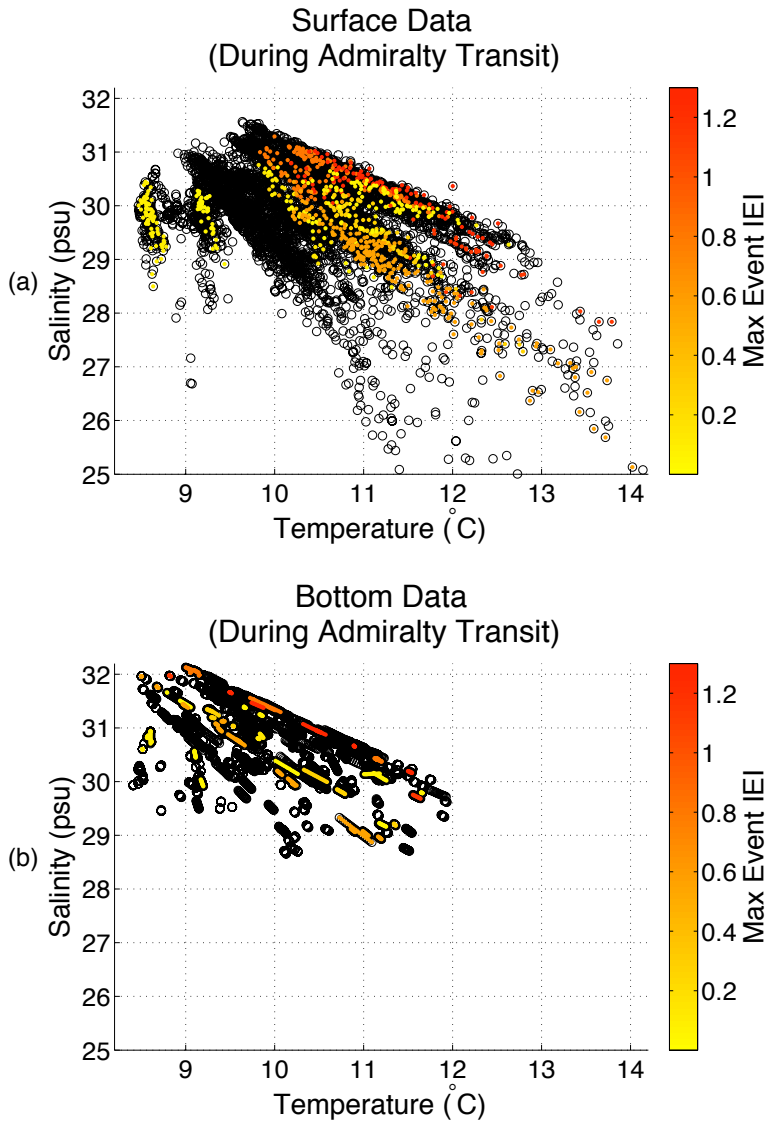

Figure 2.9: Salinity (PSU) versus temperature (C) at Admiralty Inlet from June 2012 to January 2013. Open circles represent the entire sample of observations. Data points corresponding to observations made during a distinct active intrusion event are colored according to the maximum IEI reached during that event. (a) observations at surface from Victoria Clipper, (b) observations at bottom from tripod.

tween these surface and bottom signals for salinity and temperature on the 1-mintue scale for each of the distinct intrusion events observed. Because this data is on a tidal scale and is sorted based on an index on a sub-tidal scale, these relationships are not strong. Re-

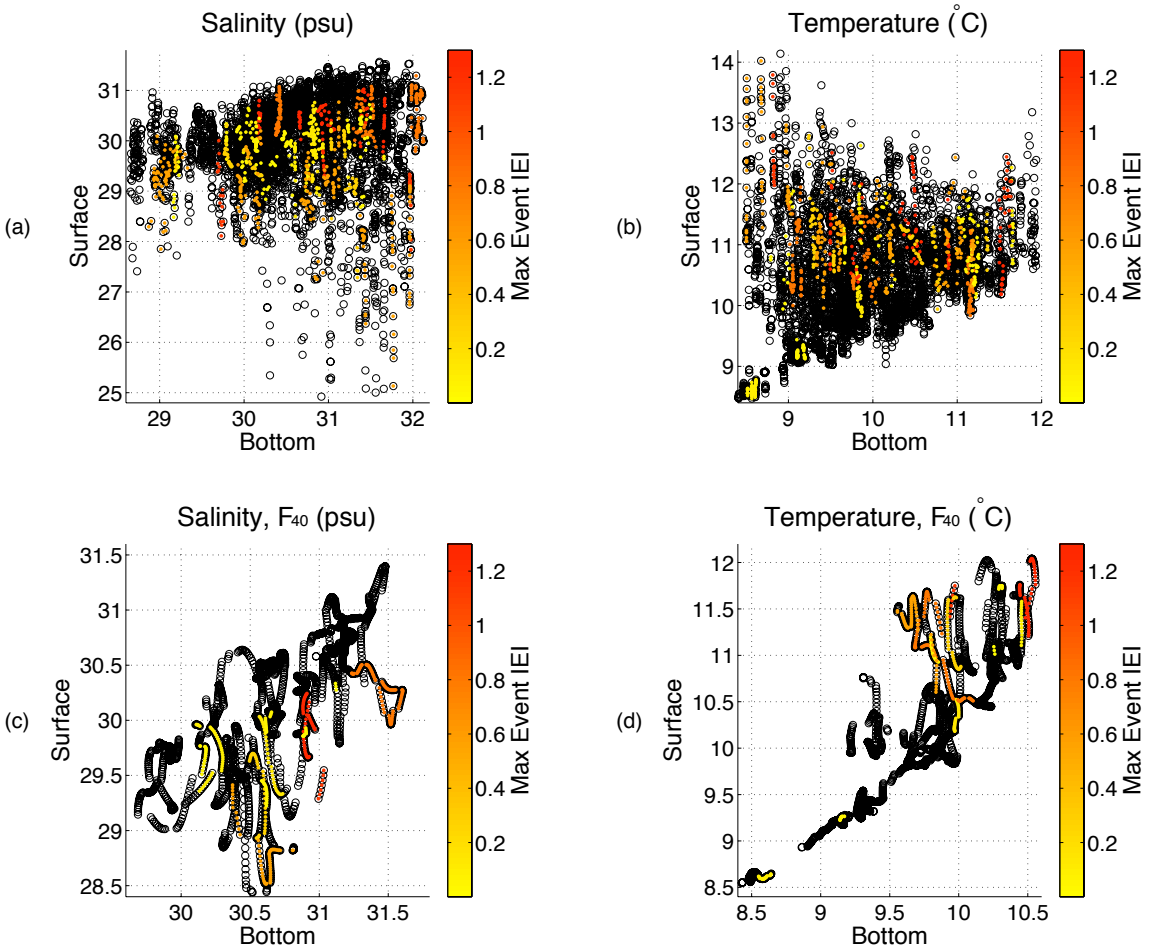

Figure 2.10: Diagrams showing the relationship between coincident observations at the surface (Victoria Clipper) and bottom (tripod) at Admiralty Inlet from June 2012 to January 2013. Open circles represent the entire sample of observations. Data points corresponding to observations made during a distinct active intrusion event are colored according to the maximum IEI reached during that event. (a) salinity observations on 1-minute scale, (b) temperature observations on 1-minute scale, (c) sub-tidal filtered salinity data, (d) sub-tidal filtered temperature data,

creating the same surface-vs-bottom plots using the sub-tidal, low-pass filtered salinity and temperature sets (Figure 2.10c,d), avoids this mismatch in signal scales. For the sub-tidal signal comparison, there is an overall positive relation between surface and bottom data for salinity and temperature, presumably due to estuarial-scale seasonal trends. Conversely, during many individual intrusion events, there is a relatively strong negative correlation be-

Table 2.3: Surface-to-Bottom Event Correlations

	1-Minute Scale			Sub-Tidal ($\mathcal{F}_{40}$)		
		Correlation Coefficient[a]			Correlation Coefficient[b]	
Event Number	Sample Points	Salinity	Temperature	Sample[c] Points	Salinity	Temperature
1	240	-0.47	-0.53	60 , 62	-0.73	-0.78
2	46	——	——	15	-0.78	-0.92
3	99	-0.20	-0.31	37	-0.62	-0.59
4	33	——	-0.56	7	0.99	0.99
5	68	——	-0.35	15	0.72	——
6	14	——	-0.69	11	0.81	——
7	96	——	-0.31	49	——	0.31
8	0	——	——	3	-0.99	-1.00
9	168	——	-0.37	94	-0.73	-0.80
10	34	——	-0.52	29	-0.97	0.76
11	46	——	——	18	——	0.82
12	79	——	0.33	36	——	0.63
13	0	——	——	0	——	——

[a]Statistically significant based on 95% confidence

[b]Statistically significant based on 95% confidence

[c]Intrusion events with more coincident sample points would be more likely to exhibit a negative correlation between the surface and bottom signals because the intrusion event has more time to develop and influence the parameter signals (the sub-tidal filter has a 40-hour half amplitude period)

tween the surface and bottom sub-tidal signals for salinity and/or temperature, especially for events that reach a high IEI. This is demonstrated in the second half of Table 2.3 for the sub-tidal scale for intrusion events with larger numbers of coincident surface and bottom sample points. Events with coincident data points for over 50 hours have fairly strong correlation for both temperature and salinity. The events with statistically significant positive correlations for salinity have less than 20 sample hours (keeping in mind that the sub-tidal filter has a 40-hour half amplitude period). Events that are identified to have a positive correlation between the surface and bottom signals do not appear to follow the slope of the overall data from the time period (Figure 2.10c,d). A negative correlation between surface

and bottom salinity during intrusion events relative to the larger-scale seasonal trends supports that during period of intrusions of dense bottom water, Admiralty Inlet shows the characteristics of a two-layer exchange flow, with fresher water leaving Puget Sound at the surface and more saline water entering the Sound at depth.

As was done to determine the Dissolved Oxygen Deficit in Section 2.1.7, a salinity surplus for the bottom signal and a salinity deficit for the surface signal are calculated by taking the difference between the sub-tidal filter $\mathcal{F}_{40}$ and the seasonal filter $\mathcal{F}_{610}$ of the hourly signals.

$$SalinitySurplus_{Bttm} = -(F_{610}\left(Sal_{Bttm}\right) - \mathcal{F}_{40}\left(Sal_{Bttm}\right)) \tag{2.11}$$

$$SalinityDeficit_{Surf} = \mathcal{F}_{610}\left(Sal_{Surf}\right) - \mathcal{F}_{40}\left(Sal_{Surf}\right) \tag{2.12}$$

The development of these parameters during an intrusion event is illustrated in Figure 2.11. Intrusion events clearly influence a surplus in bottom salinity and a deficit in surface salinity compared with the background, seasonal signals of salinity. A similar procedure is used to determine a temperature deficit for the bottom signal and a temperature surplus for the surface signal.

$$TempDeficit_{Bttm} = \mathcal{F}_{610}\left(Temp_{Bttm}\right) - \mathcal{F}_{40}\left(Temp_{Bttm}\right) \tag{2.13}$$

$$TempSurplus_{Surf} = -(F_{610}\left(Temp_{Surf}\right) - \mathcal{F}_{40}\left(Temp_{Surf}\right)) \tag{2.14}$$

Figure 2.12 follows the development of these temperature modulations over the course of an intrusion event. As for salinity, temperature modulation from the background seasonal signals are tied to the influence of intrusion events. During an intrusion event, a deficit in bottom temperature and a surplus in surface temperature are observed. These observations illustrate that bottom water intrusions are part of a estuarial two-layer exchange flow at Admiralty Inlet characterized by the inflow of relatively dense, high salinity, cool water at the bottom, and the outflow of relatively fresh, warm water at the surface. During the late-summer and early-autumn, these exchange flows are characterized by hypoxic water tied to seasonally high salinity, oceanic water.

Based on the similarity between the Surface Temperature Surplus, the Surface Salinity Deficit, and the bottom Dissolved Oxygen Deficit, a multilinear regression to the sub-tidal

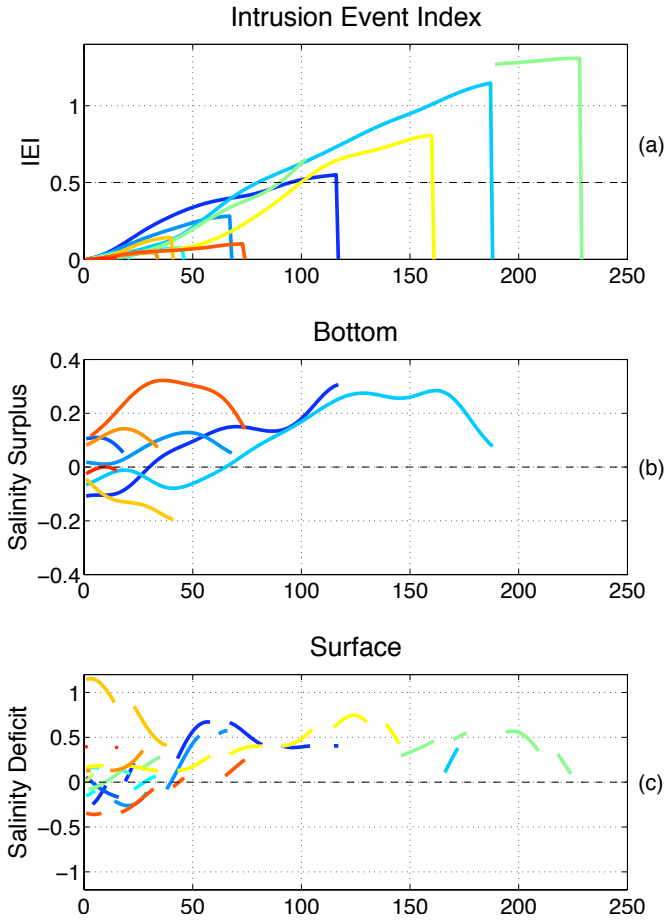

Figure 2.11: Composite in time of intrusion events from June 2012 to January 2013, showing the signals of (a) Intrusion Event Index, (b) Salinity surplus (psu) at the bottom, (c) Salinity deficit (psu) at the surface.

$\mathcal{F}_{40}$ bottom dissolved oxygen signal was conducted using the data of the sub-tidal $\mathcal{F}_{40}$ surface salinity and the sub-tidal $\mathcal{F}_{40}$ surface temperature. This resulted in a significantly strong sub-tidal dissolved oxygen prediction with an R-squared value of 0.92, based on surface measurements in Admiralty Reach.

$$_{ST}DO_P = 32.6253 - [0.6094 \times \mathcal{F}_{40}\,(Sal_{Surf})] - [0.8084 \times \mathcal{F}_{40}\,(Temp_{Surf})], \qquad (2.15)$$

The prediction compared to the sub-tidal dissolved oxygen data is demonstrated in Figure 2.13. Unfortunately, matching data for dissolved oxygen at the bottom and surface

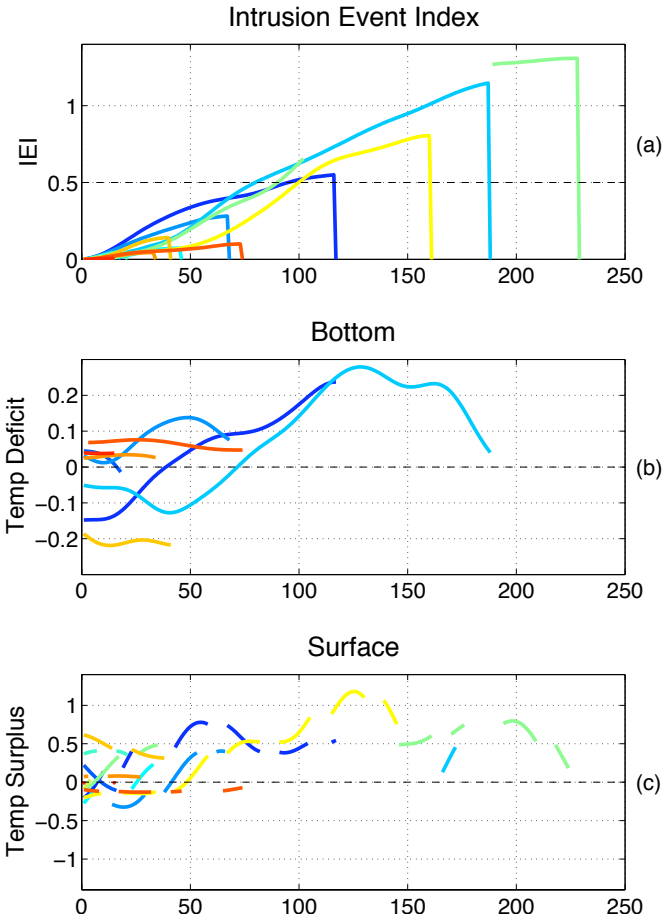

Figure 2.12: Composite in time of intrusion events from June 2012 to January 2013, showing the signals of (a) Intrusion Event Index, (b) Temperature deficit (°C) at the bottom, (c) Temperature surplus (°C) at the surface.

temperature and salinity are linked to mostly September through December 2012. However, the strength of this regression is much higher than the regression in Section 2.2.2 and empirically predicts a signal that is a temporal scale of variability higher than the seasonal prediction. This regression is very promising for using as a method to predict the sub-tidal dissolved oxygen signal and for identifying when the sub-tidal signal is low enough to support hypoxic bottom water intrusions. Surface temperature and salinity data to make these predictions can be collected using ships and the ferries that transit Admiralty Inlet many times each day (if proper instrumentation were to be installed). The proposed method,

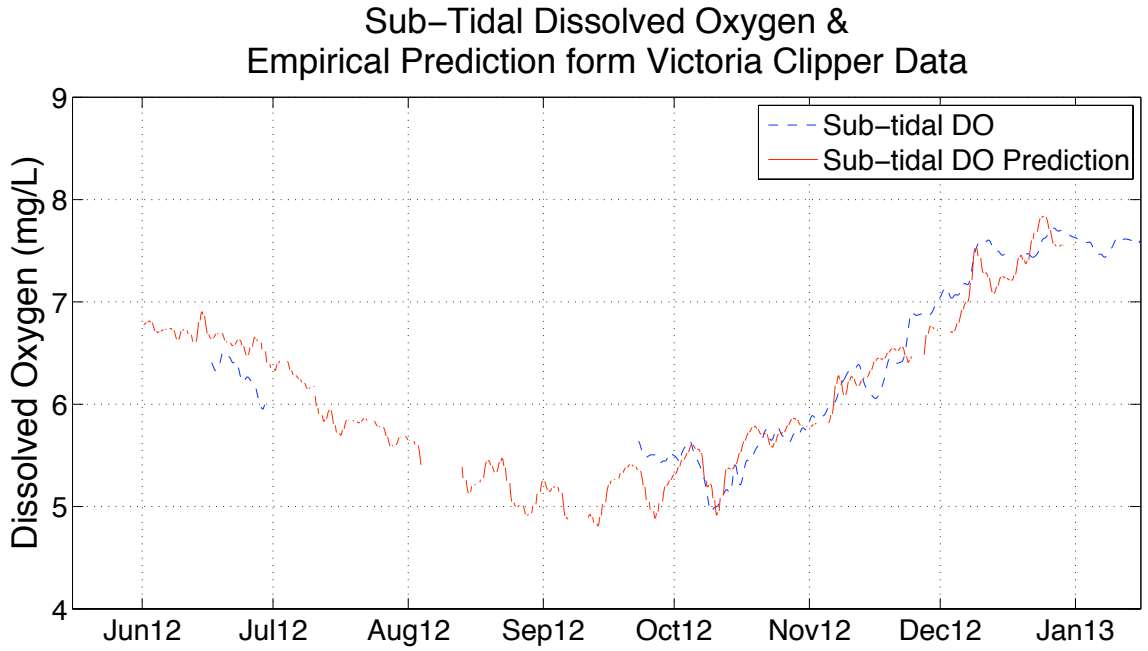

Figure 2.13: Time Series of observed sub-tidal filtered DO from June 2012 to January 2013 and the Sub-Tidal Dissolved Oxygen Prediction constructed though regression.

which uses the vertical water mass balances associated with two-layer exchange flows, could supplement and refine the method presented in Sections 2.1 to 2.3 to enhance the predictions of hypoxic intrusions into Puget Sound from the ocean. The set of code presented in Appendix C (Sub-Tidal Dissolved Oxygen Prediction Method) can be used to run this prediction with inputs from Victoria Clipper data sets.

2.5 Float Plane: CTD Cast Observations

The Washington State Department of Ecology conducts CTDO (Conductivity, Temperature, Depth, Oxygen) casts at a number of stations in Puget Sound and the Strait of Juan de Fuca about once a month as part of a marine water quality monitoring effort. The timing of these casts is fairly random in terms of neap and spring tidal cycles, ebb and flood cycles, and diurnal inequality. Despite the variety of conditions at which these casts are conducted, examining the vertical structure of dissolved oxygen concentration, salinity, and tempera-

ture, in the water column based on tidal conditions, can help demonstrate the importance of the spring-neap cycle and diurnal inequality in the development of two-layer exchange flows in Admiralty Inlet. Two stations, ADM002 and ADM001, are considered here to examine the vertical structure during various combinations of tidal cycles and intrusion events from August 2009 to December 2012. Station ADM002, is located at 48.187 N, 122.843 W, in the Strait of Juan de Fuca, just seaward of Admiralty Inlet. Station ADM001 is located at 48.030 N, 122.843 W, just landward of Admiralty Inlet in Puget Sound. For each station (Figure 1.1), data for dissolved oxygen, salinity, and temperature, are given a time stamp of the nearest hour of each associated cast time. This allows for a comparison with tidal and intrusion conditions measured at the Admiralty Inlet mooring.

The Neap Tide Index (NTI) and Intrusion Event Index (IEI) from Section 2.1 were used to determine whether a cast was conducted during a neap or spring tidal cycle and whether the cast was taken during an intrusion event (on the sub-tidal scale). Since the Diurnal Inequality Index (DII) measures degree of diurnal inequality on the sub-tidal scale, a new index was developed to differentiate if a cast was conducted during a 12.5-hour period of a small ebb and small flood (during the small-amplitude portion of a strong diurnal inequality) or during a period with a large ebb and large flood (during the large-amplitude portion of a strong diurnal inequality or either portion of a near-diurnal equality). To accomplish this, the absolute value of the time gradient of the Tidal Elevation Index (TEI) was low-pass filtered with a half-amplitude period of 12.5 hours ($\mathcal{F}_{12.5}$). The result of the time series was normalized on a scale from 0 to 1, producing the Tidal Gradient Index.

$$TGI = \mathcal{F}_{12.5}\left(\left|\frac{d}{dt}TEI\right|\right) \tag{2.16}$$

Values closer to 1 suggest the half-day amplitude is large, characterized by strong mixing, while values closer to 0 suggest the half-day amplitude is small, characterized by minimal mixing.

In Figure 2.14, dissolved oxygen concentrations from discrete casts at both stations are categorized based on whether the cast was taken during a spring or neap period and whether there was an active, sub-tidal intrusion event occurring at the time of the individual cast. The casts are colored based on the Tidal Gradient Index computed for the hour at which the

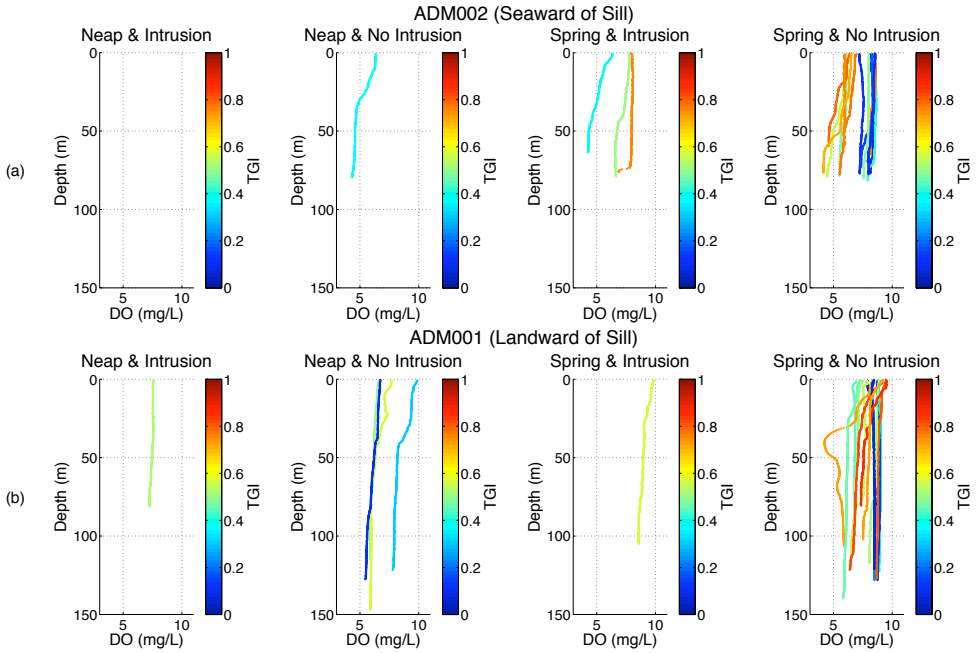

Figure 2.14: Vertical dissolved oxygen profiles from casts made between August 2009 and October 2013 during 4 different combinations of the spring-neap conditions and intrusion status, colored according to tidal gradient index (TGI) at the time of each cast, at 2 locations near Admiralty Inlet, (a) seaward of Admiralty Head at station ADM002 and (b) landward of Admiralty Head at station ADM001.

cast was conducted. It is obvious from this conditional selection that the casts are under-sampled for this purpose (i.e., there are few casts that were conducted during neap tides and few during observed intrusion events). The tidal and intrusion conditions in which the majority of casts were taken, spring tides with no intrusion, are the conditions in which little vertical change in water properties are expected due to strong mixing over Admiralty Sill [2]. The lack of vertical gradient in dissolved oxygen concentrations is evident in the plots for spring tides with no observed intrusion. A demonstration of a vertically mixed water column during these conditions is also evident for salinity in Figure 2.15 and temperature in Figure 2.16, particularly at ADM002, seaward of the sill. At ADM001, we find in some instances that there is vertical variation at the top, but these observations are likely due to transient freshwater plumes at the surface originating from Whidbey Basin river discharge leaving the Sound. This structure is not seen on the seaward side of the sill because vertical

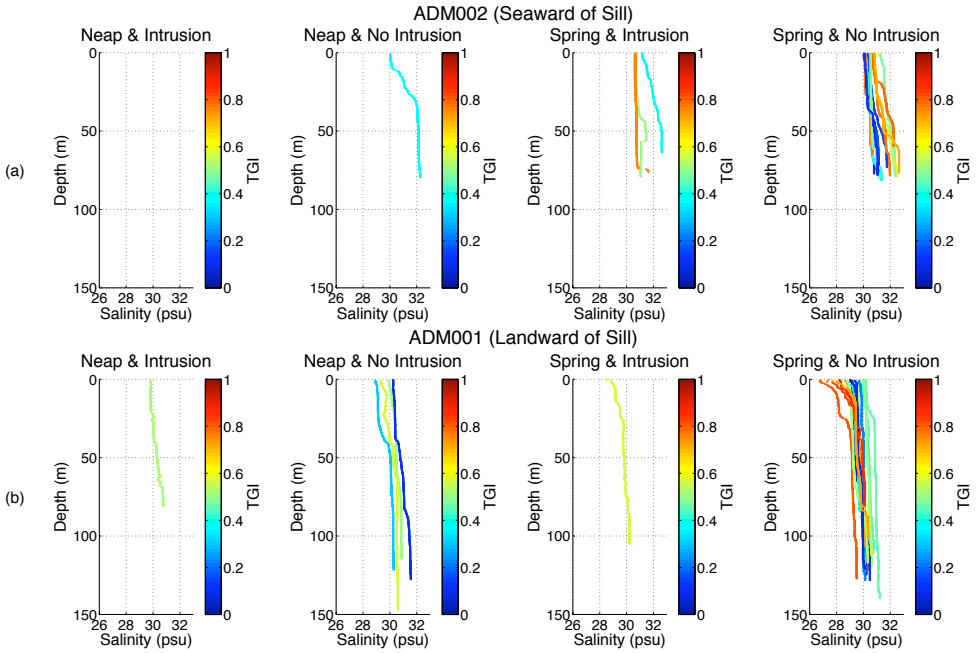

Figure 2.15: Vertical salinity profiles from casts made between August 2009 and October 2013 during 4 different combinations of the spring-neap conditions and intrusion status, colored according to tidal gradient index (TGI) at the time of each cast, at 2 locations near Admiralty Inlet, (a) seaward of Admiralty Head at station ADM002 and (b) landward of Admiralty Head at station ADM001.

variation from these freshwater plumes would be mixed out as the water passes over the sill, during spring tides.

Because the spring-neap tidal condition was based on the NTI ≥ 0.5 (neap) or ≤ 0.5 (spring), some casts in the spring tide condition could possibly exhibit exchange flow structure if taken during the neap-to-spring transition period or during an active intrusion event. However, such an instance would require that the cast was taken during a time with a low TGI (small ebb or small flood), where mixing is minimal. The importance of the small-amplitude portion of the tidal cycle for two-layer exchange flows is illustrated quite well in the cast plots for all three parameters at ADM002, during the "Spring and Intrusion" condition Figure 2.14a-2.16a. The blue line (low TGI) has significant vertical variability and reaches hypoxic levels in dissolved oxygen concentration with high salinity at great depth, while the green line (higher TGI) is more vertically uniform and the orange line (high TGI)

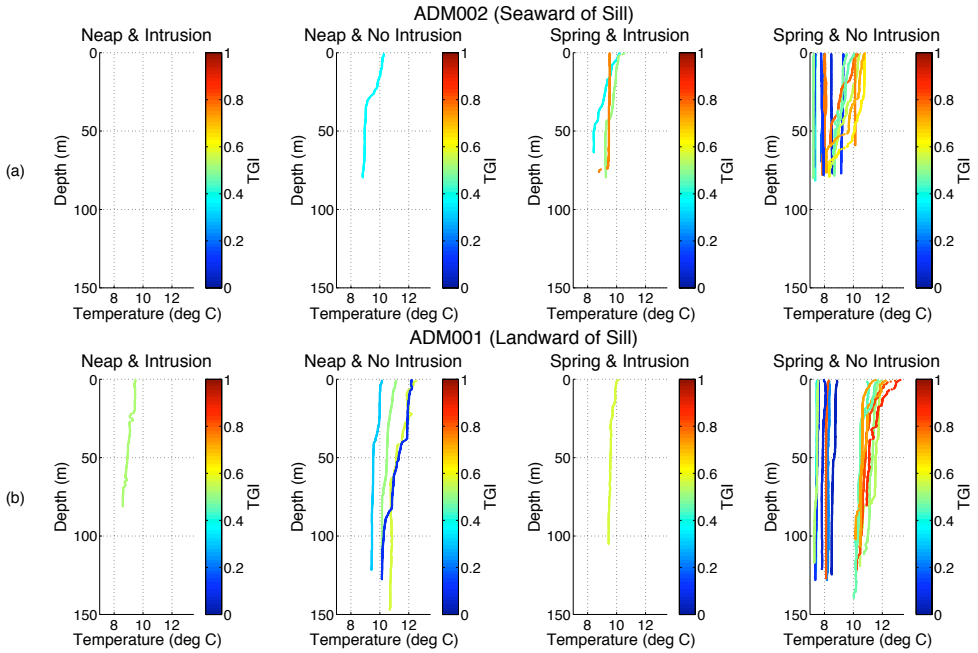

Figure 2.16: Vertical temperature profiles from casts made between August 2009 and October 2013 during 4 different combinations of the spring-neap conditions and intrusion status, colored according to tidal gradient index (TGI) at the time of each cast, at 2 locations near Admiralty Inlet, (a) seaward of Admiralty Head at station ADM002 and (b) landward of Admiralty Head at station ADM001.

appears to be uniform with no change over depth. The small-amplitude portion of the tidal cycle is important for the development of exchange flows on a tidal time-scale [2].

Unfortunately, only six casts were conducted between both stations during the neap tidal cycle. The only one taken during an active intrusion was at ADM001 during a time with a moderate TGI when the two-layer exchange flow would be undeveloped due to mixing by strong currents during the large-amplitude portion of the diurnal inequality [2]. The conditions most favorable for a well-developed two-layer exchange flow is an active intrusion event during a neap tide with a very low TGI. There were no casts taken during these conditions that would have allowed for illustrating this relationship.

The example of a vertical structure that best resembles a two-layer exchange flow is the cast taken during a neap tide with no active sub-tidally identified intrusions and a low TGI at ADM002, seaward of the sill. The vertical gradient in parameters is most pronounced for

salinity, in Figure 2.15 a. An increase in salinity by 2 psu over about 30 meters occurred until a large mass of dense, salty water was reached. The signal is also observed for dissolved oxygen, which drops to hypoxic levels in the dense water mass, and for temperature, which drops to less than 9 °C. While this observation occurs when there is no active intrusion event identified from the residual currents, it does not preclude that a short intrusion developed during the tidal cycle that was not accounted after the sub-tidal filtering.

No cast observation at ADM001 during neap tides and no active intrusion events was as striking in two-layer exchange flow patterns as the cast at ADM002. This may be a bias of under-sampling so that no temporary intrusion events were captured. This would still agree with the sub-tidal intrusion event observations. It could also point to the fact that exchange flows are harder to identify by observing the vertical variation in water properties on the landward side of the sill. A dense, bottom intrusion that clears the sill would turn into a gravity current and would likely take the form of a relatively thin layer near the bottom. Since casts do not consistently touch the bottom on the landward side of Admiralty Inlet, the intrusion signal could have been missed.

The data from these float plane casts are too few to provide a complete picture of the development of exchange flows during different tidal conditions. However, the limited number of casts agree with the expected dynamics proposed by Geyer and Canon [2]. The ability for a two-layer exchange flow to develop at Admiralty Inlet is governed by the degree of tidally-forced mixing over the sill (TGI).

2.6 Local Conclusions (Admiralty Inlet)

Low dissolved oxygen water measured at the Northern extreme of Puget Sound , Admiralty Inlet, is associated with deep ocean water masses, as determined by temperature and salinity. This ocean water can intrude across the sill into Puget Sound near the seabed under two-layer exchange flow conditions of minimal mixing, nominally coincident maximum diurnal inequality and neap tides during equinoxes. Tidal elevation data can be used as an indicator for such exchange flow, as shown by the use of combined Neap Tide Index and Diurnal Inequality Index thresholds. Residual current analysis from ADCP data validates the threshold basis for identifying intrusions, but alone is not sufficient to identify hypoxic

events. Hypoxic events also are controlled by coastal upwelling and river discharge, which set the availability of dense, low dissolved oxygen water in the Strait of Juan de Fuca. A regression of dissolved oxygen background levels to an Upwelling Persistence Index and Fraser River Discharge Index results in an empirical Dissolved Oxygen Availability Prediction that correlates well with observations. Ultimately, an Intrusion Event prediction combines the background oxygen levels to successfully identify 98% of events with $DO < 4.0$ mg/L and 84% of events with $DO < 4.5$ mg/L.

Observations of surface signals in salinity and temperature at Admiralty Inlet from the Victoria Clipper nicely compliment the continuous observations at the bottom at Admiralty Sill. The established temporal tie between episodicsalinity increases at the bottom and temporarily fresher water at the surface are consistent with the dynamics of a two-layer exchange flow over a sill as described by Helfrich [8]. There is value in this observation as it was demonstrated that by interpolating and sub-tidally filtering the salinity and temperature observations made by the Victoria Clipper and processing them with the empirically derived regression equation, a strong prediction of the sub-tidal dissolved oxygen signal was made. While data is limited to test this for a short period of months, it is a promising prediction method to supplement and independently validate the main hypoxic intrusion prediction method described in this document.

Despite a limited number of the CTDO cast data sets from the Ecology float plane program, the vertical profiles did agree with the expected observations based on tidal cycle, tidal amplitude, and residual intrusion activity. If intrusion conditions were to be considered when developing flight plans, individual casts could better target and explore intrusion events. Some observations at the surface and in the vertical profiles are consistent with two-layer exchange flows during observed intrusion events, but these data are limited in number. Chapter 3 will provide a comparison of the signals at Admiralty Inlet with dissolved oxygen signals at other locations in Puget Sound to explore the lags between correlation between Admiralty Reach and more landward stations. The approach will help develop a better understanding of the transport of hypoxic water from the ocean once it reaches the main basin and travels through Puget Sound.

Chapter 3

REGIONAL CONTEXT AND EXPLORATION

It is a complicated task to determine where low dissolved oxygen water flows after it traverses the Admiralty Inlet sill. Literature proposes that, after inflow, the dense water is no longer governed by strong tidal currents and acts as a gravity current that carries this water through the main basin until it is eventually mixed by other processes [1][2][5][9]. This is investigated by looking for a low dissolved oxygen signature at other locations in Puget Sound after low dissolved oxygen inflows occur at Admiralty Inlet. The spatial and temporal dynamics of the main-basin-transport will be important to understand if the predictive methods developed here are to be useful in decisions and policy making for water quality management.

This analysis examines the question of where hypoxic water is transported after passing over Admiralty Sill and explores the average speed of propagation. There are two main schemes that a signal of low dissolved oxygen could follow. In the first scheme, when hypoxic intrusions occur at Admiralty Inlet, the intrusion signature is apparent in a consequent drop in dissolved oxygen concentration at other points in the Sound. In this case, hypoxic intrusions at the mouth have a direct effect on the dissolved oxygen signal in the basin of Puget Sound. The second scheme is a diffuse signal in which hypoxic intrusions have a cumulative effect of lowering dissolved oxygen levels in the Sound over time. Lavelle, et al., and Holbrook, et al., provide useful insight into expected gravity current propagation speeds for intrusions and the influences of certain bathymetry features, such as interior sills [9][10]. The work in this chapter will characterize the nature of the dissolved oxygen modulations in the Main Basin of Puget Sound (main Sound) and in Hood Canal.

This chapter specifically examines the relationships between the signals of dissolved oxygen concentration, salinity, and temperature, at Admiralty Inlet and the signals in the basin of Puget Sound by independently focusing on the Main Basin and Hood Canal. Section

Table 3.1: Main Sound, CTDO Sensor Depths.

Mooring Station	Mukilteo	Manchester	Squaxin
Water Depth	—	11.8 m	8.9 m
Sensor Depth	12.6 m	10.4 m	7.8 m

3.1 examines the modulation of dissolved oxygen at three different moorings in the main Sound. Section 3.2 analyzes the dissolved oxygen signal in Hood Canal.

3.1 Main Puget Sound Mooring Observations

Of the three different moorings used in this section, two are located in the main basin (Manchester Inlet and Mukilteo) and one in the South Sound (Squaxin), as shown in Figure 1.1. Data is analyzed from CTDO's near the sea bed at each location. The CTDO at Mukilteo (47.954 N, 122.288 W) has data records available from September 2009 to April 2013 and is situated near the bottom at 12.6 m depth relative to MLLW[1]. At Manchester Inlet (47.574 N, 122.545 W), the CTDO is situated 1.4 m above the bottom at a depth of 10.4 m relative to MLLW. It has data records available from July 2008 to December 2012. The CTDO at Squaxin (47.182 N, 122.937 W), situated 1.1 m above the bottom at 7.8 m depth relative to MLLW, has data records available from September 2009 to April 2013. The mooring depth information is catalogued in Table 3.1.

By examining the relationship between different water properties at the different sites, conclusions can be drawn concerning the source of hypoxic water (Figure 3.1). If hypoxic water at the sites originated exclusively from Admiralty Inlet at depth (and previously the Strait of Juan de Fuca and the Pacific Ocean), it would be tied to a high-salinty water mass. There is not sufficient evidence to tie hypoxic water at these locations exclusively to Admiralty Inlet. At Mukilteo at 12.6 m (Figure 3.1a), which is the closest to Admiralty Inlet, a relation between low dissolved oxygen and high salinity with a narrow temperature

[1]This CTDO at Mukilteo is not at the full water depth. It is situated on a shallow plateau so we miss bottom information here

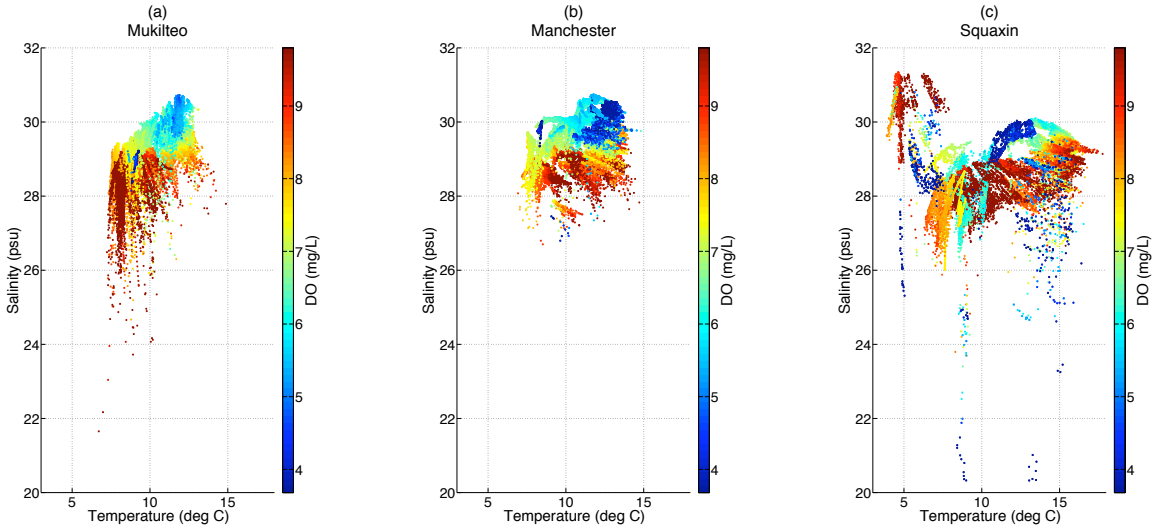

Figure 3.1: Salinity (psu) versus temperature (C) at 3 moorings in the main basin of Puget Sound during the full periods of active data collection. Data colored according to corresponding dissolved oxygen concentration (mg/L). Observations from (a) Mukilteo (23066 data points), (b) Manchester (27052 data points), and (c) Squaxin (20507 data points).

range exists (despite a few outliers), but the water mass is less salty than that of hypoxic water at Admiralty Inlet. This suggests that the primary source of hypoxic water during the observation period at this sensor site is from Admiralty Inlet, but that the signal is diffuse. Figure 3.1b suggests that the signal is even more diffuse at Manchester Inlet as the high-salinity hypoxic water mass has a much wider temperature range. Also, there are some instances of hypoxic water being tied to lower-salinity water masses, suggesting that hypoxic intrusions at Admiralty Inlet are not the only main drivers of dissolved oxygen modulation at this location. At Squaxin (Figure 3.1c), hypoxic water is tied to many different kinds of water masses. Part of the signal here may be a very diffuse result of hypoxic intrusions at Admiralty Inlet, but there are clearly many other sources of hypoxic water at this site. The lack of a traceable signal at this location is quite expected, as water in the main basin must traverse another sill at Tacoma Narrows in order to make its way to this location [9]. The mixing that occurs at this sill would prevent any direct signal from propagating over the sill, but there could still be a very diffuse cumulative effect on dissolved oxygen levels.

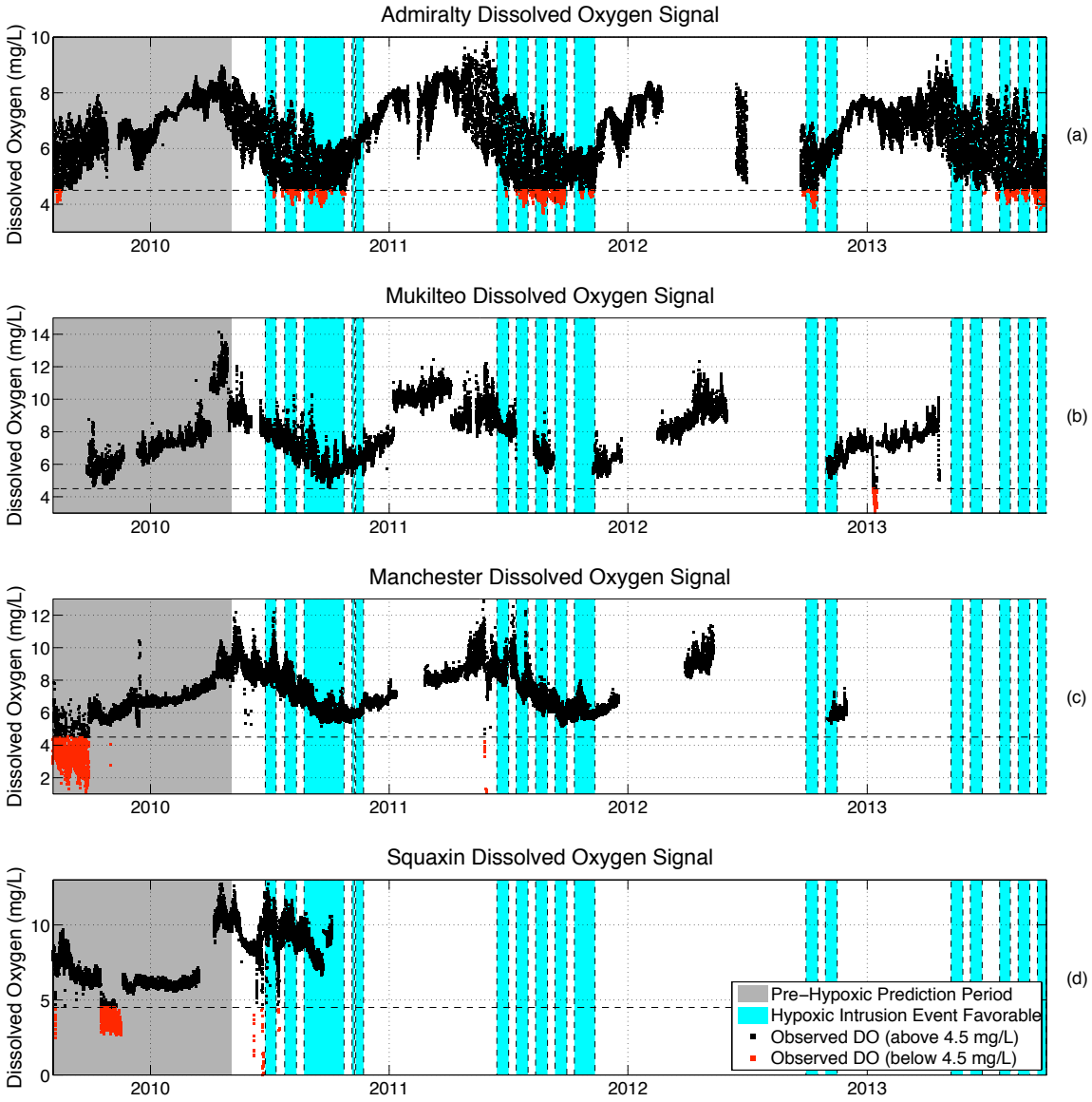

Figure 3.2: Hourly dissolved oxygen observations at 3 different moorings in the main basin of Puget Sound compared to those at Admiralty Sill (points less than or equal to 4.5 mg/L marked red) from August 2009 to October 2013, The background is shaded blue for Hypoxic Intrusion Event Favorable Periods predicted at Admiralty Inlet. The period before intrusion predictions were made is shaded gray. Observations from (a) Admiralty Sill, (b) Mukilteo, (c) Manchester, and (d) Squaxin.

Table 3.2: Main Sound, Lags and Correlation to Admiralty Signal.

Mooring Station	DO Signal Lag	Correlation[a]	DO Deficit Lag	Correlation[b]
Mukilteo	956 hr	0.619	135 hr	0.173
Manchester	1344 hr	0.647	166 hr	0.144
Squaxin	1840 hr	0.450	499 hr	0.104

[a]Statistically significant based on 95% confidence

[b]Statistically significant based on 95% confidence

The comparison of the hourly dissolved oxygen time series from the four different CTDO's in Figure 3.2, observed during the Admiralty mooring deployment time period, reinforces these observations. The seasonal behavior of dissolved oxygen modulation in the main Sound follows the signal at Admiralty Inlet, lagged slightly, suggesting a cumulative response. However, resultant drops in dissolved oxygen concentration from the seasonal trend at the other sites following hypoxic intrusion events at Admiralty Sill are not obvious. This suggests that the modulations of dissolved oxygen levels at Mukilteo, Manchester, and Squaxin, have a cumulative relation to the water masses entering the Sound rather than a direct response.

A cross-correlation analysis was performed between the dissolved oxygen signals at Admiralty Inlet and the other sites for this time period and the results are catalogued in Table 3.2. For each site, the closest positive, statistically significant lag at which the cross-correlation between the signals reached a maximum was determined. This was performed using the hourly dissolved oxygen signals to assess the cumulative response lag, and using the dissolved oxygen deficits determined from equation (2.7) to assess the direct response lag. For both cases, the most reasonable statistically significant positive lag where a local maximum occurs in the cross-correlation signal between each mooring and Admiralty Inlet was identified. The modest correlation coefficients between the hourly dissolved oxygen signals at lags between 1 to 3 months agree with the idea that there is a detectable, yet diffuse,

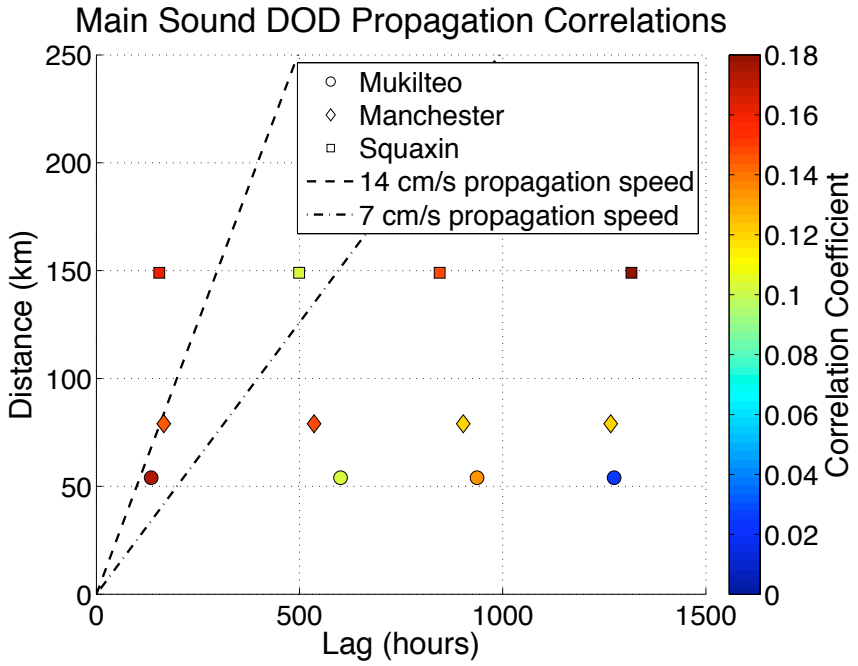

Figure 3.3: Approximate along channel distance (km) to different main Sound moorings are plotted against the positive lag (in hours) at which a statistically significant (based on 95% confidence) local maximum occurs in the cross-correlation signal for the dissolved oxygen deficit (DOD) signals between each mooring and Admiralty Inlet. Shape of points are determined by the mooring location and color is determined by the magnitude of the correlation coefficient at the lag. The dotted lines show the envelope of expected distances for an intrusion signal to reach over time based on gravity current propagation speeds between 7 and 14 cm/s [9][10].

cumulative response to the dynamics at Admiralty Inlet at most sites. The increase in signal lag from Mukilteo to Squaxin, where the correlation is lowest, suggests that water mass properties propagate from North to South in the Sound after traversing Admiralty Inlet and become increasingly diffuse along the way, particularly after passing over the Tacoma Narrows sill.

The very low correlation coefficients determined for the relationship between the dissolved oxygen deficit at Admiralty and the other sites confirm the absence of a trace-able direct response in the Sound to hypoxic intrusion events at these sites. However, the lag times do fall within the range that a water mass would be expected to require to move

from Admiralty to these points in the Sound based on a gravity current velocity of 7 to 14 cm/s as mentioned in Lavelle, et al. [9][10]. The concept for this estimation is presented in Figure 3.3. The presented correlation assessment in this section supports the scheme that hypoxic intrusion events have a cumulative effect of lowering dissolved oxygen levels in Puget Sound over time, but the direct propagation into the existing water masses of the rest of the Sound is very diffuse. The diversity of water masses with low DO in Figure 3.1 imply that there are other sources of hypoxic water than oceanic intrusions in certain areas of Puget Sound.

3.2 Hood Canal Mooring Observations

Data analyzed in this section is collected from four different moorings in Hood Canal that are maintained by the ORCA group at the University of Washington. In order from North to South, the moorings are the North Buoy(47.907 N, 122.627 W), Dabob Bay (47.803 N, 122.803 W), Hoodsport (47.4218 N, 123.113 W), and Twanoh (47.375 N, 123.01 W), as seen in Figure 1.1. Each mooring has a setup that conducts CTDO casts from surface-to-bottom from a buoy on the surface. In this analysis, only data from the deepest point with sufficient data coverage is considered at each mooring, assuming that water properties are similar to those at the bottom of the water column. Parameter data are linearly interpolated to the chosen depth. The depth used for analysis compared to the water depth at each mooring location is catalogued in Table 3.3. From the North Buoy, located at the mouth of Hood Canal, there is salinity, temperature, and dissolved oxygen data available span from November 2005 to October 2012. The mooring at Dabob Bay, a Northward branch off of the main channel of Hood Canal, has data records available from June 2010 to July 2013. At Hoodsport, data records available from a mooring in the main channel of Southern Hood Canal at 113 m depth has data available from September 2006 to June 2011. The mooring at Twanoh, in the Southern hook of Hood Canal, has data spanning from January 2005 to November 2013.

The unique water properties at depth for each site are illustrated in Figure 3.4 for the full time periods of active data collection. As for other sites in Puget Sound, hypoxic water that is associated with high salinity suggests that the water masses are historically tied

Table 3.3: Hood Canal, Data Analysis Depths.

Mooring Station	North Buoy	Dabob Bay	Hoodsport	Twanoh
Water Depth	100 m	100 m	120 m	35 m
Analysis Depth	85 m	96 m	113 m	26 m

to a bottom water intrusion over Admiralty Sill. For the North Buoy (Figure 3.4a), the dissolved oxygen color scale matches the range as the temperature-salinity diagrams from the Admiralty mooring and the main Sound moorings. At the North Buoy, some hypoxic water is tied to fairly high salinity and likely has a source in Admiralty Inlet, however the most hypoxic water is concentrated in moderate salinity ranges with very high temperatures. In this case, there may be another source for much of the hypoxic water, such as a water mass from further up Hood Canal that has been altered by biogeochemical processes in Hood Canal. The signal here is also likely strongly modulated by mixing over the sill at the mouth of Hood Canal [9].

Because the dissolved oxygen levels at the other three moorings are so low, the color scale in Figure 3.4(b,c,d) highlights a different, lower range of dissolved oxygen concentrations. On the dissolved oxygen color scale for these three moorings, dissolved oxygen concentrations below 4.5 mg/L (orange through blue) would be considered hypoxic on the color scale used in the the Hood Canal North Buoy, main Sound, and Admiralty Inlet diagrams. Being that the majority of points in the diagrams for these Hood Canal moorings would be considered hypoxic on the other scale, it is important to point out that none of the water samples reach salinity levels of greater than 31 psu. The hypoxic intrusions at Admiralty Inlet were characterized by water masses with salinity of at least 31 psu and much higher. Therefore, none of the hypoxic water at these three moorings can be directly traced to Admiralty Inlet. Again, this is likely related to the mixing over the sill at the mouth of Hood Canal which likely disperses the signal and mixes different water masses. Therefore, hypoxic water within Hood Canal originating from Admiralty Sill cannot be identified using this water mass analysis.

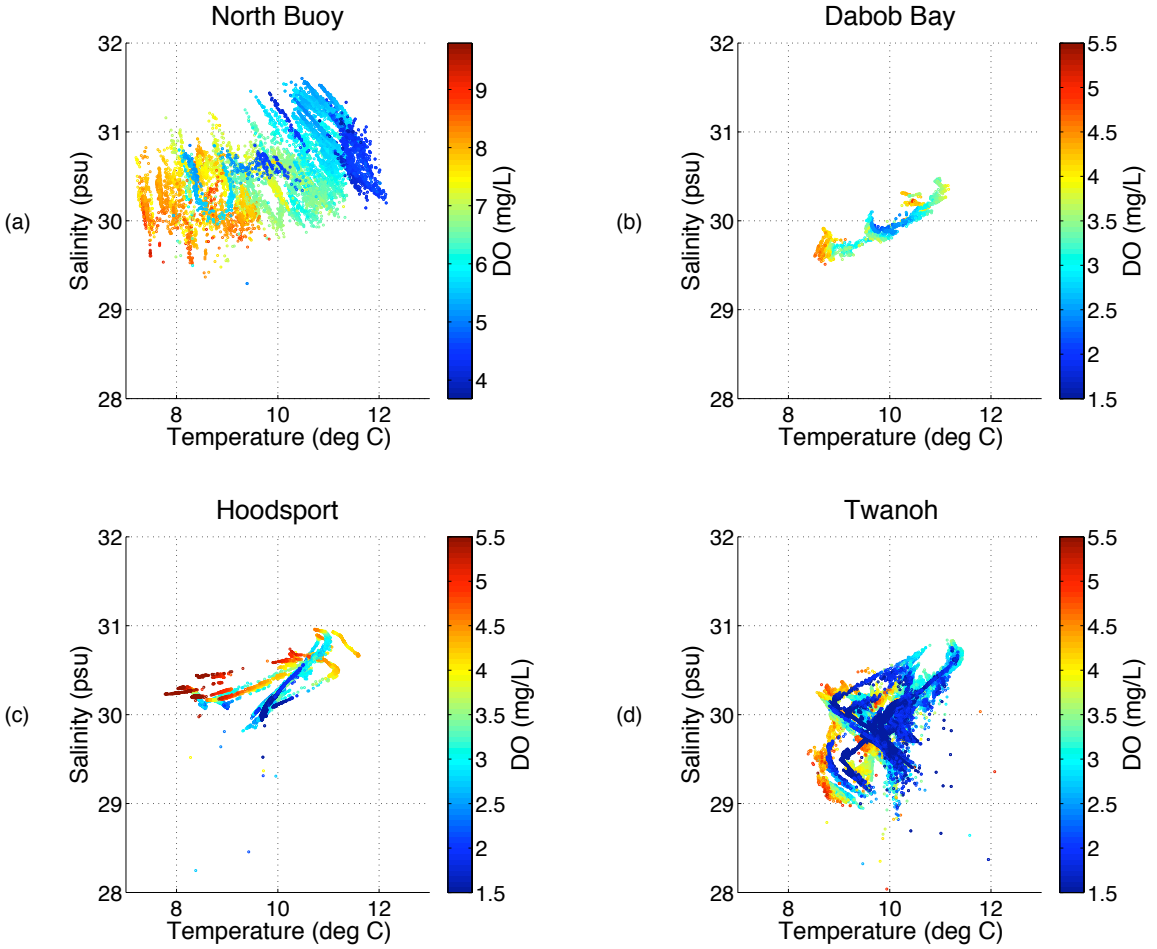

Figure 3.4: Salinity (psu) versus temperature (C) at 4 moorings in Hood Canal during the full periods of active data collection. Data colored according to corresponding dissolved oxygen concentration (mg/L). Observations from (a) North Buoy (8890 data points), (b) Dabob Bay (2296 data points), (c) Hoodsport (9006 data points), and (d) Twanoh (23368 data points).

At Dabob Bay (Figure 3.4b), water properties fall within a fairly narrow, moderate salinity range, but data records at this site are incomplete. Most hypoxic water masses are concentrated at moderate temperatures and salinities with no indication to suggest a distinct local or external source. For Hoodsport (Figure 3.4c), extremely low dissolved oxygen levels seem to be tied to water masses with relatively low salinity and moderate temperatures, suggesting a local source. The extremely hypoxic water observations at the Twanoh

(Figure 3.4d) mooring are tied to a large variety of different water masses. Additionally, there is a staggering number of extremely hypoxic observations. This may be a result of the fact that this mooring is much shallower than the others and, therefore, more directly affected by benthic respiration or other modulating factors. It is unlikely to find a distinct water mass from Admiralty at Hoodsport and Twanoh as the deepest portions of Hood Canal limit the ability for a gravity current to propagate to these regions further to the South. Hypoxic water at these moorings is likely locally dominated, with a very diffuse response to modulations at Admiralty Inlet cumulatively affecting the overall concentrations of dissolved oxygen in the water of Puget Sound and Hood Canal.

Figure 3.5 shows a comparison between the dissolved oxygen records from Admiralty Inlet and the four Hood Canal moorings, interpolated to an hourly time-scale as observed during the Admiralty mooring deployment time period. From the concurrent data available, it appears that the seasonal trends in dissolved oxygen at the Hood Canal moorings follow those of Admiralty Inlet. At the North Buoy (Figure 3.5b), this slightly lagged signal also seems to be strikingly similar in magnitude and trend to Admiralty Inlet's signal. This is corroborated by the cross-correlation analysis performed between the dissolved oxygen signals at Admiralty Inlet and the Hood Canal sites for this time period presented in Table 3.4. As for the main Sound, the most reasonable statistically significant positive lag at which the cross-correlation between the signals reached a maximum was determined for each mooring. The analysis was based on the hourly dissolved oxygen signals to examine a cumulative response lag and for the dissolved oxygen deficits, using equation 2.7, to assess a direct response lag. A graphical approach in Figure 3.6 was used to rationalize the choice of a lag and a local maximum correlation coefficient with a signal propagation speed 7 to 14 cm/s from Lavelle, et al. [9][10]. The strong correlation coefficient in the hourly dissolved oxygen signal for the North Buoy at a lag of approximately 7 days suggests that there is a rapid response at this site to the cumulative effects from the dissolved oxygen modulations over Admiralty Sill. Despite a strong cumulative tie, there is no indication that a measurable direct response occurs as a result of individual Admiralty intrusion events, supported by the low correlation coefficient in the dissolved oxygen deficit signal. A 14.5-day lag was identified whichdoes not fall within the range of time that a water mass would be expected

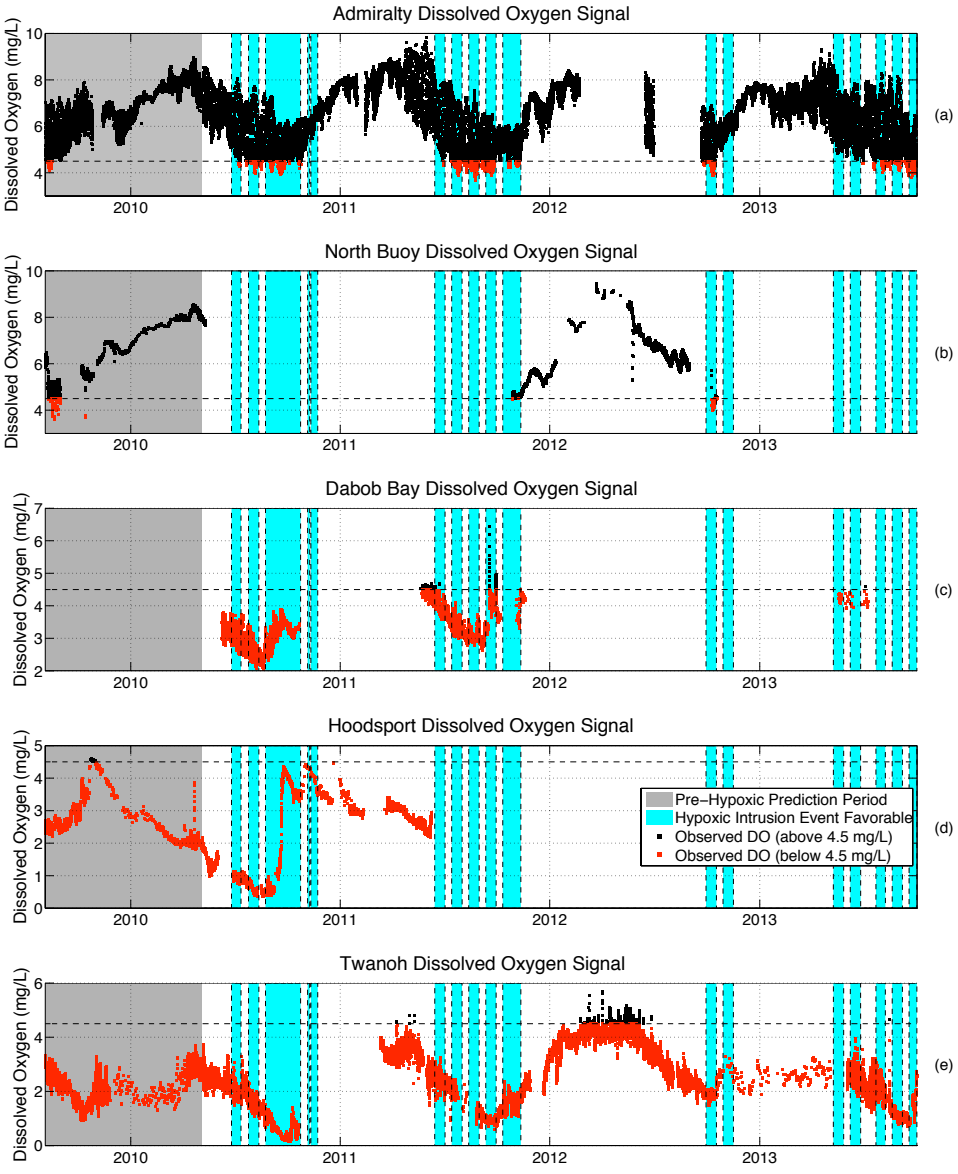

Figure 3.5: Hourly dissolved oxygen observations at 4 different moorings in Hood Canal compared to those at Admiralty Sill (points less than or equal to 4.5 mg/L marked red) from August 2009 to October 2013, The background is shaded blue for Hypoxic Intrusion Event Favorable Periods predicted at Admiralty Inlet. The period before intrusion predictions were made is shaded gray. Observations from (a) Admiralty Sill, (b) North Buoy, (c) Dabob Bay, (d) Hoodsport, and (e) Twanoh.

Table 3.4: Hood Canal, Lags and Correlation to Admiralty Signal.

Mooring Station	DO Signal Lag	Correlation[a]	DO Deficit Lag	Correlation[b]
North Buoy	175 hr	0.767	351 hr	0.156
Dabob Bay[c]	467 hr	0.296	276 hr	0.201
Hoodsport	0 hr	0.135	362 hr	0.358
Twanoh	175 hr	0.691	476 hr	0.097

[a]Statistically significant based on 95% confidence

[b]Statistically significant based on 95% confidence

[c]Insufficient data records to analyze the full seasonal signal response

to take to move from Admiralty Inlet to this mooring based on the expected gravity current velocity [9][10]. The mixing at the Hood Canal sill likely masks a correlation in the signal.

At the remainder of the moorings, the average dissolved oxygen concentrations are significantly lower than the average level at Admiralty Inlet. At Dabob Bay (Figure 3.5c), the dissolved oxygen record is limited to the Summer and Fall, precluding conclusions about the seasonal signal and its cumulative response to Admiralty Inlet. While there is a low correlation coefficient for the direct response of the dissolved oxygen deficit to that at Admiralty Inlet, a determined 11.5-day lag identified seems reasonable based on expected intrusion propagation velocities [9][10]. While the dissolved oxygen signal reaches a minimum at around the same time at Hoodsport (Figure 3.5d) and Admiralty Inlet, the shape of the signal differs tremendously. At Hoodsport, there is a sharp increase from near-anoxic levels to higher dissolved oxygen concentrations during the Fall of 2010, contrasting with the gradual seasonal increase at Admiralty Inlet. From this observation and the low correlation at a zero-hour lag (the correlation was higher for negative lags), it seems that the seasonal signal at Hoodsport cannot be attributed to a cumulative response from modulations at Admiralty Inlet and is likely dominated by local modulating factors such as oxygen uptake by algae blooms, and flushing due to higher-oxygen, fresh water input associated with rain

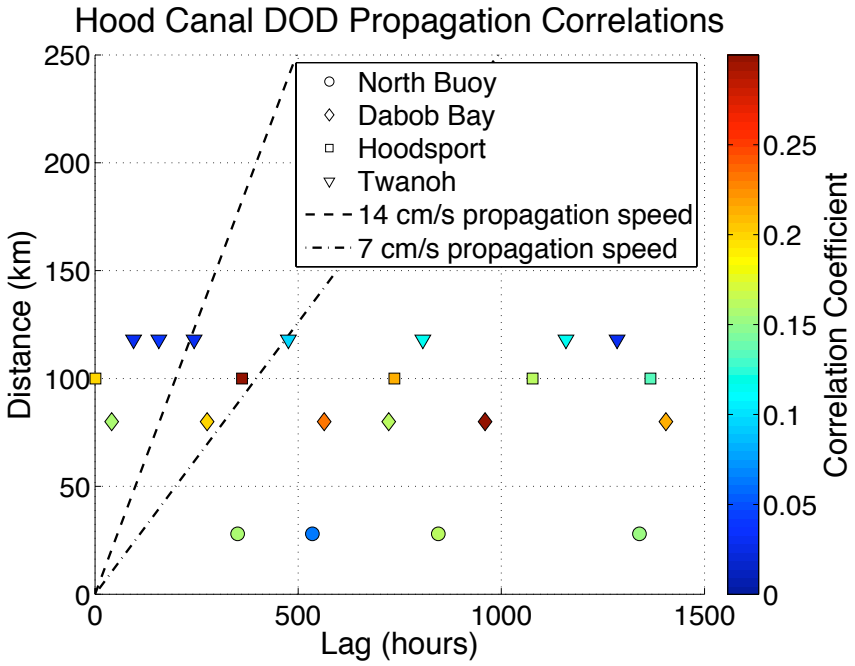

Figure 3.6: Approximate along channel distance (km) to different Hood Canal moorings are plotted against the positive lag (in hours) at which a statistically significant (based on 95% confidence) local maximum occurs in the cross-correlation signal for the dissolved oxygen deficit (DOD) signals between each mooring and Admiralty inlet. Shape of points are determined by the mooring location and color is determined by the magnitude of the correlation coefficient at the lag. The dotted lines show the envelope of expected distances for an intrusion signal to reach over time based on gravity current propagation speeds between 7 and 14 cm/s [9][10].

in the Fall. Interestingly, the 15-day lag identified for the direct response of the dissolved oxygen deficit to that at Admiralty Inlet still seems reasonable and falls within the expected propagation velocities [9][10]. The dissolved oxygen seasonal trends at Twanoh (Figure 3.5e) tightly follow those of Admiralty Inlet with a robust correlation at a lag of a little over 7 days. However, the fact that this lag is identical to the lag identified for the North Buoy and that the mooring location is much further away, past an uncorrelated Hoodsport site, and around the Great Bend suggests that the correlation may be a coincidence. It is more likely that these local trends are driven to a low degree by a cumulative response to the Admiralty modulation, and more by local modulating factors (algae blooms and precipitation

responses) with similar seasonality. Despite this, a direct dissolved oxygen deficit response lags almost 20 days and falls within the expected propagation velocity [9][10], though the correlation is very weak, suggesting a predominantly diffuse direct response.

Based on the data, evidence is presented detailing a seasonal modulation of dissolved oxygen at the mouth of Hood Canal (North Buoy) as a result of the cumulative effects of modulation at Admiralty Inlet. However, the mixing at the sill at the entrance to Hood Canal causes this propagation of water properties to carry a diffuse signal. For the other three moorings, average dissolved oxygen concentrations are significantly lower and there is insufficient evidence to conclude that the seasonal trends are a result of the cumulative response from Admiralty Inlet. Local modulating factors likely have a dominant role in seasonal the trends at these sites. At all four moorings, there is no traceable direct response to hypoxic intrusions. Compared to the main Sound, occurrences of hypoxic and anoxic water in Hood Canal seem to be predominantly locally driven.

3.3 Regional Conclusions (Puget Sound)

Observing the water mass properties at moorings throughout Puget Sound, the propagation of dense water intrusions from Admiralty Inlet is diffuse and is dependent on bathymetry characteristics and proximity to the mouth of the Sound. While hypoxic water at Admiralty Sill is tied to a narrow temperature range of high salinity, a signal is only predominant in the main basin, closer to Admiralty Inlet. When water traverses internal sills, e.g. entering Hood Canal or the Tacoma Narrows, the signal is mixed by strong tidal currents into the existing water mass. In areas that are far away from Admiralty Inlet and/or on the other side of a sill, hypoxic bottom water seems to have additional low oxygen sources that are tied to local effects. This is particularly apparent in Southern Hood Canal and in the South Sound, where some hypoxic water is associated with relatively fresh water masses. At these locations, hypoxic water cannot be attributed to a source of an intrusion over Admiralty Sill.

In the Main Basin of the Sound, in the South Sound, and at the mouth of Hood Canal, the seasonal, cumulative signal of dissolved oxygen modulations can be reasonably related to the regional modulations at Admiralty Inlet. Further into Hood Canal, while dissolved

oxygen levels follow a similar seasonal modulation, concentrations are significantly lower, poorly correlated, and likely modulated by local factors that operate on a similar seasonal cycle. As a consequence, temporary deficits in dissolved oxygen cannot be directly tracked and attributed to intrusion events at any point in the Sound. While correlation between these signals is very low, on average, the lag between some of these signals does seem to be reasonably associated with an intrusion propagation of between 7 and 14 cm/s [9][10] even though DO modulations associated with intrusion events cannot be directly tracked. In conclusion, hypoxic intrusions at Admiralty Inlet do not account for observable direct modulations of water quality in Puget Sound, but their propagations landward and seasonal modulation do seem to contribute to cumulative seasonal water mass characteristics in the main portion of the Sound. In contrast, Hood Canal seems to be primarily driven by local modulation factors.

Chapter 4

OPERATIONAL TEST OF PREDICTION METHOD AND IMPLEMENTATION

This chapter compares the results of the prediction method using water level data from NOAA for the TEI (operational version) to those using in situ pressure data to determine the TEI (in Chapter 2). The prediction methods for intrusion event identifications and hypoxic intrusion favorable periods in Chapter 2 were developed using in situ pressure observations from the CTDO sensor on the tripod at the bottom of Admiralty Inlet to determine tidal elevation signals. This data will not always be available (it might be available from tidal turbine monitoring starting in 2015). Therefore, it is important for the operation of the intrusion prediction method that all inputs are publicly available from online databases. For this purpose, the operational version of the intrusion prediction method will rely on tidal elevation data from NOAA at the Port Townsend, WA, station 9444900 [16]. This water level data should be downloaded in meters, relative to MLLW, as an hourly time series in GMT. This time series will take the place of the Tidal Elevation Index (TEI), from equation 2.1, and no de-meaning or normalization is necessary. After making this adjustment, the methods outlined in Sections 2.1 and 2.2 are used as presented. The first set of codes presented in Appendix C (Operational Intrusion Prediction Method) can be used to operationally run the intrusion prediction methods with only time series inputs of:

- Hourly time-step vector constructed based on chosen analysis period
- Tidal elevation from NOAA [16]
- Moon phase from USNO [14]
- Upwelling Index at N 48, W 125, from PFEL [12]
- Fraser River discharge at Hope, BC, Canada, from the Water Survey of Canada [15]

Table 4.1: Operational Test, Intrusion Event prediction results

	Operational Test		Using In Situ Tidal Data	
Intrusion Events with IEI	Number of Events	Percent Identified	Number of Events	Percent Identified
≥ 1.0	9	100	same	
≥ 0.9	10	100	same	
≥ 0.8	15	100	same	
≥ 0.5	26	100	25	100
≥ 0.4	29	93.1	28	92.9
≥ 0.3	35	85.7	33	84.8
≥ 0.2	39	79.5	37	78.4
≥ 0.1	52	69.2	49	69.4
> 0.0	102	41.18	88	43.2

Table 4.1 compares the success rates of Intrusion Event predictions for the operational methods and for the in situ version from Chapter 2. The operational method is shown to correctly identify intrusion events just as well as with the in situ data method and is able to predict additional intrusion events during times in which there were data gaps from the in situ data due to instrument failure. The operational method produces a false positive prediction 1.68 % of the times that the true Intrusion Event Index is zero, as compared to 1.52 % for the Chapter 2 analysis. Figure 4.1a shows when intrusion predictions are made using both methods (green), using only the operational method (blue), and using only the in situ data method (orange). This demonstrates the overwhelming agreement of the two versions. In fact, the only prediction made using the in situ data that is not also made by the operational method is not during an active intrusion event. Figure 4.1b compares the prediction results for the two method inputs for predicted hypoxic intrusion favorable periods. The operational method correctly identifies hypoxic intrusion favorable periods just as well as with the in situ data method, including periods not covered by in situ data.

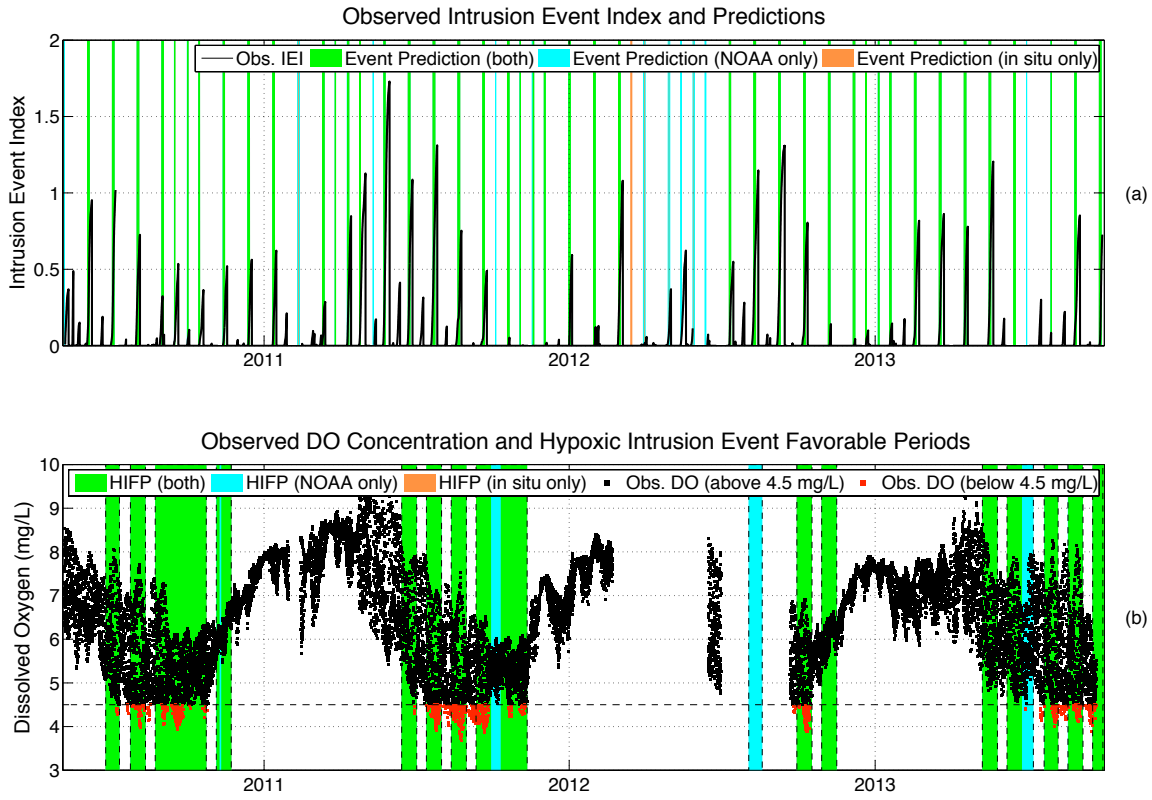

Figure 4.1: Presentation of results from operational test of hypoxic intrusion event predictions. Blue indicates that a prediction was made only by the operational method using tidal elevation data from NOAA [16]. Orange indicates that a prediction was made only by the method using in situ pressure data from the CTDO. Green indicates that a prediction was made using both methods. (a) The observed Intrusion Event Index time series from May 2010 to October 2013 with marks indicating when the tidal condition indices are both above the proposed threshold for prediction ($NTI > 0.8$, $DII > 0.72$). (b) Hourly dissolved oxygen observations (points less than or equal to 4.5 mg/L marked red) from May 2010 to October 2013, with background shaded for Hypoxic Intrusion Event Favorable Periods.

Results for hypoxic intrusions are shown in Table 4.2 and compared to success rates of the predicted hypoxic intrusion event favorable periods at Admiralty Sill.

The operational test of the hypoxic intrusion prediction method successfully predicts intrusion events with comparable precision as using in situ data. Using the codes presented in Appendix C, this method can be implemented without requiring in situ measurements. Data for inputs is readily available from routinely-updated databases. For more accurate

Table 4.2: Operational Test, Hypoxic Intrusion Event prediction results.

	Operational Test	Using In Situ Tidal Data
Observed DO (mg/L) Below	Percent of Points Identified	Percent of Points Identified
4.0	97.8	same
4.25	90.4	same
4.50	83.9	83.7
4.75	81.9	80.7
5.0	80.1	77.9
5.25	78.3	74.9
5.5	77.7	73.7
5.75	75.4	71.0
6.0	73.0	68.9
6.25	69.8	66.2
6.5	66.1	62.8

predictions, it is recommended that larger continuous data sets over several years be used. This is important because additional seasonal cycles will improve calculations for the de-trending methods for the Upwelling Persistence Index (UPI) outlined in Section 2.1.5, and improve normalization techniques for other indices. The Pacific Fisheries Environmental Laboratory has Upwelling Index data for N 48, W 125, since 1967 [12]. This long record could be used to maximize the de-trending method quality for the UPI. The Neap Tide Index (NTI) and the Diurnal Inequality Index (DII) are not as sensitive to long-term de-trending and normalization as the UPI (the most sensitive parameter due to the de-trending necessary after the conditional integration) and the Fraser River Discharge Index (FRDI). This is because the UPI and FRDI have a much higher degree of interannual variability than the NTI and DII.

Chapter 5

CONCLUSION

Observations and analysis presented in this thesis agree with the literature that assesses the conditions necessary to develop a hypoxic, oceanic, dense bottom water intrusion at Admiralty Inlet. Implications for the water quality of the Main Basin of Puget Sound are shown to be mostly cumulative and diffuse. The following list summarizes the most important conclusions and products developed in this analysis.

1. The hypoxic intrusion prediction method developed in Chapter 2 and operationalized in Chapter 4 is successful in conditionally identifying periods favorable for oceanic hypoxic bottom water intrusions at Admiralty Inlet. In Appendix C, MATLAB codes are provided to operationally run this prediction method using publicly available data from the websites of government agencies.

2. Dense bottom water intrusions at Admiralty Inlet develop during neap tides, coincident with periods of maximum diurnal inequality. Periods in which intrusion events are observed exhibit the larger-scale characteristics associated with a two-layer estuarine exchange flow over Admiralty Sill.

3. The availability of hypoxic water at the entrance of Puget Sound is a product of the larger-scale estuarine exchange flow in the Strait of Juan de Fuca. Intrusions therefore only carry hypoxic water over Admiralty Sill if they coincide with high Fraser River discharge and prolonged periods of upwelling at the mouth of the Strait.

4. Temperature and salinity data observed in the surface waters of Admiralty Inlet can alternatively be used to predict the sub-tidal near-bottom signal of dissolved oxygen at Admiralty Inlet. The MATLAB codes for making these predictions can be found at the end of Appendix C.

5. In the main basin of Puget Sound, the dissolved oxygen signal at Admiralty Inlet contributes to a diffuse, lagged seasonal modulation in dissolved oxygen.

6. In Hood Canal, dissolved oxygen modulation is not directly linked to oceanic intrusions at Admiralty Sill, but is rather driven by local forcing factors.

7. Internal sills in Puget Sound are influential in diffusing the signal of hypoxic intrusions.

Much of the precise dynamics of hypoxic intrusions entering Puget Sound from the ocean, their propagation landward, and exact effects on water quality still need to be studied with greater temporal and spatial resolution. The two-stage prediction method developed here helps to confirm the importance of the forces that modulate sill dynamics. Two-layer exchange flows can only develop during tidal cycles at Admiralty Inlet that induce minimal mixing. The availability of hypoxic water at the site is seasonally modulated by larger-scale estuarine factors that are sensitive to climate variations. Multiple conditions must be satisfied to produce a hypoxic intrusion over Admiralty Sill. The prediction method developed in this thesis successfully identifies intrusion events and the conditions necessary for hypoxic dense-water intrusions for the time period from May 2010 to October 2013. Climate shifts and interannual variability might affect these relationships in unforeseen ways. It is important to point out that these method are currently limited to a binary prediction of hypoxic intrusions. Additional approaches will be required to assess the severity or duration of intrusion events or the flux of oxygen and other constituents through Admiralty Inlet.

BIBLIOGRAPHY

[1] T. Khangaonkar, B. Sackmann, W. Long, T. Mohamedali, and M. Roberts, "Simulation of annual biogeochemical cycles of nutrient balance, phytoplankton bloom(s), and do in Puget Sound using an unstructured grid model," *Ocean Dynamics*, vol. 62, pp. 1353–1379, 2012.

[2] W. R. Geyer and G. A. Cannon, "Sill processes related to deep waterrenewal in a fjord," *Journal of Geophysical Research*, vol. 87, no. C10, pp. 7985–7996, 1982.

[3] J. Thomson, B. Polagye, V. Durgesh, and M. Richmond, "Measurements of turbulence at two tidal energy sites in Puget Sound, WA," *Journal of Oceanic Engineering*, vol. 37, no. 3, pp. 363–374, 2012.

[4] R. E. Thomson, "Physical oceanography of the Strait of Georgia-Puget Sound-Juan de Fuca Strait system," in *Review of the Marine Environment and Biota of Strait of Georgia, Puget Sound and Juan de Fuca Strait. Proceedings of the BC/Washington Symposium on the Marine Environment. Canadian Technical Report of Fisheries and Aquatic Science, NO.1948*, R. Wilson, R. Beamish, F. Aitkens, and J. Bell, Eds., 1994, pp. 36–100.

[5] C. A. Barnes and E. E. Collias, "Some considerations of oxygen utilization rates in Puget Sound," *Journal of Marine Research*, vol. 17, pp. 68–80, 1958.

[6] Z. Yang and T. Wang, "Tidal residual eddies and their effect on water exchange in Puget Sound," *Ocean Dynamics*, vol. 63, no. 8, pp. 995–1009, 2013.

[7] G. A. Cannon, J. R. Holbrook, and D. J. Pashinski, "Variations in the onset of bottom-water intrusions over the entrance sill of a fjord," *Estuaries*, vol. 13, no. 1, pp. 31–42, 1990.

[8] K. R. Helfrich, "Time-dependent two-layer hydraulic exchange flows," *Journal of Physical Oceanography*, vol. 25, pp. 359–373, 1995.

[9] J. W. Lavelle, E. D. Cokelet, and G. A. Cannon, "A model study of density intrusions into and circulation within a deep, silled estuary: Puget sound," *Journal of Geophysical Research*, vol. 96, no. C9, pp. 16,779–16,800, 1991.

[10] J. R. Holbrook, G. A. Cannon, and E. T. Baker, "Propagation of renewed deep water in the puget sound estuary," *Eos Trans. AGU*, vol. 64, p. 1033, 1983.

[11] B. Polagye and J. Thomson, "Tidal energy resource characterization: methodology and field study in Admiralty Inlet, Puget Sound, WA (USA)," *Proceedings of the Institution of Mechanical Engineers, Part A: Journal of Power and Energy ceedings of the Institution of Mechanical Engineers, Part A: Journal of Power and Energy*, vol. 227, no. 3, pp. 352–367, 2013.

[12] N. O. A. A. Pacific Fisheries Environmental Laboratory. Index values at 48N 125W (1967-present). [Online]. Available: http://www.pfeg.noaa.gov/products/PFEL/modeled/indices/upwelling/upwelling.html

[13] S. D. Hicks, R. L. Sillcox, C. R. Nichols, B. Via, and E. C. McCray, "Tide and current glossary. Silver Spring, MD: NOAA National Ocean Service," *Center for Operational Oceanographic Products and Services*, pp. 1–29, 2000.

[14] U. S. N. O. Astronomical Applications Department. Fraction of the moon illuminated. [Online]. Available: http://aa.usno.navy.mil/data/docs/MoonFraction.php

[15] E. C. Water Survey of Canada. Hydrometric data. [Online]. Available: http://www.wsc.ec.gc.ca/applications/H2O/index-eng.cfm

[16] NOAA/NOS/CO-OPS. Observed water levels at 9444900, port townsend wa. [Online]. Available: http://tidesandcurrents.noaa.gov/waterlevels.html?id=9444900

Appendix A

SENSOR COMPARISON (SEABIRD AND HOBO)

The purpose of this Appendix section is to determine how well the HOBO CT and DO loggers performed in comparison to the Seabird CTDO during the three deployments within December 2012 to October 2013. The first deployment considered in this analysis was from December 18, 2012, to April 1, 2013. The second was from April 2 to July 1, 2013, and the third was from July 2 to October 1, 2013. In the graphical comparisons in this section, the distinct deployment periods are easy to pick out based on recovery gaps. Data sets from the recovered sensors were processed with the appropriate software and interpolated to hourly values for comparison of Salinity, Dissolved Oxygen, and Temperature readings. For each parameter, a visual comparison is presented in which the top panel of the figure is a plot of the hourly values from the processed data for each sensor. The bottom panel(s) shows difference between the HOBO sensor data and the Seabird sensor data over the time series. The uncertainty envelope around this difference time series is calculated as follows, with expected values based on the error (accuracy and resolution) provided by the manufacturer:

- The upper bound is the difference between maximum expected value from the HOBO sensor and the minimum expected value from the Seabird sensor.

- The lower bound is the difference between minimum expected value from the HOBO sensor and the maximum expected value from the Seabird sensor.

The uncertainty envelope, therefore, describes the range of the possible difference between sensor readings, based on manufacturer-stated error. If the uncertainty envelope encompasses the zero-line a given point, it is possible that the instruments are reading the same value within their rated error at that time.

The HOBO CT logger has a maximum rated accuracy of 5 percent of the conductivity value in a range of $\pm$ 3,000 μS/cm from the field calibration point (the company released

a statement on April 15, 2013, amending the accuracy ratings for the instrument from previous ones to ± 5,000 μS/cm and subsequently has updated the manual (16844-B MAN-U24-002-C) to these specifications of ± 3,000 μS/cm). The readings on this deployment fall within that range of measured conductivity values, so it is reasonable to use ± 5 percent conductivity as the accuracy. The rated resolution is 2 μS/cm. The error value used for the HOBO salinity reading is 5 percent of the salinity reading, using an assumption that salinity and conductivity vary proportionally. The Seabird CTD sensor has a rated accuracy of 0.0005 μS/m and a rated resolution of 0.00005 μS/m (about 0.4 ppm). The error value for each Seabird DO reading was taken to be 0.004 psu (4 ppm), making assumptions for the conductivity/salinity comparison. These error values were used in determining the uncertainty envelope for instrument comparison.

A different calibration scheme was used for each deployment. For the December to April deployment, since no field calibrations were made for the HOBO CT sensor, Seabird CTDO readings were used as starting and ending field calibrations during the HOBO data processing. For the April to July deployment, no field calibration was conducted at deployment so a reading from the Seabird was used as the start calibration point. At recovery, a specific conductivity solution (10,000 μS/m) was used to make a field calibration for the end calibration point. For the final deployment (July to October), a field calibration using the conductivity solution was used at both ends. It is also important to note that HOBO CT temperature values are used when processing HOBO CT salinity data. Therefore, an error in the CT sensor temperature could potentially propagate into the processed salinity values.

Comparison plots for salinity readings of the Seabird CTDO and the HOBO CT logger are shown in Figure A.1. It becomes immediately clear that the calibration method using the Seabird salinity values results in the best agreement with the Seabird salinity observations, which are reasonable given the expected salinity values at this site. During this first deployment, the sensor difference plot shows that the two sensors agree within the bounds of the uncertainty envelope for the majority of the data but there is a drift away from agreement in the middle of the deployment that then returns to agreement at the end to match calibration. The HOBO sensor data appears to follow a similar structure to that of the Seabird.

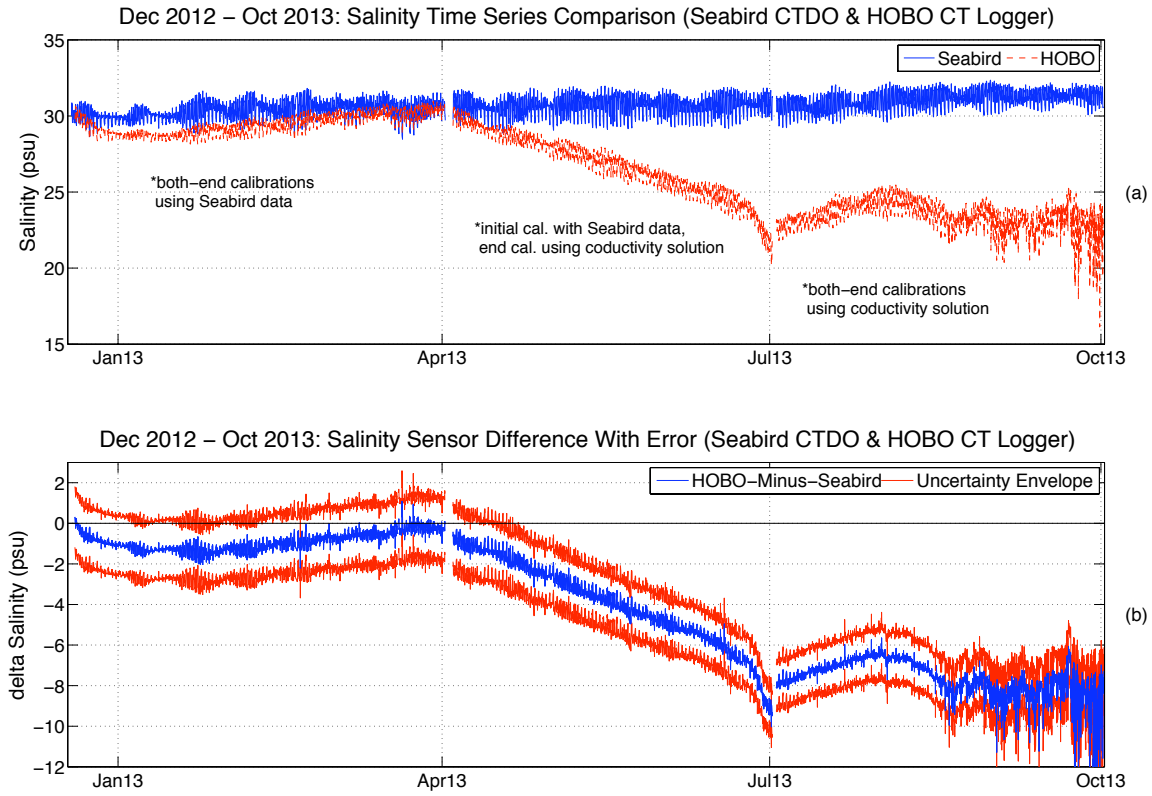

Figure A.1: Comparison of Salinity readings from HOBO CT logger and Seabird CTDO from Dec 2012 to Oct 2013. Panel (a) shows processed hourly data from sensors. Panel (b) shows differences in instrument readings and uncertainty envelope based on instrument error from manufacturer.

The new accuracy values for the HOBO CT sensor from the manufacturer result in very large uncertainties of about $\pm$ 1.5 psu and accuracy is much worse if conductivity values vary outside of the range of $\pm$ 3,000 μS/cm from the field calibration point. Calibrations can only be expected to hold over this limited range. This is most likely the source of the overwhelming disagreement between the HOBO observations calibrated with the conductivity solution and the Seabird observations. Estuarine water such as this has conductivity levels on the order of 45,000 μS/cm, which is well over 3,000 μS/cm than the 10,000 μSc/m conductivity of the solution used for calibration. This conductivity solution may be useful in environments with much lower salinity, but it seems that using it for field calibrations

at a site like this does not work due to the parameters of the instrument. Conducting field calibrations with a solution rated for a conductivity of closer to 45,000 μS/cm would likely work much better since, in most applications, another device with which to derive calibration readings with will not be available. However, according to the updated manual, "For conductivities within $\pm$ 30,000 μS/cm, there will be less than 4% error added to the DO measurements (percent of the DO reading in mg/L)" (16844-B MAN-U24-002-C).

The HOBO DO logger has a rated accuracy of 0.2 mg/L up to 8 mg/L and 0.5 mg/L from 8-20 mg/L. The rated resolution is 0.02 mg/L. The error value used for the HOBO dissolved oxygen reading is the sum of the accuracy and resolution at each reading. The Seabird DO sensor has a rated accuracy of 2 percent of DO saturation readings. Making the assumption that there is a proportional relation between DO saturation and mg/L, this accuracy percentage was used to compute the error value for each Seabird DO reading. Resolution for the instrument was not listed in the documentation. These error values were used in determining the uncertainty envelope for instrument comparison.

Figure A.2 shows the DO comparison plots for the Seabird CTDO and the HOBO DO logger. It should be considered that the DO (mg/L) values are processed using salinity values from the HOBO CT sensor deployed simultaneously. Therefore, an error in the CT sensor could propagate into the processed DO values. The sensor difference plot shows that, during the first deployment, which is calibrated using the reasonable salinity data, the two instruments initially agree within the bounds of the uncertainty envelope. However, over time the HOBO DO logger becomes biased high, beyond the uncertainty envelope. The HOBO sensor data appears to follow a similar structure to that of the Seabird data. For the second and third deployments, there appears to be a much larger variance in the signal (likely due to the accuracy problems associated with calibrating DO data using largely-incorrect salinity data from the HOBO CT), but the observations do seem to follow the Seabird DO observations reasonably well in structure and trend. It seems that in taking the Seabird data to be true, low DO intrusions are not accurately observed at Admiralty Inlet using the HOBO sensor (at least when calibrated with poor salinity data) as it sometimes falsely identifies points below 4 mg/L and overestimates at some instances of critically low DO levels.

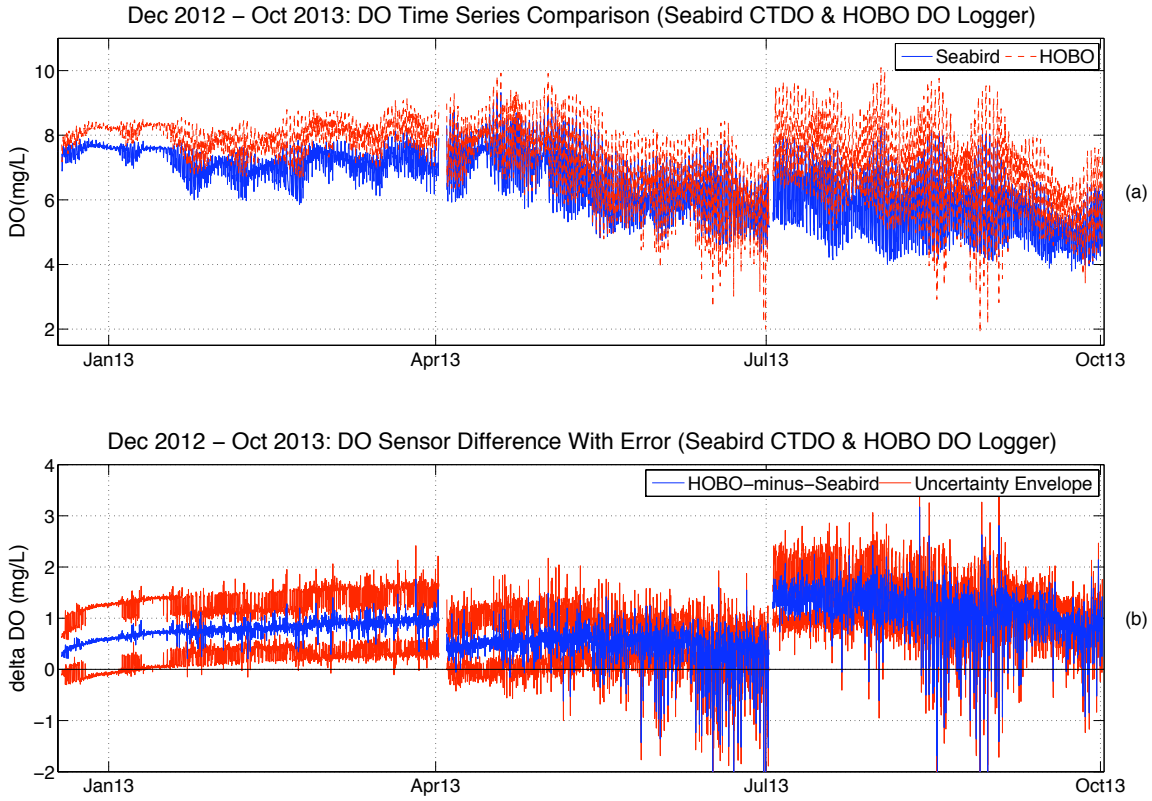

Figure A.2: Comparison of Dissolved Oxygen readings from HOBO DO logger and Seabird CTDO from Dec 2012 to Oct 2013. Panel(a) shows processed hourly data from sensors. Panel (b) shows differences in instrument readings and uncertainty envelope based on instrument error from manufacturer.

The HOBO DO logger has a rated temperature accuracy of 0.2 °C and a rated resolution of 0.02 °C. For the HOBO CT logger, the rated temperature accuracy is 0.1 °C and the rated resolution is 0.01 °C. The error values used for the respective HOBO temperature readings are the sum of the sensor accuracy and resolution at each reading. The Seabird CTD sensor has a rated accuracy of 0.005 °C and resolution of 0.0001 °C. The error value used for the Seabird temperature readings is the sum of the accuracy and resolution at each reading. These error values were used in determining the uncertainty envelope for instrument comparison.

Figure A.3 shows comparison plots for temperature readings of the Seabird CTDO, the HOBO DO logger, and the HOBO CT logger. According to the first sensor difference plot (Figure A.3b), the Seabird CTDO and the HOBO DO logger agree within the bounds of the uncertainty envelope for the entire time series. Additionally the actual value difference between the two is nearly zero. The HOBO DO logger temperature values are therefore accurate if the Seabird values are taken to be true. The second sensor difference plot (Figure A.3c) shows that the Seabird CTDO and the HOBO CT logger have temperature readings that are different, even when accounting for instrument error at low temperatures. However, this difference seems to be relatively low and to improve at higher temperatures (or possibly due to sensor drift). The HOBO CT logger seems to be biased low at low temperatures and there is no method to calibrate temperature reading in the data processing software.

Despite some discrepancies in comparison with the Seabird CTDO, the HOBO sensors give reasonable values and could most likely detect a low dissolved oxygen water intrusion at Admiralty Inlet when using the CT sensor calibration method that uses in situ data. However, using field calibrations taken using a conductivity solution that is not close to 45,000 μS/m, results in large inaccuracies in salinity observations and less accurate, more variable DO observations. If the manufacturer fixes the newfound problems with accuracy of the CT sensors, the next generation of HOBO CT loggers has the potential to more accurately measure salinity.

HOBO DO and CT sensors have some inherent advantages not related to sensor accuracy. The HOBO sensors cost less than the Seabird sensors and are much smaller, allowing for easy deployment without requiring extensive mooring space. Also, the HOBO DO loggers have no moving parts, eliminating potential problems with clogging or pump damage that the Seabird DO sensors are susceptible to. Calibration is extremely important for these instruments, and due to calibration accuracy requirements, the HOBO CT sensor cannot be used in environments where conductivity values outside of the range of $\pm$ 3,000 μS/cm around the calibration point are expected to occur, as demonstrated in the second and third deployment.

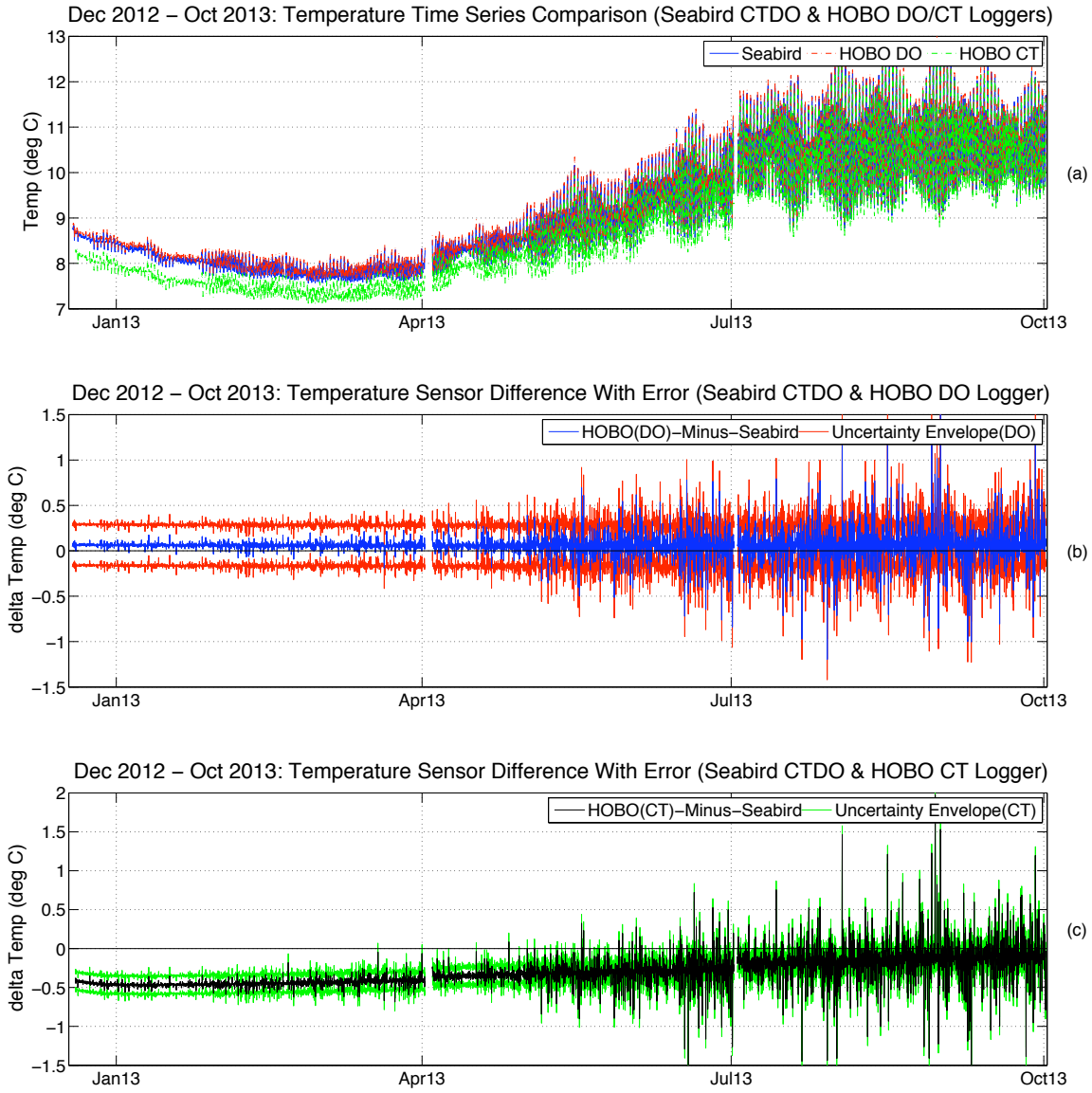

Figure A.3: Comparison of Temperature readings from HOBO DO logger, HOBO CT logger, and Seabird CTDO from Dec 2012 to Oct 2013. Panel (a) shows processed hourly data from sensors. Panels (b) and (c) show differences in instrument readings and uncertainty envelope based on instrument error from manufacturer.

Appendix B

SENSITIVITY TO DE-TRENDING IN UPWELLING PERSISTENCE INDEX CALCULATION

The analysis for the Interim Report for the Department of Ecology and for the OCEANS'13 conference paper was done using data through the April 2013 recovery. After adding all data through the final October 2013 recovery, the original scheme for making hypoxic intrusion event predictions was ill-suited for the data set due to the method for removing the cumulative bias from the Upwelling Persistence Index. Therefore, a new scheme for removing this bias was introduced, which is the one reported in Section 2.1.5 of the main body of the thesis. Instead of demeaning the conditionally-integrated upwelling index, a 2nd-order polynomial was fit to the data between January 2010 and January 2013. Then the set was de-trended by subtracting the trend for the full data set fit to this polynomial equation to create the new version of the UPI. However, this new UPI trend removal made it necessary to determine a new threshold for the Dissolved Oxygen Availability Prediction due to a different regression fit to the seasonal dissolved oxygen data. This new threshold was determined to be $DO_{AP} < 6.241$ instead of $DO_{AP} < 6.4$. This new scheme works efficiently for the new, full data set, and has agrees with the previously determined prediction success rates for the portion of data considered in the Interim Report. A comparison of these schemes is shown in Table B.1. Using the new de-trending method for the Upwelling Persistence Index results in a higher, more consistent R-squared value in the multi-linear regression.

Table B.1: Comparison between success of different Hypoxic Intrusion Event prediction results.

	New data, through October			Data through April		
UPI	Detrended	Demeaned		Detrended		Demeaned
R-squared Value	0.7745	0.5525	—	0.7796	—	0.7407
	Percent of Points Identified					
Observed DO (mg/L) Below	——	w/ Reg.	w/ Eqn.	w/Reg.	w/ Eqn.	——
4.0	97.83	45.65	97.83	100	100	100
4.25	90.43	71.91	90.43	95.05	95.05	95.05
4.50	83.68	69.34	83.07	90.81	90.81	90.81
4.75	80.71	67.01	78.94	87.69	87.69	87.69
5.0	77.86	62.60	74.85	84.09	84.09	84.09
5.25	74.87	57.53	71.51	80.37	80.37	80.37
5.5	73.70	54.44	70.16	77.89	77.89	77.89
5.75	71.05	52.28	67.55	74.52	74.54	74.54
6.0	68.87	51.35	65.56	72.11	72.17	72.17
6.25	66.17	49.93	62.81	68.83	69.04	69.03
6.5	62.81	47.55	59.56	64.73	64.92	64.90
% of TS Predicted	35.72	26.67	33.48	32.75	35.34	34.46
% False Positives						
by window coverage	29.41	27.27	31.25	25.00	30.77	30.77
by ID point	25.17	23.65	24.69	18.39	23.51	23.95

Appendix C

MATLAB PREDICTION CODES

Codes may be accessed with the following link:

http://faculty.washington.edu/jmt3rd/DeppeCodes/

- Operational Intrusion Prediction Method:

  `Deppe_HIpredict_16Nov2013.m`

- Test-case input data for Intrusion Prediction Method:

  `Raw_Nov_2013_Operational.mat`

- Sub-Tidal Dissolved Oxygen Prediction Method (Victoria Clipper):

  `Deppe_VCdo_16Nov2013.m`

OPERATIONAL INTRUSION PREDICTION METHOD

```
%% PREDICTION METHOD (Operational Version)

%Intrusion Events & Hypoxic Intrusion Events

%R. Walt Deppe
%November 16, 2013
```

```
%% Import NOAA Tideal Elevation Data

% from 9444900 Port Townsend, WA
% [http://tidesandcurrents.noaa.gov/waterlevels.html?id=9444900]

% download data by hour in GMT in reference to MLLW
% in year-length chunks and combine
% (excel time + 695422 = matlab time)

% NOAA_Tides = uiimport('NOAA_TidalElevation.csv');
% NOAA_Time = NOAA_Tides.NOAA_Time_Matlab;
% NOAA_TE = NOAA_Tides.NOAA_TE_hr;


%% Choose time period for analysis / Set up hourly time steps

% hourly time from (05 Aug 2009) to (02 Oct 2013)
Hour = (733990:(1/24):735509)';

% Be sure that [pl66tn.m] and [dynamicDateTicks.m],
% are in the current folder

%% TEI (Tidal Elevation Index)

TEI_noaa = interp1(NOAA_Time,NOAA_TE,Hour);

% **check interpolation**
% plot(NOAA_Time,NOAA_TE,'k');
% hold on; plot(Hour,TEI_noaa,'--r');
```

```
% hold off;
% dynamicDateTicks();

%% NTI (Neap Tide Index)

% Import MoonPhase data from the Astronomical Applications Department of
% the US Naval Observatory
% (MoonTime = day from data set)
% (MoonPhase = moon phase, 1=full, 0=new)
% http://aa.usno.navy.mil/data/docs/MoonFraction.php

% Set: 1 = Peak Neap , 0 = Peak Spring
NTIraw = (-2*abs(MoonPhase-0.5))+1;
%interpolate to hourly time scale
NTI = interp1(MoonTime,NTIraw,Hour);

clear NTIraw
% **check interpolation**
% plot(MoonTime,MoonPhase);hold on;plot(Hour,NTI,'r');hold off;

%% DII (Diurnal Inequality Index)

% alsolute value of gradient of Tidal Amplitude Index [tidal time-scale]
tgi_noaa = abs(gradient(TEI_noaa));
% match residual current time-scale [subtidal signal]
tgi66_noaa = pl66tn(tgi_noaa,1,40);
% remove parts of filtered signal biased by NaN values
tgi40_noaa = tgi66_noaa;
for i = 1:length(tgi66_noaa);
    if (i<41 || i>(length(tgi66_noaa)-40));
```

```
        tgi40_noaa(i) = NaN;
    elseif(isnan(tgi66_noaa(i)));
        tgi40_noaa((i-40):(i+40),1) = NaN(81,1);
    end
end
% normalize/reverse sign
DII = (-(tgi40_noaa-max(tgi40_noaa)))/...
            max(-(tgi40_noaa-max(tgi40_noaa)));
% 1 = Max. Diurnal Inequality ; 0 = Diurnal Equality

clear tgi tgi66 tgi40 i tgi_noaa tgi66_noaa tgi40_noaa
% **check against TEI**
% plot(Hour,TEI_noaa,'b');hold on;
% plot(Hour,DII,'r');
% hold off; dynamicDateTicks();

%% Lagged Upwelling Index (UI - 7.25 days)

% Import Raw_Upwell data from Upwelling Index from PFEL (NOAA)
% for site 48 N, 125 W
% (Raw_Ut = day from data set)
% (Raw_Upwell = upwelling index observations)
% http://www.pfeg.noaa.gov/products/PFEL/modeled/indices/upwelling/NA/data_download.html
% **Raw_Ut range currently used: [733980 735415] 26-Jul-2009 to 30-Jun-2013

% QC raw UI set
for j = 1:length(Raw_Upwell);
    if (Raw_Upwell(j,1) <= -9999);
        Raw_Upwell(j,1) = NaN;
    end
```

```
end
%due to missing values in june 2013 record
for j = 5628:5744;
    if (isnan(Raw_Upwell(j,1)));
        Raw_Upwell(j,1) = (Raw_Upwell(j-1,1)+Raw_Upwell(j+1,1))/2;
    end
end
%find start and end points (with lag) to match Hour
start = find(Raw_Ut == Hour(1)-7.25);
final = find(Raw_Ut == Hour(length(Hour))-7.25);
%find Time start and end points (withOUT lag) to match Hour
Tstart = find(Raw_Ut == Hour(1));
Tfinal = find(Raw_Ut == Hour(length(Hour)));
%select Lagged Raw Upwelling section of data corresponding to time period
Raw_Utime = Raw_Ut(Tstart:Tfinal,1);
Raw_UI = Raw_Upwell(start:final,1);
% interpolate to hourly
UI_hr = interp1(Raw_Utime,Raw_UI,Hour);

clear j start final Raw_upwell Raw_Ut
% ** check interpolation**
% plot(Raw_Utime,Raw_UI);
% hold on;
% plot(Hour,UI_hr,'r');
% hold off; grid on;
% dynamicDateTicks();

%% UPI (Upwelling Persistance Index)

% match residual current time-scale [subtidal signal]
```

```
ui66 = pl66tn(UI_hr,1,40);
% remove parts of filtered signal biased by NaN values
UI_lpf40 = ui66;
for i = 1:length(ui66);
    if (i<41 || i>(length(ui66)-40));
        UI_lpf40(i) = NaN;
    elseif(isnan(ui66(i)));
        UI_lpf40((i-40):(i+40),1) = NaN(81,1);
    end
end

clear ui66 i
% **check filter**
% plot(Hour,UI_hr);hold on;plot(Hour,UI_lpf40,'r');hold off;

% conditional integration of UI_lpf40
UI_lpf40_integral = NaN(length(UI_lpf40),1);
UI_lpf40_sign = NaN(length(UI_lpf40),1);
for i = 1:length(UI_lpf40_sign);
    if (isfinite(UI_lpf40(i)));
        if (UI_lpf40(i)>0 );
            UI_lpf40_sign(i) = 1;
        elseif (UI_lpf40(i)<0);
               UI_lpf40_sign(i) = -1;
        else
                UI_lpf40_sign(i) = 0;
        end
    end
end
% begin integration following NaN's at beginning
```

```
Reals = find(isfinite(UI_lpf40_sign));
start = Reals(1,1);
for t=start:length(UI_lpf40_integral);
    if (t>start);
        if (isfinite(UI_lpf40_sign(t)));
            UI_lpf40_integral(t) = UI_lpf40_sign(t)+UI_lpf40_integral(t-1);
        else
            UI_lpf40_integral(t) = UI_lpf40_integral(t-1);
        end
    else
        UI_lpf40_integral(t) = UI_lpf40_sign(t);
    end
end
% detrend to create UPI
UPI = NaN(length(UI_lpf40_integral),1);
%determine 2nd order polynomial coefficients
%using time period between the First and Last
%01January in the time series (for seasonal trend consistency)
startSeason = find(Hour==datenum(2010,01,01));
endSeason = find(Hour==datenum(2013,01,01));
poly2 = polyfit(Hour(startSeason:endSeason),...
    UI_lpf40_integral(startSeason:endSeason),2);
%fit 2nd order polynomial
UItrend = polyval(poly2,Hour(start:length(UI_lpf40_integral)));
% detrend
UPI(start:length(UI_lpf40_integral)) = ...
    UI_lpf40_integral(start:length(UI_lpf40_integral))-UItrend;

% **check conditonal integration**
%  plot(Hour,UI_lpf40);hold on;
```

```
%  plot(Hour, UI_lpf40_integral,'k');
%  plot(Hour(start:length(UI_lpf40_integral)), UItrend,'c');
%  plot(Hour, UPI,'g');
%  hold off; grid on; dynamicDateTicks();

clear Reals start t i UI_lpf40_integral UI_lpf40_sign UItrend poly2...
        startSeason endSeason

%% FRDI (Fraser River Discharge Index)

% import Fraser Data from Hope, BC, Canada
% downloaded from the Water Survey of Canada Website
% *must download recent and older data seperately and combine
% http://www.wateroffice.ec.gc.ca/graph/graph_e.html?stn=08MF005
% http://www.wsc.ec.gc.ca/applications/H2O/graph-eng.cfm?station=08MF005&report=daily&year=201
% rename as (Fraser_Discharge) and (Fraser_time)

% switch to UTC time
UTC_time_fraser = Fraser_time + (8/24);
% interpolate to hourly
Fdis_hr = interp1(UTC_time_fraser,Fraser_Discharge,Hour);

% **check interpolation**
% scatter(UTC_time_fraser,Fraser_Discharge,'x');
% hold on;
% plot(Hour,Fdis_hr,'r');
% hold off;

% discharge index (normalization)
dMax = max(Fdis_hr);
```

```
dMin = min(Fdis_hr);
FDI_prefilter = (Fdis_hr - dMin)/(dMax-dMin);
% match residual current time-scale [subtidal signal]
fdi66 = pl66tn(FDI_prefilter,1,40);
% remove parts of filtered signal biased by NaN values
fdi40 = fdi66;
for i = 1:length(fdi66);
    if (i<41 || i>(length(fdi66)-40));
        fdi40(i) = NaN;
    elseif(isnan(fdi66(i)));
        fdi40((i-40):(i+40),1) = NaN(81,1);
    end
end
% normalize
FRDI = (fdi40-min(fdi40))/max(fdi40-min(fdi40));

% **check filter**
% plot(Hour,FDI_prefilter);hold on;plot(Hour,FRDI,'r');hold off;

clear fdi40 fdi66 i dMax dMin UTC_time_fraser Fraser_time...
    Fraser_Discharge FDI_prefilter

%% DOAP (Dissolved Oxygen Availibility Prediction)

% use equation derived from regression
DOAP = 7.0343 - (0.0013*UPI) - (2.0535*FRDI);

%% Intrusion Event Predictions

IEconditions = find(NTI>=0.8 & DII>=0.72);
```

```
%% Hypoxic Intrusion Event Predictions

HIEconditions = find(NTI>=0.8 & DII>=0.72 & DOAP<=6.241);

%% HIFP (Hypoxic Intrusion Favorable Period)

HIFP = NaN(length(Hour),1);
% HIFP is the hour vector that is set to NAN if it is not within 8
% days of a hypoxic intrusion event prediction point
for i = 1:length(HIFP);
    if (i>192 && i<(length(HIFP)-192));
        if (any(NTI(((i-192):(i+192)),1)>=0.8 &...
                DII(((i-192):(i+192)),1)>=0.72 &...
                DOAP(((i-192):(i+192)),1)<=6.241));
            HIFP(i) = Hour(i);
        end
    elseif (i<=192);
        if (any(NTI((1:(i+192)),1)>=0.8 &...
                DII((1:(i+192)),1)>=0.72 &...
                DOAP((1:(i+192)),1)<=6.241));
            HIFP(i) = Hour(i);
        end
    else
        if (any(NTI(((i-192):length(HIFP)),1)>=0.8 &...
                DII(((i-192):length(HIFP)),1)>=0.72 &...
                DOAP(((i-192):length(HIFP)),1)<=6.241));
            HIFP(i) = Hour(i);
        end
    end
```

```
end

clear i

%% Plot Intrusion Predictions and HIFP's

IntP = NaN(size(Hour));
for i = 1:length(IntP);
    if (any(i==IEconditions));
        IntP(i) = 1;
    else
        IntP(i) = 0;
    end
end

a=subplot(2,1,1);
area(Hour,IntP,...
    'FaceColor','g','EdgeColor','none');
hold on;
area(Hour,IntP,...
    'FaceColor','none','EdgeColor','g','LineStyle','-');
plot(Hour,zeros(size(Hour)),'k');
plot(Hour,1*ones(size(Hour)),'k');
title('Intrusion Event Predictions','FontSize',22);
dynamicDateTicks();
set(gca,'YDir','normal','FontSize',18,'Layer','top');
grid on;
legend('Intrusion Event Prediction');
hold off;
```

```
HypIntP = NaN(size(Hour));
for i = 1:length(HypIntP);
    if (isfinite(HIFP(i)));
        HypIntP(i) = 10;
    else
        HypIntP(i) = 0;
    end
end

b=subplot(2,1,2);
area(Hour,HypIntP,...
    'FaceColor','c','EdgeColor','none');
hold on;
plot(Hour,DOAP,'--b');
area(Hour,HypIntP,...
    'FaceColor','none','EdgeColor','k','LineStyle','--');
plot(Hour,3*ones(size(Hour)),'k');
plot(Hour,10*ones(size(Hour)),'k');
title('Hypoxic Intrusion Event Favorable Periods','FontSize',22);
ylabel('Dissolved Oxygen (mg/L)','FontSize',20);
legend('Hypoxic Intrusion Event Favorable',...
    'Dissolved Oxygen Availibility Prediction (seasonal)');
hold off;
grid on; set(gca,'YDir','normal','FontSize',18,'Layer','top');
ylim([3 10]);

linkaxes([a b],'x');
dynamicDateTicks([a b], 'link');
xlim([Hour(1,1),Hour(length(Hour),1)]);
```

```
set(gcf, 'PaperPosition', [0.5 2 18 12]);

clear a b IntP HypIntP
```

SUB-TIDAL DISSOLVED OXYGEN PREDICTION METHOD (VICTORIA CLIPPER)

```
%% SUB-TIDAL DO PREDICTION

%Using Victoria Clipper T-S observations

%R. Walt Deppe
%November 16, 2013

%% Import Data Sets

VC_30Jun2012 = uiimport('2012-06-30_vc_csv_export.mat');
VC_31Jul2012 = uiimport('2012-07-31_vc_csv_export.mat');
VC_31Aug2012 = uiimport('2012-08-31_vc_csv_export.mat');
VC_30Sep2012 = uiimport('2012-09-30_vc_csv_export.mat');
VC_31Oct2012 = uiimport('2012-10-31_vc_csv_export.mat');
VC_30Nov2012 = uiimport('2012-11-30_vc_csv_export.mat');
VC_31Dec2012 = uiimport('2012-12-31_vc_csv_export.mat');

%% TSNH sets

Pars_TSNH = [1 5 6 8 9 10 11 12];

VC_TSNH_raw_26 = VC_30Jun2012.TSNH;
```

```
VC_TSNH_raw_27 = VC_31Jul2012.TSNH;
VC_TSNH_raw_28 = VC_31Aug2012.TSNH;
VC_TSNH_raw_29 = VC_30Sep2012.TSNH;
VC_TSNH_raw_30 = VC_31Oct2012.TSNH;
VC_TSNH_raw_31 = VC_30Nov2012.TSNH;
VC_TSNH_raw_32 = VC_31Dec2012.TSNH;

VC_TSNH_26 = VC_TSNH_raw_26(1:size(VC_TSNH_raw_26,1),Pars_TSNH);
VC_TSNH_27 = VC_TSNH_raw_27(1:size(VC_TSNH_raw_27,1),Pars_TSNH);
VC_TSNH_28 = VC_TSNH_raw_28(1:size(VC_TSNH_raw_28,1),Pars_TSNH);
VC_TSNH_29 = VC_TSNH_raw_29(1:size(VC_TSNH_raw_29,1),Pars_TSNH);
VC_TSNH_30 = VC_TSNH_raw_30(1:size(VC_TSNH_raw_30,1),Pars_TSNH);
VC_TSNH_31 = VC_TSNH_raw_31(1:size(VC_TSNH_raw_31,1),Pars_TSNH);
VC_TSNH_32 = VC_TSNH_raw_32(1:size(VC_TSNH_raw_32,1),Pars_TSNH);

clear VC_TSNH_raw_26 VC_TSNH_raw_27 VC_TSNH_raw_28 VC_TSNH_raw_29...
   VC_TSNH_raw_30 VC_TSNH_raw_31 VC_TSNH_raw_32 VC_30Jun2012...
   VC_31Jul2012 VC_31Aug2012 VC_30Sep2012 VC_31Oct2012...
   VC_30Nov2012 VC_31Dec2012

%% combine TSNH

%Time
col = 1;
VC_TSNH_Time_sets = vertcat(...
    vertcat(VC_TSNH_26(1:size(VC_TSNH_26,1),col)),...
    vertcat(VC_TSNH_27(1:size(VC_TSNH_27,1),col)),...
    vertcat(VC_TSNH_28(1:size(VC_TSNH_28,1),col)),...
    vertcat(VC_TSNH_29(1:size(VC_TSNH_29,1),col)),...
    vertcat(VC_TSNH_30(1:size(VC_TSNH_30,1),col)),...
```

```
    vertcat(VC_TSNH_31(1:size(VC_TSNH_31,1),col)),...
    vertcat(VC_TSNH_32(1:size(VC_TSNH_32,1),col)));
%Temperature
col = 2;
VC_TSNH_Temp_sets = vertcat(...
    vertcat(VC_TSNH_26(1:size(VC_TSNH_26,1),col)),...
    vertcat(VC_TSNH_27(1:size(VC_TSNH_27,1),col)),...
    vertcat(VC_TSNH_28(1:size(VC_TSNH_28,1),col)),...
    vertcat(VC_TSNH_29(1:size(VC_TSNH_29,1),col)),...
    vertcat(VC_TSNH_30(1:size(VC_TSNH_30,1),col)),...
    vertcat(VC_TSNH_31(1:size(VC_TSNH_31,1),col)),...
    vertcat(VC_TSNH_32(1:size(VC_TSNH_32,1),col)));
%Salinity
col = 3;
VC_TSNH_Salinity_sets = vertcat(...
    vertcat(VC_TSNH_26(1:size(VC_TSNH_26,1),col)),...
    vertcat(VC_TSNH_27(1:size(VC_TSNH_27,1),col)),...
    vertcat(VC_TSNH_28(1:size(VC_TSNH_28,1),col)),...
    vertcat(VC_TSNH_29(1:size(VC_TSNH_29,1),col)),...
    vertcat(VC_TSNH_30(1:size(VC_TSNH_30,1),col)),...
    vertcat(VC_TSNH_31(1:size(VC_TSNH_31,1),col)),...
    vertcat(VC_TSNH_32(1:size(VC_TSNH_32,1),col)));
%Time_GPS
col = 4;
VC_TSNH_Time_GPS_sets = vertcat(...
    vertcat(VC_TSNH_26(1:size(VC_TSNH_26,1),col)),...
    vertcat(VC_TSNH_27(1:size(VC_TSNH_27,1),col)),...
    vertcat(VC_TSNH_28(1:size(VC_TSNH_28,1),col)),...
    vertcat(VC_TSNH_29(1:size(VC_TSNH_29,1),col)),...
    vertcat(VC_TSNH_30(1:size(VC_TSNH_30,1),col)),...
```

```
    vertcat(VC_TSNH_31(1:size(VC_TSNH_31,1),col)),...
    vertcat(VC_TSNH_32(1:size(VC_TSNH_32,1),col)));
%Lattitude
col = 5;
VC_TSNH_Latt_sets = vertcat(...
    vertcat(VC_TSNH_26(1:size(VC_TSNH_26,1),col)),...
    vertcat(VC_TSNH_27(1:size(VC_TSNH_27,1),col)),...
    vertcat(VC_TSNH_28(1:size(VC_TSNH_28,1),col)),...
    vertcat(VC_TSNH_29(1:size(VC_TSNH_29,1),col)),...
    vertcat(VC_TSNH_30(1:size(VC_TSNH_30,1),col)),...
    vertcat(VC_TSNH_31(1:size(VC_TSNH_31,1),col)),...
    vertcat(VC_TSNH_32(1:size(VC_TSNH_32,1),col)));
%Longitude
col = 6;
VC_TSNH_Long_sets = vertcat(...
    vertcat(VC_TSNH_26(1:size(VC_TSNH_26,1),col)),...
    vertcat(VC_TSNH_27(1:size(VC_TSNH_27,1),col)),...
    vertcat(VC_TSNH_28(1:size(VC_TSNH_28,1),col)),...
    vertcat(VC_TSNH_29(1:size(VC_TSNH_29,1),col)),...
    vertcat(VC_TSNH_30(1:size(VC_TSNH_30,1),col)),...
    vertcat(VC_TSNH_31(1:size(VC_TSNH_31,1),col)),...
    vertcat(VC_TSNH_32(1:size(VC_TSNH_32,1),col)));
%Speed
col = 7;
VC_TSNH_Speed_sets = vertcat(...
    vertcat(VC_TSNH_26(1:size(VC_TSNH_26,1),col)),...
    vertcat(VC_TSNH_27(1:size(VC_TSNH_27,1),col)),...
    vertcat(VC_TSNH_28(1:size(VC_TSNH_28,1),col)),...
    vertcat(VC_TSNH_29(1:size(VC_TSNH_29,1),col)),...
    vertcat(VC_TSNH_30(1:size(VC_TSNH_30,1),col)),...
```

```
    vertcat(VC_TSNH_31(1:size(VC_TSNH_31,1),col)),...
    vertcat(VC_TSNH_32(1:size(VC_TSNH_32,1),col)));
%Direction
col = 8;
VC_TSNH_Dir_sets = vertcat(...
    vertcat(VC_TSNH_26(1:size(VC_TSNH_26,1),col)),...
    vertcat(VC_TSNH_27(1:size(VC_TSNH_27,1),col)),...
    vertcat(VC_TSNH_28(1:size(VC_TSNH_28,1),col)),...
    vertcat(VC_TSNH_29(1:size(VC_TSNH_29,1),col)),...
    vertcat(VC_TSNH_30(1:size(VC_TSNH_30,1),col)),...
    vertcat(VC_TSNH_31(1:size(VC_TSNH_31,1),col)),...
    vertcat(VC_TSNH_32(1:size(VC_TSNH_32,1),col)));

clear col VC_TSNH_26 VC_TSNH_27 VC_TSNH_28 VC_TSNH_29...
    VC_TSNH_30 VC_TSNH_31 VC_TSNH_32

%remove blank cells
cut = [64:72];
VC_TSNH_Time_sets(cut) = [];
VC_TSNH_Temp_sets(cut) = [];
VC_TSNH_Salinity_sets(cut) = [];
VC_TSNH_Time_GPS_sets(cut) = [];
VC_TSNH_Latt_sets(cut) = [];
VC_TSNH_Long_sets(cut) = [];
VC_TSNH_Speed_sets(cut) = [];
VC_TSNH_Dir_sets(cut) = [];

clear cut

%% fix length-match problems
```

```
for i = 1:size(VC_TSNH_Time_sets,1);
    if (size(VC_TSNH_Time_sets{i,1,:},1)>...
            size(VC_TSNH_Temp_sets{i,1,:},1));
        dsize = size(VC_TSNH_Time_sets{i,1,:},1) - ...
                   size(VC_TSNH_Temp_sets{i,1,:},1);
        Tempfix = VC_TSNH_Temp_sets{i,1,:};
        Tempfix(length(Tempfix)+1:length(Tempfix)+dsize,1) = NaN(dsize,1);
        VC_TSNH_Temp_sets{i,1,:} = Tempfix;
    end
    if (size(VC_TSNH_Time_sets{i,1,:},1)>...
            size(VC_TSNH_Salinity_sets{i,1,:},1));
        dsize = size(VC_TSNH_Time_sets{i,1,:},1) - ...
                   size(VC_TSNH_Salinity_sets{i,1,:},1);
        Salfix = VC_TSNH_Salinity_sets{i,1,:};
        Salfix(length(Salfix)+1:length(Salfix)+dsize,1) = NaN(dsize,1);
        VC_TSNH_Salinity_sets{i,1,:} = Salfix;
    end
end

clear i Tempfix Salfix dsize

%% ready sets for interpolation, make time set

Step = 1;   %set time step in minutes

N = size(VC_TSNH_Time_sets,1);

%remove foul time value-------------
for i = 1:N;
```

```
    SetFix = VC_TSNH_Time_sets{i,1,:};
    for j = 1:length(SetFix);
        if (SetFix(j)<datenum(2012,05,31) ...
                || SetFix(j)>datenum(2013,01,02));
            SetFix(j) = NaN;
        end
    end
    VC_TSNH_Time_sets{i,1,:} = SetFix;
end
%------------------------------

TIME_sets = cell(N,1);
Raw_TimeSets = VC_TSNH_Time_sets;
Raw_TempSets = VC_TSNH_Temp_sets;
Raw_DirSets = VC_TSNH_Dir_sets;
Raw_LattSets = VC_TSNH_Latt_sets;
Raw_LongSets = VC_TSNH_Long_sets;
Raw_SpeedSets = VC_TSNH_Speed_sets;
Raw_SalinitySets = VC_TSNH_Salinity_sets;
for i = 1:N;
    %create time set
    Set = [VC_TSNH_Time_sets{i,:,:}];
    TIME_sets{i,:,:} = (floor(min(Set)):((1/24)/(60/Step)):ceil(max(Set)))';
    %remove time-repeats in data
    RawSetTime = [Raw_TimeSets{i,:,:}];
    RawSetTemp = [Raw_TempSets{i,:,:}];
    RawSetDir = [Raw_DirSets{i,:,:}];
    RawSetLatt = [Raw_LattSets{i,:,:}];
    RawSetLong = [Raw_LongSets{i,:,:}];
    RawSetSpeed = [Raw_SpeedSets{i,:,:}];
```

```
    RawSetSalinity = [Raw_SalinitySets{i,:,:}];
    for j = 2:length(Set);
        if (Set(j,1)==Set(j-1,1));
            RawSetTime(j,1)=NaN;
        end
    end
    cut = find(isnan(RawSetTime));
    RawSetTime(cut) = [];
    RawSetTemp(cut) = [];
    RawSetDir(cut) = [];
    RawSetLatt(cut) = [];
    RawSetLong(cut) = [];
    RawSetSpeed(cut) = [];
    RawSetSalinity(cut) = [];
    Raw_TimeSets{i,:,:} = RawSetTime;
    Raw_TempSets{i,:,:} = RawSetTemp;
    Raw_DirSets{i,:,:} = RawSetDir;
    Raw_LattSets{i,:,:} = RawSetLatt;
    Raw_LongSets{i,:,:} = RawSetLong;
    Raw_SpeedSets{i,:,:} = RawSetSpeed;
    Raw_SalinitySets{i,:,:} = RawSetSalinity;
end

clear N i j Set cut RawSetTime RawSetTemp RawSetDir RawSetLatt...
    RawSetLong RawSetSpeed RawSetSalinity VC_TSNH_Time_sets VC_TSNH_Temp_sets...
    VC_TSNH_Dir_sets VC_TSNH_Latt_sets VC_TSNH_Long_sets VC_TSNH_Speed_sets...
    VC_TSNH_Salinity_sets VC_TSNH_Time_GPS_sets SetFix

%% interpolate to time step specified
```

```
N = size(TIME_sets,1);
%Salinity
Salinity_sets = cell(N,1);
for i = 1:N;
    Set = [Raw_SalinitySets{i,:,:}];
    RawTimeSet = [Raw_TimeSets{i,:,:}];
    timeSet = [TIME_sets{i,:,:}];
    Salinity_sets{i,:,:} = interp1(RawTimeSet,Set,timeSet);
end
%Temp
Temp_sets = cell(N,1);
for i = 1:N;
    Set = [Raw_TempSets{i,:,:}];
    RawTimeSet = [Raw_TimeSets{i,:,:}];
    timeSet = [TIME_sets{i,:,:}];
    Temp_sets{i,:,:} = interp1(RawTimeSet,Set,timeSet);
end
%Dir
Dir_sets = cell(N,1);
for i = 1:N;
    Set = [Raw_DirSets{i,:,:}];
    RawTimeSet = [Raw_TimeSets{i,:,:}];
    timeSet = [TIME_sets{i,:,:}];
    Dir_sets{i,:,:} = interp1(RawTimeSet,Set,timeSet);
end
%Latt
Latt_sets = cell(N,1);
for i = 1:N;
    Set = [Raw_LattSets{i,:,:}];
    RawTimeSet = [Raw_TimeSets{i,:,:}];
```

```
    timeSet = [TIME_sets{i,:,:}];
    Latt_sets{i,:,:} = interp1(RawTimeSet,Set,timeSet);
end
%Long
Long_sets = cell(N,1);
for i = 1:N;
    Set = [Raw_LongSets{i,:,:}];
    RawTimeSet = [Raw_TimeSets{i,:,:}];
    timeSet = [TIME_sets{i,:,:}];
    Long_sets{i,:,:} = interp1(RawTimeSet,Set,timeSet);
end
%Speed
Speed_sets = cell(N,1);
for i = 1:N;
    Set = [Raw_SpeedSets{i,:,:}];
    RawTimeSet = [Raw_TimeSets{i,:,:}];
    timeSet = [TIME_sets{i,:,:}];
    Speed_sets{i,:,:} = interp1(RawTimeSet,Set,timeSet);
end

clear Set RawTimeSet timeSet i N Raw_TimeSets Raw_TempSets...
    Raw_SalinitySets Raw_DirSets Raw_LattSets Raw_LongSets...
    Raw_SpeedSets

%% TSNH combine full series
TIME_VC_TSNH = cell2mat(TIME_sets);

Salinity_VC_TSNH = cell2mat(Salinity_sets);
 for i=1:length(Salinity_VC_TSNH);
     if (Salinity_VC_TSNH(i)<=0 || Salinity_VC_TSNH(i)>40);
```

```
         Salinity_VC_TSNH(i)=NaN;
     end
 end
Temp_VC_TSNH = cell2mat(Temp_sets);
 for i=1:length(Temp_VC_TSNH);
     if (Temp_VC_TSNH(i)<=0 || Temp_VC_TSNH(i)>30);
         Temp_VC_TSNH(i)=NaN;
     end
 end
Dir_VC_TSNH = cell2mat(Dir_sets);
Latt_VC_TSNH = cell2mat(Latt_sets);
Long_VC_TSNH = cell2mat(Long_sets);
Speed_VC_TSNH = cell2mat(Speed_sets);

clear i TIME_sets Salinity_sets Temp_sets Dir_sets Latt_sets...
        Long_sets Speed_sets

%% GPS Range Limit

GPS_ADM = find(Long_VC_TSNH<=-122.6 & Long_VC_TSNH>=-122.8 ...
            & Latt_VC_TSNH>=48.1 & Latt_VC_TSNH<=48.2);

%** check location **
% scatter(Long_VC_TSNH,Latt_VC_TSNH);hold on;
% scatter(Long_VC_TSNH(GPS_ADM),Latt_VC_TSNH(GPS_ADM),'x');
% scatter(-122.6862,48.1529,'or','filled');
% hold off;
% grid on;

%% Limit Data to Admiralty
```

```
VCsal_Adm = NaN(length(Salinity_VC_TSNH),1);
VCtemp_Adm = NaN(length(Temp_VC_TSNH),1);
VClatt_Adm = NaN(length(Latt_VC_TSNH),1);
VClong_Adm = NaN(length(Long_VC_TSNH),1);
T_Adm = NaN(length(TIME_VC_TSNH),1);
for i = GPS_ADM;
    VCsal_Adm(i) = Salinity_VC_TSNH(i);
    VCtemp_Adm(i) = Temp_VC_TSNH(i);
    VClatt_Adm(i) = Latt_VC_TSNH(i);
    VClong_Adm(i) = Long_VC_TSNH(i);
    T_Adm(i) = TIME_VC_TSNH(i);
end

%** check location **
% scatter(VClong_Adm,VClatt_Adm,'x');hold on;
% scatter(-122.6862,48.1529,'or','filled');
% hold off;
% grid on;

clear i


%% Choose time period for analysis / Set up hourly time steps

% hourly time from (16 May 2009) to (16 Jan 2013)
Hour = (datenum(2012,05,16):(1/24):datenum(2013,01,16))';

% Be sure that [pl66tn.m] and [dynamicDateTicks.m],
% are in the current folder
```

```
%% Interpolate VC Salinity data at Admiralty to hourly time scale

VCsal_raw = VCsal_Adm;
VCtime_raw = T_Adm;
cut = find(isnan(T_Adm));
VCtime_raw(cut) = [];
VCsal_raw(cut) = [];

%set up distinct value vector to eliminate NaN periods through rounding
Sal_VC_Finite = NaN(length(Salinity_VC_TSNH),1);
count = 0;
for i = 1:length(Sal_VC_Finite);
    if (isfinite(Salinity_VC_TSNH(i)));
        count = count+1;
        Sal_VC_Finite(i) = count;
    end
end

VCsal_raw_Nan = Sal_VC_Finite;
VCtime_raw_Nan = TIME_VC_TSNH;
cutNan = find(isnan(Sal_VC_Finite));
VCtime_raw_Nan(cutNan) = [];
VCsal_raw_Nan(cutNan) = [];

VCsal_hr = interp1(VCtime_raw,VCsal_raw,Hour);
VCsal_hr_NAN = interp1(VCtime_raw_Nan,VCsal_raw_Nan,Hour);
 for i = 1:length(VCsal_hr);
     if (VCsal_hr_NAN(i)~=round(VCsal_hr_NAN(i)));
         VCsal_hr(i) = NaN;
```

```
     end
 end

%***check interp
% plot(TIME_VC_TSNH,VCsal_Adm,'r');hold on;
% scatter(Hour,VCsal_hr,'xk');
% plot(Hour,VCsal_hr);hold off;grid on;dynamicDateTicks();
% xlim([TIME_VC_TSNH(1) TIME_VC_TSNH(length(TIME_VC_TSNH))]);

clear cut VCsal_raw VCtime_raw cutNan VCtime_raw_Nan VCsal_raw_Nan...
        VCsal_hr_NAN i count

%% Interpolate VC Temp data at Admiralty to hourly time scale

VCtemp_raw = VCtemp_Adm;
VCtime_raw = T_Adm;
cut = find(isnan(T_Adm));
VCtime_raw(cut) = [];
VCtemp_raw(cut) = [];

Temp_VC_Finite = NaN(length(Temp_VC_TSNH),1);
count = 0;
for i = 1:length(Temp_VC_Finite);
    if (isfinite(Temp_VC_TSNH(i)));
        count = count+1;
        Temp_VC_Finite(i) = count;
    end
end

VCtemp_raw_Nan = Temp_VC_Finite;
```

```
VCtime_raw_Nan = TIME_VC_TSNH;
cutNan = find(isnan(Temp_VC_Finite));
VCtime_raw_Nan(cutNan) = [];
VCtemp_raw_Nan(cutNan) = [];

VCtemp_hr = interp1(VCtime_raw,VCtemp_raw,Hour);
VCtemp_hr_NAN = interp1(VCtime_raw_Nan,VCtemp_raw_Nan,Hour);
 for i = 1:length(VCtemp_hr);
     if (VCtemp_hr_NAN(i)~=round(VCtemp_hr_NAN(i)));
         VCtemp_hr(i) = NaN;
     end
 end

%***check interp
% plot(TIME_VC_TSNH,VCtemp_Adm,'r');hold on;
% scatter(Hour,VCtemp_hr,'xk');
% plot(Hour,VCtemp_hr);hold off;grid on;dynamicDateTicks();
% xlim([TIME_VC_TSNH(1) TIME_VC_TSNH(length(TIME_VC_TSNH))]);

clear cut VCtemp_raw VCtime_raw cutNan VCtime_raw_Nan VCtemp_raw_Nan...
        VCtemp_hr_NAN i count

%% 40-hour LowPassFilter & Seasonal Filter
% match residual current time-scale [subtidal signal]

VCsal_lpf40 = pl66tn(VCsal_hr,1,40);
% **check filter**
% plot(TIME_VC_TSNH,VCsal_Adm,'g');hold on;
% scatter(Hour,VCsal_hr,'xk');
% plot(Hour,VCsal_lpf40,'b');
```

```
% hold off;grid on;dynamicDateTicks();
% xlim([TIME_VC_TSNH(1) TIME_VC_TSNH(length(TIME_VC_TSNH))]);

VCtemp_lpf40 = pl66tn(VCtemp_hr,1,40);
% **check filter**
% plot(TIME_VC_TSNH,VCtemp_Adm,'g');hold on;
% scatter(Hour,VCtemp_hr,'xk');
% plot(Hour,VCtemp_lpf40,'b');
% hold off;grid on;dynamicDateTicks();
% xlim([TIME_VC_TSNH(1) TIME_VC_TSNH(length(TIME_VC_TSNH))]);

%% ST_DOP (Sub-Tidal Dissolved Oxygen Prediction)

% use equation derived from regression
ST_DOP = 32.6253 - (0.6094*VCsal_lpf40) - (0.8084*VCtemp_lpf40);

%% ST_DOP plot

plot(Hour,ST_DOP,'--b');
title('Empirical Sub-Tidal Dissolved Oxygen Prediction form Victoria Clipper Data'...
    ,'FontSize',22);
ylabel('Dissolved Oxygen (mg/L)','FontSize',22);
set(gca,'YDir','normal','FontSize',18);
legend('Sub-tidal DO Prediction');
grid on;
ylim([4 9]);
dynamicDateTicks();

set(gcf, 'PaperPosition', [0.5 2 12 6]);
```

```
clear ticks
```

VITA

Walt Deppe graduated from the University of Virginia in May 2012 with a B.S. in Mechanical Engineering and a minor in Environmental Science. He is working towards a M.S. in Mechanical Engineering, with plans to graduate from the University of Washington in March 2014.